ÉCOLE DE TECHNOLOGIE SUPÉRIEURE
UNIVERSITÉ DU QUÉBEC

THESIS M. ENG
PRESENTED TO
ÉCOLE DE TECHNOLOGIE SUPÉRIEURE

IN PARTIAL FULFILLEMENT OF THE REQUIREMENTS FOR
THE DEGREE OF MASTER'S OF ENGINEERING
M. Eng.

BY
Philippe PHAM

IMPROVEMENT OF THE INITIALIZATION OF THE WEST WIND RESSOURCE SOFTWARE FOR MOUNTAINOUS REGION IN COLD CLIMATES

MONTREAL, MARCH 6TH 2013

BOARD OF EXAMINERS

THIS THESIS HAS BEEN EVALUATED

BY THE FOLLOWING BOARD OF EXAMINERS

Dr. Robert Benoit, Thesis Supervisor
Department of Mechanical Engineering at École de technologie supérieure

Dr. Christian Masson, Thesis Co-supervisor
Department of Mechanical Engineering at École de technologie supérieure

Dr. François Brissette, President of the Board of Examiners
Department of Construction at École de technologie supérieure

Dr. Jean-Paul Pinard, External Evaluator
Consultant

THIS THESIS WAS PRESENTED AND DEFENDED

IN THE PRESENCE OF A BOARD OF EXAMINERS AND PUBLIC

<FEBRUARY 7TH 2013>

AT ÉCOLE DE TECHNOLOGIE SUPÉRIEURE

ACKNOWLEDGMENT

First of all, I would like to thank Dr. Christian Masson and the École de technologie supérieure (ETS) for giving me the opportunity to be part of the Chaire de recherche sur l'aérodynamique des éoliennes en milieu nordique (AEMN) and do research on projects related to wind and renewable energies, a subject I feel strongly about. I would also like to acknowledge the Wind Energy Strategic Network (WESNet) for funding this research.

I would also like to thank my supervisor, Dr. Robert Benoit, a very knowledgeable, understanding and brilliant scientist. He has aided me and offered insights countless times whenever I encountered issues and obstacles in my research. I am also grateful of the help Dr. Wei Yu and Dr. Jean-Paul Pinard for their occasional inputs and assistance during my research. In addition, Dr. Pinard has been a great help for providing me with the observation data used in this study.

Finally, I would like to acknowledge my friends and family for being there and supporting me throughout this endeavour.

AMÉLIORATION DE L'INITIALISATION DU LOGICIEL WEST EN SAISON FROIDE POUR LES RÉGIONS MONTAGNEUSES, THÈSE M. ING

Philippe PHAM

RÉSUMÉ

Cette recherche vise à améliorer l'initialisation du logiciel WEST qui est utilisé pour cartographier le potentiel éolien. Il a été démontré dans Pinard, Benoit *et al.* (2009) que WEST ne reproduisait pas correctement la climatologie du vent dans le Yukon et la stratification thermique du Yukon durant les saisons froides n'était pas bien représentée. Cela entraînait les prédictions des vents dans la couche limite à être trop grandes. La première modification introduit le nombre de Froude, un nouveau critère de classification qui prendra en considération la stratification thermique, et des facteurs de correction. Les expériences démontrent que le nombre de Froude réussit à capturer les stratifications thermiques, et les facteurs de correction ont été capables de modifier la fréquence des états climatique en se basant sur les données des Radiosondes, ce qui a permis d'obtenir des vitesses de vent réduites. Les differences moyennes avec les observations passent de 0.8 m/s à 0.1 m/s. La deuxième modification augmente le niveau du plan initial à un niveau approprié à la région modélisée afin de minimiser les pentes fortes tout autour du domaine. Ce changement a permis de réduire davantage les vitesses des vents. La troisième modification vise à modifier les directions des vents modélisées en utilisant les profils de vent à un niveau plus élevé et en interpolant vers les niveaux plus bas avec le principe du vent thermique. Les corrections des vents ont été minimes, mais dépendant des expériences, les directions du vent ont pu être corrigées. Les résultats de cette recherche démontrent une réduction des vitesses originalement surestimées pour la région de Whitehorse, et qu'il est possible de corriger les directions des vents lorsque nécessaire.

Mot-clé : modèle meso-échelle, éolien, Yukon, Whitehorse, Froude, initialisation, WEST.

IMPROVEMENT OF THE INITIALIZATION OF WEST SOFTWARE FOR MOUNTAINOUS REGION IN COLD CLIMATES, THESIS M. ENG

Philippe PHAM

ABSTRACT

This study aims to improve the WEST software for wind resource assessment purposes, and obtain better simulated results of the wind for the mountainous region of Whitehorse. It was found that the model overestimated the wind speeds, and Pinard *et al.* (2009) suggested several improvements and modifications to the model, where some of these modifications were considered and implemented in this study. The first suggestion was the introduction of the Froude number and correction factors in the classification scheme. The Froude number was successful in capturing stable climate states and thermal stratification. The correction factors were able to modify the frequency of certain climate states to match the frequency of their occurrence as seen in the observations through Radiosondes. These stable climate states would reduce the speed of the wind, and mean difference of the simulation with respect to the wind stations, would go from 0.8 m/s to 0.1 m/s. The second suggestion was to raise the initial reference topography to a level appropriate to the region, in order to attenuate the spurious cliffs seen around the domain. It was shown that these cliffs would affect the flow and cause an outflow of the wind. By implementing this modification, the modeled wind speeds were further reduced. The third suggestion did not aim to reduce the wind speeds, but to correct the simulated wind directions that were found to be erroneous in previous studies. A modification to the code during the initialization of the model was implemented, where the data levels below the terrain for initialization profiles were replaced by extrapolated values from values at higher levels. This correction provided a minimal change to the simulation of this study; however it was able to correct the directions when applied to the simulations presented in past studies using a different set of climate states. These results show that a reduction of the simulated wind speeds for the region of Whitehorse was achieved, and it was possible to correct the wind directions if needed.

Keywords: mesoscale model, wind, Yukon, Whitehorse, Froude, initialization, WEST.

TABLE OF CONTENTS

Page

INTRODUCTION 1

CHAPTER 1 DESCRIPTION OF MODEL 7
1.1 WEST model 7
1.2 Initialization of model 9
1.3 Computation aspects 11

CHAPTER 2 THE NEW CLASSIFICATION 15
2.1 Froude Number 15
2.2 Correction Factors 20
2.3 Climate States 27
2.4 Stable Climate States 30
2.5 Results 39

CHAPTER 3 INITIAL REFERENCE TOPOGRAPHY 43
3.1 Method 43
3.2 Theoretical Topography 45
3.3 Results 49

CHAPTER 4 LOW LEVEL PROFILES 51
4.1 Profile Modifications 51
4.2 Results 56

CHAPTER 5 COMPARISON OF RESULTS 59
5.1 Wind Stations 59
5.2 Modeled Results 62
5.2.1 Classification Variants 63
5.2.2 Initial Reference Topography 70
5.2.3 Low level profiles 73
5.2.4 Effects on Past Studies 77

CHAPTER 6 FINAL SIMULATION 81
6.1 Results 81
6.2 Comparison 84

CONCLUSION 89

ANNEX I CLASSIFICATION ALGORITHM 91

ANNEX II PROCEDURE TO CHANGE CLASSIFICATION VARIANT 99

ANNEX III CALCULATED CORRECTION FACTORS 103

ANNEX IV FROUDE FREQUENCY CURVE....105

ANNEX V FROUDE FREQUENCY CURVE WITH MERGED FACTORS....109

ANNEX VI RESULTS AND ANALYSIS OF CLASSIFICATION VARIANT 3....113

ANNEX VII WIND SPEEDS CONTOUR LINES FOR ORIGINAL CLASSIFICATION....117

ANNEX VIII WIND SPEED CONTOUR LINES FOR CLASSIFICATION VARIANT 1....119

ANNEX IX WIND SPEED CONTOUR LINES FOR CLASSIFICATION VARIANT 2....121

ANNEX X WIND SPEED CONTOUR LINES FOR INITIAL REFERENCE TOPOGRAPHY....123

ANNEX XI DESCRIPTION OF KEY KNCEP_DROP....125

ANNEX XII DETAILED DESCRIPTION OF WIND STATIONS....127

ANNEX XIII SIMULATED WIND SPEED OF SIMULATIONS....129

ANNEX XIV DIFFERENCE BETWEEN OBSERVATIONS AND SIMULATIONS....131

ANNEX XV WIND FREQUENCY ROSE OF FINAL SIMULATIONS AT 16 WIND STATION....133

LIST OF BIBLIOGRAPHICAL REFERENCES....137

LIST OF TABLES

Page

Table 2.1 Correction factors of Whitehorse 24

Table 2.2 Limits for Froude bins 28

Table 2.3 Description of different classification scheme and number of climate states 30

Table 2.4 Initialization variables for ANU1D225C04 climate states 31

Table 2.5 Brunt-Väisälä frequency of Climate states for 0 and 1500 m 36

Table 2.6 Parameters used in the MC2 simulation 39

Table 3.1 Initialization profile of theoretical topography 47

Table 4.1 Horizontal temperature gradient of Whitehorse Reanalaysis grid point 55

Table 5.1 Description of wind stations and wind measured wind speeds 60

Table 5.2 Wind speed difference between Original and Variant 1 66

Table 5.3 Wind speed difference between Variant 1 and Variant 2 69

Table 5.4 Wind speed difference between Variant 2 and Variant 2 with init_topo 71

Table 5.5 Difference between Variant 2 and Variant 2 with kdrop 76

Table 6.1 Wind speed difference between the final simulation and Variant 2 with init_topo 84

Table 6.2 Wind speed difference between the final simulations and the observations 85

LIST OF FIGURES

Page

Figure 0.1.1	Map of Yukon and region of Whitehorse	3
Figure 1.1	WEST flowchart	7
Figure 2.1	Position of Reanalysis grid points around Whitehorse	16
Figure 2.2	Map of the location and the type of the upper air Radiosondes network used in Canada	23
Figure 2.3	The Froude number frequency curve of Whitehorse modified by correction factors	25
Figure 2.4	Froude number frequency curve of Whitehorse modified by merged correction factors	27
Figure 2.5	The simulated wind flow of climate state ANU1D225C04A at 40 m AGL	33
Figure 2.6	The simulated wind flow of climate state ANU1D225C04D at 40 m AGL	33
Figure 2.7	The vertical velocity of the cross-section of Whitehorse valley cross-section for ANU1D225C04A	34
Figure 2.8	The vertical velocity of Whitehorse valley cross-section for ANU1D225C04D	35
Figure 2.9	The vertical profile of the vertical velocity WZ for climate state ANU1D225C04-	37
Figure 2.10	The temperature profile of climate state ANU1D225C04-	38
Figure 2.11	The simulated wind flow for original classification	41
Figure 2.12	The simulated wind flow for classification variant 1	42
Figure 2.13	The Simulated wind flow for classification variant 2	42
Figure 3.1	The vertical cross-section of topography for entire domain for the region of Regina (Saskatchewan) in m ASL	44

Figure 3.2 The vertical cross-section of topography for entire domain for the region of Regina (Saskatchewan), with initial reference topography set at 500m ASL....44

Figure 3.3 The cross-section of theoretical topography with initial reference topography at 0m 45

Figure 3.4 The cross-section of theoretical topography with initial reference topography at 500m 46

Figure 3.5 The superposition of the wind flow over theoretical topography with init_topo at 0 and 500m ASL....47

Figure 3.6 The vector difference between initial reference topography at 0m ASL and 500m ASL 48

Figure 3.7 Vector difference of the simulated wind flow for the cases of "classification variant 2"with initial reference topography at 0m ASL and initial reference topography" at 600m ASL 50

Figure 4.1 The wind energy frequency roses of Reanalysis (shaded) and Radiosondes (outlined) for Whitehorse 52

Figure 4.2 Geopotential heights of Reanalysis over the Yukon....53

Figure 4.3 Average temperature field of Reanalysis over the Yukon....56

Figure 4.4 The simulated wind flow for classification variant 2 with module kdrop 57

Figure 5.1 The topography and location of the 16 wind stations....61

Figure 5.2 Map of Whitehorse area and wind energy frequency of the 16 wind stations and the upper-air Radiosondes (plus Mt.Sumanik) 62

Figure 5.3 The comparison of the wind speed in m/s of the observations and the "original classification" (not using Froude) for the 16 wind stations....64

Figure 5.4 The comparison of the wind speed in m/s of the observations and the "classification variant 1 (without correction factors) for the 16 wind stations 65

Figure 5.5 The comparison of the wind speed in m/s of the observations and the "classification variant 2" (using correction factors) for the 16 wind stations 67

Figure 5.6 Total frequencies of climate states in same speed class with and without correction factors 68

Figure 5.7 The comparison of wind speeds in m/s of the observations and the "classification variant 2 with initial reference topography" for the 16 wind stations 70

Figure 5.8 Map of wind speed difference of the classification variant 2 with respect to the classification variant 2 with init_topo at 600m 73

Figure 5.9 The wind energy frequency roses of Reanalysis from Original Classification....75

Figure 5.10 Comparison of wind speeds in m/s of the observations and the "classification variant 2 with kdrop" for the 16 wind stations....77

Figure 5.11 The simulated wind flow of the climate states from WEST database and used in Pinard *et al.* (2009) 78

Figure 5.12 The simulated wind flow of the climate states from WEST database and used in Pinard *et al.* (2009) 79

Figure 6.1 The simulated wind flow for the climate states of the final simulation involving all the modifications 82

Figure 6.2 Wind speed for final simulations 82

Figure 6.3 Simulated direction frequency rose of Whitehorse at height levels 83

Figure 6.4 Comparison of wind speed in m/s between the observations and the final simulations 87

LIST OF ABREVIATIONS

AGL	Above ground level
ASL	Above sea level
BAEC	Boreal Alternative Energy Centre
KAMM	Karlsruhe Atmospheric Mesoscale Model
MSC	Meteorological Service of Canada
NARR	North American Regional Reanalysis
NCAR	National Center for Atmospheric Research
NCEP	National Center for Environmental Prediction
MC2	Mesoscale Compressible Community
RA	Reanalysis
RPN	Recherche en Prévision Numérique
RS	Radiosondes
SGE	Sun Grid Engine
WEST	Wind Energy Simulation Toolkit
YG	Yukon Government

LIST OF SYMBOLS

m	metre (unit of length)
km	kilometre (unit of length)
kg	kilogram (unit of mass)
s	second (unit of time)
rad	radian (unit of angle)
K	kelvin (unit of temperature)
°C	degree Celsius (unit of temperature)
m/s	metre/second (unit of speed)
knots	knots (1 knot = 1,943 844m/s) (unit of speed)
m/s^2	metre/second square (unit of acceleration)
rad/s	radian/second (unit of angular speed)
J	joule (unit of energy)
mbar	millibar (unit of pressure)
Pa	pascal (unit of pressure)
atm	atmosphere (unit of pressure)
R	universal gas constant (287 J kg^{-1} K^{-1})
T	air temperature (K)
P	air pressure in (Pa)
f	coriolis parameter ($s^{-1)}$
Ω	angular velocity of Earth (rad/s)
U	east component of horizontal wind (m/s)
V	north component of horizontal wind (m/s)

g	gravitational acceleration (m/s^2)
z	height (m)
z_s	height of ground (m)
H	height of model top (m)
T*	basic state of temperature isothermal profile (K)
T’	perturbation of temperature (K)
q	natural logarithmic of pressure (Pa)
q*	basic state of q (Pa)
q’	perturbation of q (Pa)
b	buoyancy per unit mass (m/s^2)
Fr	Froude number
N	Brunt-Väisälä frequency (s^{-1})
Θ	potential temperature (K)
U_g	incoming wind toward mountain (m/s)
H_c	characteristic topographic height (m)
uu	easterly component of wind speed for Reanalysis
vv	northerly component of wind speed for Reanalysis
tt	temperature of Reanalysis (K)
gz	geopotential height for Reanalysis (decametres)
hr	relative humidity for Reanalysis (kg/kg)
hu	specific humidity from classification scheme (kg/kg)
pp	pressure from classification scheme (millibar)
ug	geostrophic wind for classification scheme (m/s)

WZ	vertical wind speed (m/s)
ρ	density (kg/m^3)
u_g	east component of geostrophic wind (m/s)
v_g	north component of geostrophic wind (m/s)
V_T	thermal wind (m/s)
V_g	geostrophic wind (m/s)
Fcorr	correction factors
X	x coordinate component of grid
Y	y coordinate component of grid

INTRODUCTION

Context

The wind is a source of energy that has been harnessed by humans for thousands of years, from the sail of a ship to navigate the seas, to the wind mills on a farm to grind the wheat. In our modern times, one wide spread method to extract the power of the wind and transform it into electricity, is to use wind turbines and wind farms. Canada already has many wind farm installations; however, with the growing demand in energy, there is need to find and exploit additional regions with high energy potential. These regions are first usually determined by performing a wind resource assessment analysis using wind modeling softwares. One of such softwares is WEST (Wind Energy Simulation Toolkit), a software able to model the wind both in a meso and micro scale. The WEST software was developed by Recherche en Prévision Numérique of Environment Canada (RPN), and was shown to be able to obtain accurate wind potential results for the Gaspésie region in Yu *et al.* (2006), and the province of Quebec in Benoit *et al.* (2004). Furthermore, WEST was even used to create the Canadian Wind Energy Atlas to obtain coloured maps representing the average wind velocity and power for the whole country, and thus, offering an additional meteorological tool for the wind industry (Recherche en Prévision Numérique, 2003).

Literature review

In general, the mesoscale models enables us to obtain the wind climatology for large areas, and the microscale models uses the output of the mesoscale results as inputs to obtain a finer wind climatology on smaller resolutions. The use of both a mesoscale and microscale model has been used by several studies for different models.

In Frank *et al.* (2001), the authors combined the mesoscale model KAMM with the microscale model WAsP to perform wind simulations in Ireland, Denmark, Northern Portugal and Faroe Island. The simulations yielded better predictions than the simulations

using only the KAMM mesoscale component. Furthermore, the KAMM/WAsP combination was also used to map the wind atlas for Egypt in Mortensen *et al.* (2006). The atlas was able to capture the main features of the sometimes complicated flow patterns; however, the wind speeds were underestimated in some region. The KAMM mesoscale model is comparable to the MC2 mesoscale model used in this study, as they both use very similar methodology for the input and analysis of the climatology based on a large scale dataset.

Another computation of a mesoscale and microscale model is seen in Yim *et al.* (2007), where the MM5 model developed by Penn State/NCAR (Grell *et al.* 1994) is the mesoscale component, and CAMLET developed by Earth Tech Inc. (Scire *et al.* 2000) is the microscale component. In that study, Yim *et al.* (2007) simulates the wind in known complex terrain, such as Guangdong, Pearl River Delta, and Hong Kong, and the simulations did a very good job of replicating wind speeds and wind directions.

Similarly, the WEST software has also attempted to simulate the wind in complex terrain. The mountainous region of Yukon and Whitehorse (as shown in Figure 0.1.1) were chosen for simulations, and in depth studies of the climatology and wind potential has been performed in Pinard *et al.* (2005), Pinard (2007) and Pinard *et al.* (2009). The study from Pinard *et al.* (2005) attempted to simulate the southern region of the Yukon, and it was shown that the results were not congruent with the observations by the wind stations. The simulated winds had a difference of up to 40% with the measured values. WEST did not perform as well in the Yukon as it did in the region of Gaspésie, since the Yukon is complex and mountainous. In Pinard (2007) the climatology of the region of Whitehorse was further analyzed and the details of the climatology of the region was discussed and stratification issues were mentioned. In Pinard *et al.* (2009), it was highlighted that the complex terrain and temperature profile was speeding up the wind in the lee slope of the mountains and caused an overestimation of the wind speeds. The wind had a tendency to accelerate down the mountain and mix in the valley, and this phenomenon was caused by the temperature profile of the atmosphere not being sufficiently stratified, as the observations showed. It was demonstrated that if the temperature profile showed a stronger stratification, with the cold

temperatures in the bottom of the valley and warmer temperatures at higher altitudes, the wind in altitudes flowing in the lee slope of the mountain would flow over the valley as it encounters the cold area with a higher density and as a result, reduce the downward momentum transfer of the wind in the valley.

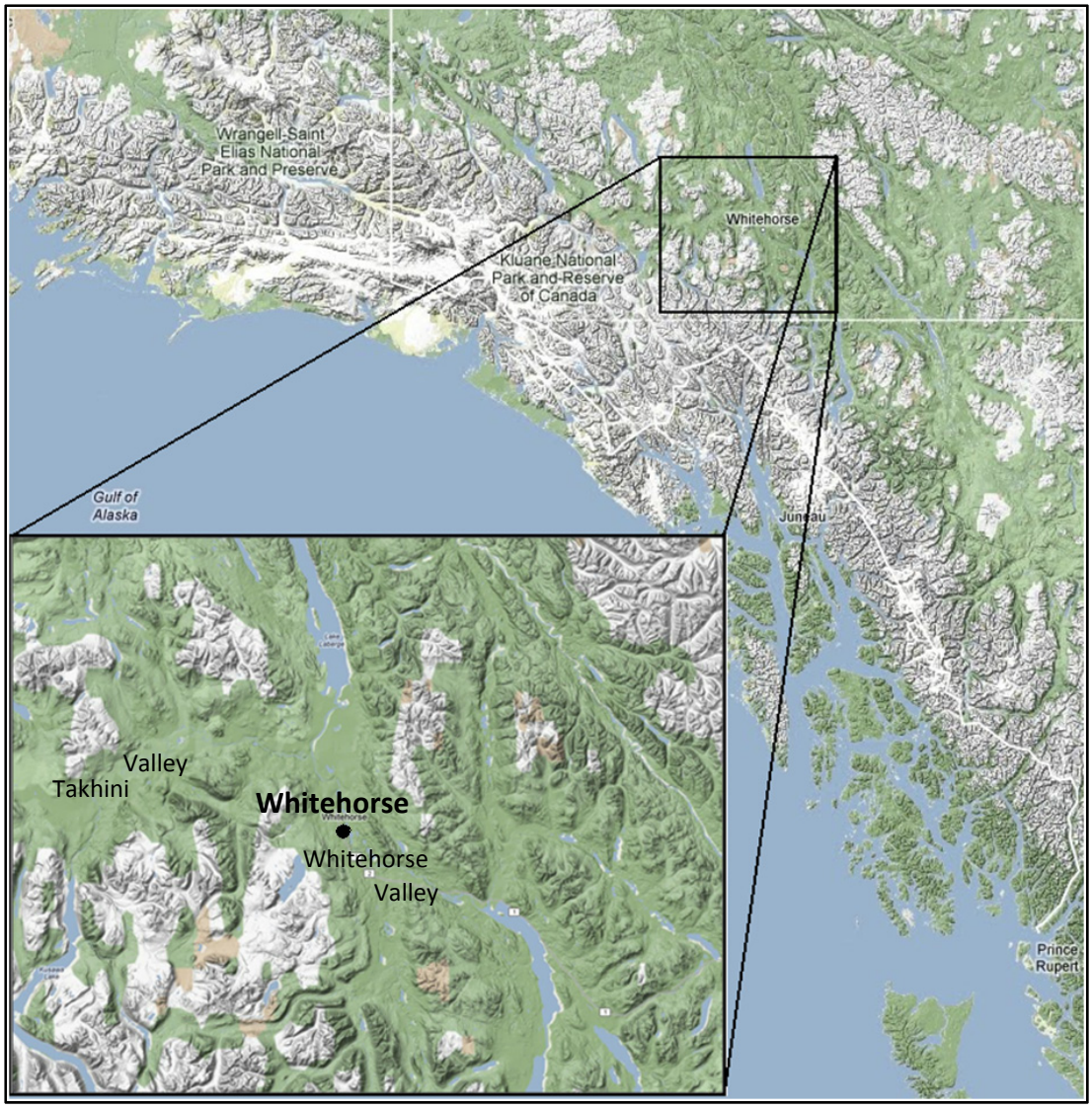

Figure 0.1.1 Map of Yukon and region of Whitehorse
Taken from Google Maps

Objective

The objective of this study is to implement several of the suggested improvements from Pinard *et al.* (2009). These suggestions aim at improving the performance of WEST by adding and modifying certain components of the software during initialization, such that the simulated winds in Whitehorse would approach the observed wind values in the region; this would provide a better wind atlas; and these new methodologies and components can be a benchmark for improvements for other similar regions that require better wind results.

The first modification suggested in Pinard *et al.* (2009) was to capture the stratified temperature profiles. It was shown that the temperature profiles currently used are not representative of the temperature profiles captured by the Radiosonde, which shows a temperature inversion. Since temperature profiles play an important part in the initialization and the simulated results obtained, a new criterion should be added to the classification scheme. This new criterion would be able to differentiate between different grades of temperature profiles, and consequently, provide a better representation of the observed temperature profile during the initialization of the model.

A second suggestion was to raise the initial reference topography used to build the topography from the geophysical files when initializing. This suggestion was added due to the hypothesis that the initial reference topography at sea-level can create an artificial topography around the model, and this may cause and force the flow into unexpected patterns.

Finally, the third improvement was to ignore the variable profiles that are below the topography during the initialization and use the values above the topography. Pinard *et al* (2009) showed that the values of the profile used to initialize the model may not always be correct and an alternative should be considered, if correct wind directions in the region is desired.

This study will attempt to implement these 3 proposed solutions and improve the simulated results of the region of Whitehorse in order to be closer to the observations. Chapter 1 of this document will introduce the software used (WEST) and the main component relevant to this study. Chapter 2 will describe the new classification scheme and modifications implemented to capture the temperature profiles needed and preliminary results. Chapter 3 will describe the modifications done to the initial reference topography, and the effects observed with this change. Chapter 4 will describe the modification that ignores the data below the topography during the initialization and its effect. Chapter 5 will describe the observation wind values used, and its comparison with the simulated results obtained from the previous chapters. Chapter 6 will analyze and discuss the final simulations involving all the modifications described in Chapter 2, 3 and 4. This report will end with a conclusion and further recommendations for future research.

CHAPTER 1

DESCRIPTION OF MODEL

1.1 WEST model

WEST (formerly known as Anemoscope) is based on a statistical-dynamical downscaling approach from Frey-Buness *et al.* (1995). It is divided into 4 major modules: A classification scheme, a mesoscale model (MC2), a statistic module (WESTATS), and a microscale model (MSMicro). Its flow chart is illustrated in Figure 1.1.

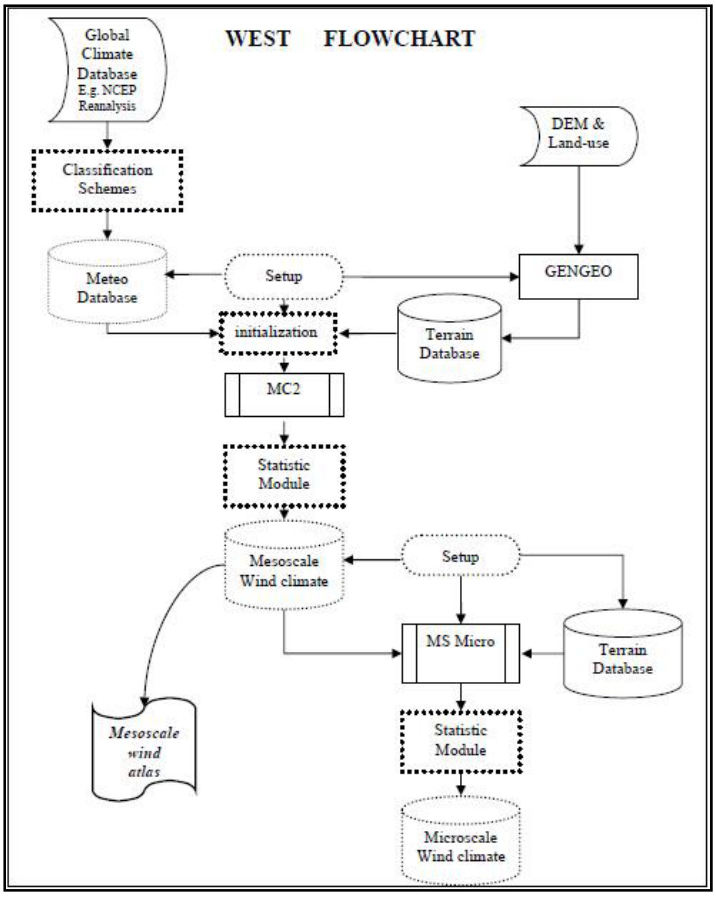

Figure 1.1 WEST flowchart
Taken from Pinard *et al.* (2005)

The downscaling procedure first uses regional climate of basic large scale situations (Global Climate Database) that were obtained by processing a long-term global-dataset through a classification scheme. This allows the meteorological and weather situations to be simplified to single atmospheric profiles (also referred as climate states) associated with specific frequency distribution that are fed into WEST to start and initialize its mesoscale component.

The mesoscale model used in WEST is the Canadian Mesoscale Compressible Community Model (MC2). MC2 is a compressible non-hydrostatic limited area model (Robert et al., 1985; Tanguay et al., 1990; Laprise et al., 1997; Thomas et al., 1998; Girard et al., 2005) and it was developed for mesocale modelling research, and operational weather forecasting. Mesoscale wind climates are obtained through MC2, and the results are processed through a statistics module.

The statistics module called WESTATS uses as inputs the mesoscale solutions and frequencies from the classification scheme to obtain a database of statistics, including mean values of the wind speed, frequency distribution of wind speed and direction, and wind power classes. The statistics can be calculated for any height in the surface region by interpolating wind speeds to the desired height from the MC2 model level closest to the target height. The interpolation uses the logarithmic profile of surface-wind assumption. A more in-depth description of WESTATS can be found in Pinard *et al.* (2005) and Anemoscope reference documentations (Canadian Hydraulic Centre, 2006).

Using the statistics database obtained from the results of WESTATS, these results are inserted in the microscale component of WEST : MSMicro of Walmsley, Taylor *et al.* (1986). MSMicro uses the theory of Jackson and Hunt (1975) as a basis for numerical modelling of 2 dimensional steady state turbulent flow over a low hill. And by coupling MSMicro with the mesoscale component, the final output yields microscale wind climates.

1.2 Initialization of model

The initialization process of MC2 is the main focus of this study, and a description of this step will be provided in this section. The original initialization process of MC2 uses as input, the vertical profiles of temperature and geostrophic wind, corresponding to each of the climate states that were obtained through the classification scheme (at 4 heights: 0, 1500, 3000, 5500m ASL). These vertical profiles are set at the center of the model domain and are interpolated and extrapolated to the rest of the model's vertical levels (this study uses 35 levels). For all the model levels between the height of 0 and 5500m ASL, a cubic interpolation is used. For the levels above those heights, the profiles are kept constant throughout the rest of the model levels.

Next, the model needs to spread the single vertical profile to the rest of the domain. The construction of the three dimensional meteorological data is done using the assumption of the hydrostatic equation 1.3, and the geostrophic balance equations 1.1 and 1.2

$$RT\frac{\partial q}{\partial X} = fV \tag{1.1}$$

$$RT\frac{\partial q}{\partial Y} = -fU \tag{1.2}$$

$$RT\frac{\partial q}{\partial z} = -g \tag{1.3}$$

where R is the gas constant for dry air (287 J kg^{-1} K^{-1}); T is air temperature; $q=ln(p)$ with p being the air pressure; f is the Coriolis parameter ($f = 2\Omega\sin\Phi$, with Ω being the angular velocity of the earth's rotation, and Φ the latitude); U and V are the components of the horizontal geostrophic wind along X and Y; and g is the effective gravitational acceleration (9.80616 m/s^2). The three components of the equation of momentum are set in a projection of the spherical earth and geometric height coordinates. The vertical coordinates follows the

work of Gal-Chen *et al.* (1975) on the terrain following scaled height coordinate system, presented in equation 1.4.

$$\zeta = \frac{H(z - z_s)}{H - z_s} \tag{1.4}$$

Where z is the height of the coordinate, z_s is the height of the ground, H is height of the top of the model, and ζ is the height in the new coordinate system.

In the model, the variables *T* and *q* are split into a basic state and perturbation component:

$$T = T^* + T' \tag{1.5}$$

and

$$q = q^* + q' \tag{1.6}$$

The basic state representing an isothermal atmosphere in hydrostatic equilibrium is:

$$\left[\frac{\partial q^*}{\partial z} = \frac{-g}{RT^*}\right] \tag{1.7}$$

Equation 1.7 is subtracted from equations 1.1, 1.2, and new variables are defined as

$$P = RT^*q' \tag{1.8}$$

and

$$b = g\frac{T'}{T^*} \tag{1.9}$$

where *P* is the generalized pressure and *b* is the buoyancy. With these changes, we obtain:

$$\left(1 + \frac{b}{g}\right)\frac{\partial P}{\partial X} = fV \tag{1.10}$$

$$\left(1+\frac{b}{g}\right)\frac{\partial P}{\partial Y}=-fU \tag{1.11}$$

$$\left(1+\frac{b}{g}\right)\frac{\partial P}{\partial z}=-b \tag{1.12}$$

Using temperature (or buoyancy) profiles at the center of the domain, the generalized pressure profile can be determined from equation 1.12. The horizontal pressure distribution is then determined by numerically integrating equations 1.10 and 1.11, starting from the center to the edges of the domain, and by keeping the geostrophic wind (U,V) uniform throughout the domain. Finally, the temperature profiles away from the center profile are obtained through another use of equation 1.12. Note that the temperature profiles away from the center are no longer identical to the original temperature profile obtained through the classification and the center point, since the temperature must change in order to maintain the hydrostatic and geostrophic balance. This is also in line with the notion of the thermal wind (see further in chapter 4.1).

Initially, no topography has been introduced yet, and the three dimensional meteorological data model is constructed on an initial reference plane set at 0 m ASL. From the first time step, the topography is slowly introduced and grows on top of the initial reference plane. The temperature of the ground takes, at each step, the temperature of the air directly in contact with it to avoid any heat flux into/from the atmosphere. Once the topography has reached its final height, the ground temperature is kept constant in time and the model is integrated for a time sufficient to reach a quasi steady state.

1.3 Computation aspects

This research involves heavy computational capabilities, due to the nature and method of the numerical experiments. A description of the procedure and computer hardware used to accomplish these simulations will be presented.

In chapter 1.1, it was mentioned that the classification scheme gives a number of climate states that describe the climatology of the desired region. These chosen climate states were fed into the software Anemoscope to prepare the runs (done independently on a personal computer) by generating the required files for the execution of the simulation for each climate state. One of such files is the *model_settings.nml* files, which controls and defines the parameters of the MC2 model, the initial conditions, and the desired output variables.

Once these setup files have been created, they were brought over to the computer cluster where the MC2 model has already been compiled. The cluster, named “Boreas” from the Institutional Research Chair on the Combustion of Biofuels for Transportation's laboratory at École de technologie supérieure (ÉTS), is a high performance supercomputer cluster with 464 processors in parallel with 928 GB of RAM, and infiniband technology. It uses the Sun Grid Engine (SGE) batch-queuing system to manage and distribute the execution of large numbers of standalone, parallel or interactive user jobs. For this study, 64 processors (8 nodes, with 8 processors per node) were used as standalone, meaning 64 climate state runs were able to be executed simultaneously.

In order to avoid submitting commands and queuing the hundreds of climate state runs into the cluster, which would put great strain on the head node, the array job option on SGE was used. Array jobs allow for the submission of any numbers of similar computations, using only a single script per node. This has the advantage of removing the need of the user to create hundreds of scripts, and gives the ability to remove and cancel all the runs by deleting one script. Since 64 processors are being used, and inherently 8 nodes, the total number of climate states for each experiments were equally divided into eight, and 8 array job scripts were written.

With so many simulations accessing the compile MC2 model on the head node, and the result files being sent back and written on this node, it was difficult for the central node to process everything. To remedy this issue, an additional procedure was added. Before submitting the

climate states on the processors, the executable files of the compiled MC2 model are copied and sent to each individual processor of the eight nodes, such that these processors no longer require connecting with the head node. Furthermore, the result files generated by the runs are stored directly on the disk space of the processors in use, and are brought back to the head node once all the climate state runs have been completed. This would allow the simulations to be run locally, and remove the need to be connected with the head node.

The procedures discussed aimed at reducing the data transfer through the head node and most importantly, to accelerate the computational time of the simulations of this research by a fold of 64. One climate state run on a modern personal computer required 90 minutes to complete, and for over 700 climate state runs, this would take more than 1 month to finish. Using the cluster, this is achievable in less than 24 hours, and allows us to do multiple experiments without too much waiting time.

CHAPTER 2

THE NEW CLASSIFICATION

2.1 Froude Number

The current classification follows the methodology used in Frank and Landberg (1997) and uses the National Center for Environmental Prediction (NCEP) and National Center for Atmospheric Research (NCAR) Reanalysis database of Kalnay, *et al.* (1996) as input to obtain the climatology that will be used to initialize the model. The NCEP/NCAR Reanalysis was chosen due to its relatively uniform quality in both space and time, and its free access to the public. It covers a period of 43 years (1958/01/01 to 2000/01/01), with a time sampling of every 6 hours; its dataset is in a latitude-longitude grid, with a spacing of 2.5 degrees; and has 17 pressure levels in the vertical, ranging from 1000 mb to 10 mb. Figure 2.1 shows the positions of the NCEP/NCAR Reanalysis grid points (in triangles) surrounding the domain of interest and the region of Whitehorse, with the grid point "17\18_table.ef" located to the north-west of Whitehorse being the Reanalysis point used as input for the classification throughout this study.

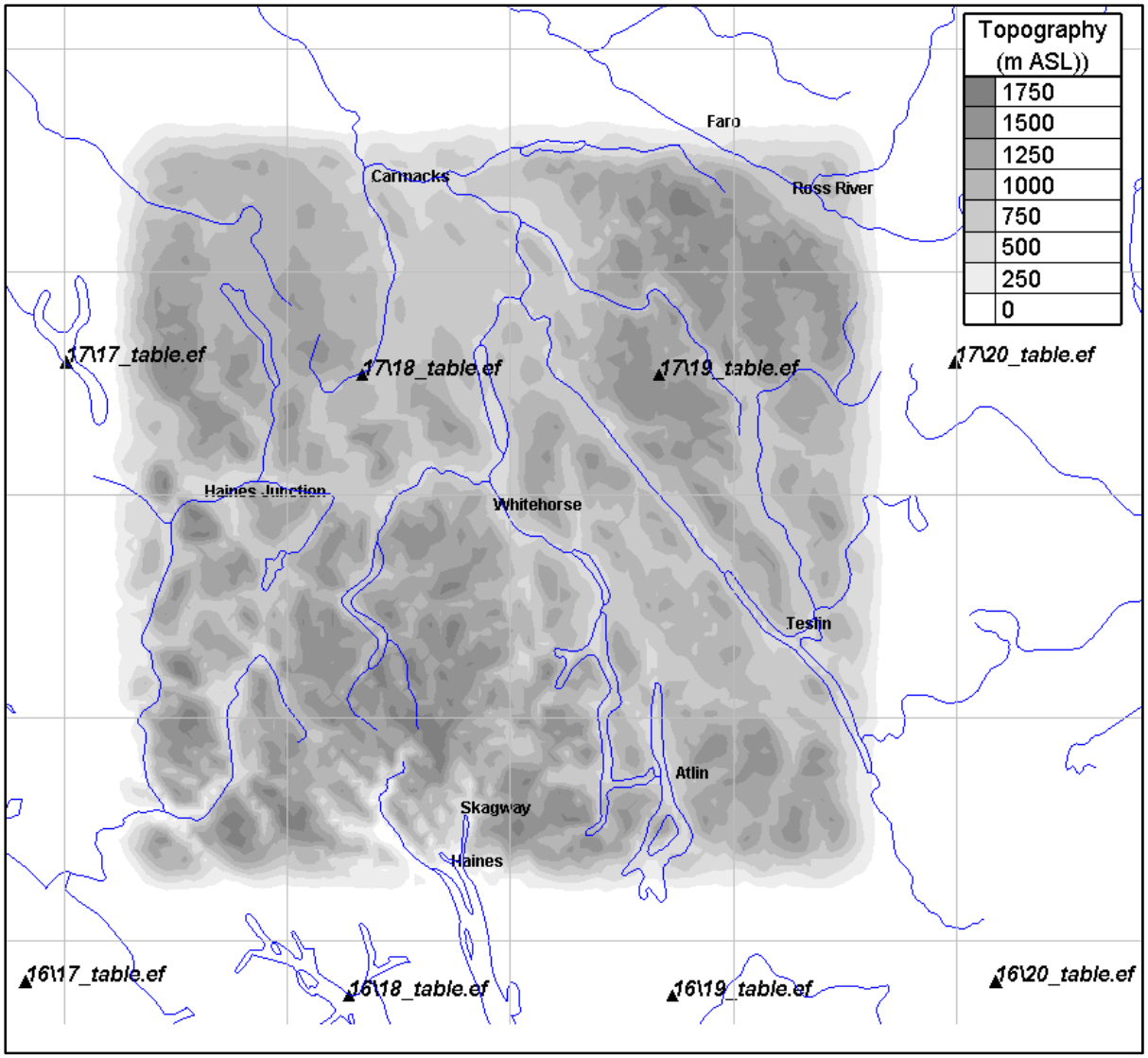

Figure 2.1 Position of Reanalysis grid points around Whitehorse

Among the data stored in the NCEP/NCAR Reanalysis, the main element of interest for the classification scheme is the geostrophic wind, since it is linked to the large pressure gradient through the geostrophic balance. The atmospheric state of the Reanalysis is defined for WEST at 4 "near-surface" heights[1] above sea level: 0, 1500, 3000 and 5500 m ASL. The respective pressures of these heights are approximately: 1000, 850, 700 and 500 mb. In the

[1] For wind energy studies, only "near-surface" winds are of interest.

classification scheme, the time series of the geostrophic wind data at 1000 mb from the NCEP/NCAR Reanalysis are classified using 3 criteria: direction (16 sectors), speed (14 classes), and shear of the geostrophic wind between the 1000 and 850 mb levels (2 bins). However, it was suggested in Pinard, Benoit *et al.* (2009), that another criterion should be added in order to capture the thermal stratification effects observed in the Yukon. The new criterion added to the classification method is the Froude number and it is calculated using the following equation:

$$Fr = \frac{U_g}{NH_c} \tag{2.1}$$

with

$$N = \sqrt{g\frac{\partial(\ln\theta)}{\partial z}} \tag{2.2}$$

where U_g is the speed of the incoming wind towards the mountain; N is the Brunt-Väisälä frequency of the oscillations due to buoyancy, and inherently, incorporates the thermal stratification; θ is the potential temperature; g is the gravitational acceleration (9.80616 m/s); and H_c is the characteristic topographic height. Practically, the Froude number from equation 2.1 indicates if the flow will go over the obstacle, or around it. The Brunt-Väisälä in equation 2.2 is the frequency at which a parcel oscillates vertically after being disturbed by an obstacle as explained in Bergstrom *et al.* (2006) for valley regions. In this study, the values for the temperature profile were taken from the Reanalysis data at the pressure levels of 1000 and 850 mb, U_g is the average of the geostrophic wind speed of the Reanalysis data at the pressure levels 1000 and 850 mb, and H_c was the approximate average height of the region of Whitehorse. The geophysical region used to calculate H_c was a 100x100 grid spanning 500 km x 500 km, with the city of Whitehorse at its center (I=50 and J=50). The calculated value for H_c was 1066 m, however, it was reduced to 1000 m for simplicity.

The Froude number seems to be a good classification criterion as it considers the issues seen in Pinard, Benoit *et al.* (2009): The wind going up the mountain and accelerating down the

mountain. This implies that a strong thermal stratification will inhibit vertical wind motion, and consequently, the bigger value the Brunt-Väisälä frequency *N* will take, the smaller value Froude number will be (Fr<1) (Holton *et al.* ,1973). Alternatively, if the thermal stratification is weak, the Froude number will take a large value (assuming the wind speed is unchanged). The Froude number has also been used in Frank *et al.* (2001) for their mesoscale modelling with KAMM (Adrian *et al.* 1991) in order to capture the stratification effects, especially with weak winds. It is worth noting that in this study, we ignore the relation between a small Froude number and the strength of the wind in the valley. For this case, Froude number is mainly a dimensionless variable that classifies the stratification.

This new Froude number criterion was added to the set of criteria (direction, speed and shear) in the existing classification algorithm developed by RPN. The algorithm uses the dataset from the NCEP/NCAR Reanalysis as input, and sorts them into categories to obtain a set of climate states, each with its own associated frequency and values at the 4 "near-surface" pressure levels (1000, 850, 700, 500 mb) for: the x-component of wind speed, *uu*; the y-component of wind speed, *vv*; and the temperature, *tt*.

The following part describes the steps the original classification method goes through, along with the new steps that are introduced by the modifications:

1) The variables, settings and parameters are defined.

2) Get the geopotential height gz, temperature tt and relative humidity hr at each grid point and for each data-time instant in the period chosen.

3) The geostrophic wind is calculated from the geostrophic balance and the ideal gas law while taking into consideration the specific humidity hu (converted from hr), the pressure pp (obtained from gz, tt and hu), and temperature tt. This also yields the direction and shear of the geostrophic wind.

4) [New] The geostrophic wind ug and potential temperature θ (converted from tt and pp) are used to calculate the Brunt-Väisälä and Froude number for each data-time instant (at each grid point).

5) The climate state categories are created from 16 direction sectors, each with 14 speed classes (with class limits as: 0.2, 2, 4, 6, 8, 12, 16, 18, 22, 26, 30 and 34 m/s), and each sector classes with 2 shear bins (positive and negative shear).

6) [New] Each shear bins are further divided into 32 Froude number bins. The bins go from Froude number 0 at the 1st bin, and progressively increase to Froude number 1.6 at the 32nd bin. Resulting in two sets of Froude number bins, one for positive shear and the other for negative shear.

7) [New] Each data-time instant is classified into their respective climate states, according to the magnitude, direction, shear of the geostrophic wind and the calculated Froude number; and their uu/vv/tt profiles are summed up. The data-time instants are counted for each climate states in order to obtain the amount of data and the overall frequency of each climate states and to average the uu/vv/tt sums.

8) [New] Using correction factors derived from Radiosondes (discussed in chapter 2.2), the frequencies of the climate states with respect to Froude number are modified in order to increase or decrease the occurrence of certain climate states and then these frequencies are globally normalized by the sum of these frequencies at the end of the corrections.

9) [New] From the 32 Froude bins for each shear signs, every 8 bins are combined together into larger Froude number bins with their respective frequencies and their uu/vv/tt profiles summed up. This result into 4 positive shear Froude bins and 4 negative shear Froude bins.

10) The shear distinction is removed from the first wind speed class, by merging both shear bins into one.

11) The shear distinction is also removed for the wind classes if the frequency is less than 0.02%, by merging both shear bins into one.

12) Each climate states have its mean values of uu/vv/tt calculated for the four heights, by dividing the summed values of uu/vv/tt by the number of occurrence in each data-time instant.

13) [New] The list of climate states are tabulated and outputted according to all classifiers, including Froude number

A more elaborate description of the classification scheme can be found in annex I. With the addition of the Froude number as a classification criterion, the number of possible climate states passes from the original 432, to 1728 climate states. The option of removing the shear as a classification criterion has also been implemented, reducing the number of possible climate states to 896 (this modification is not the main scope of this study, and further details about it will be mentioned in chapter 2.3). The procedures to switch to the different configurations of the classification scheme have been provided in annex II.

2.2 Correction Factors

The correction factors mentioned in the classification scheme (from chapter 2.1) that were used to modify the frequency of the Froude number bins were derived from the Canada Radiosonde database and the NCEP/NCAR Reanalysis data. The Froude numbers of the Reanalysis were calculated with equation 2.1 for each instance (every 6 hours) from January 1st 1958 to December 31st 2000, by using the uu/vv/tt and height values of the database at pressure level 1000 and 850 mb. The values of tt (temperature) and height give the potential temperature and the Brunt-Väisälä frequency. Using the latter and the components of the

wind, uu and vv, allow us to obtain the Froude number (assuming, a constant of 1 000m for H). In the case of the Radiosonde data, the temperature and wind speeds at the first available pressure level and the 850 mb pressure levels were extracted; and their Froude numbers were calculated using the same method as for the Reanalysis for all available data from years 1958 to 2000, by using the values of uu/vv/tt and the height of the Radiosondes.

In order to make both databases comparable, only the same time instances were used. Among the entire 67 808 reanalysis date-time instances recorded and the 34 443 Radiosonde date-time instances recorded for Whitehorse, 18 886 date-time instances were matching in time and had enough available values to be able to properly calculate the Froude numbers. The Froude numbers of these matching 18 886 date-time instances of both the Reanalysis and Radiosondes were used and were sorted into 32 bins, with the total bin limit spanning from a Froude number of 0 to 1.6. Each bin was set a limit width of 0.0516, and they were divided as follow:

1st bin: [0, 0.0516); 2nd bin: [0.0516, 0.1032); 3rd bin: [0.1032, 0.1548); .....
31st bin: [1.5485, 1.6); 32nd bin: [1.6, +]

Finally, the occurrence for each Froude number bin during the chosen period was tabulated and counted, to obtain the frequencies of each Froude number bins for both database. Knowing the frequencies of the Froude number bins of both the Reanalysis and Radiosondes, the correction factors were calculated by dividing the 32 frequency values of Radiosonde by their respective 32 frequency values of the Reanalysis, as shown in the equation 2.3.

$$[Fcorr]_i = \frac{(FREQ_{Radiosondes})_i}{\left(FREQ_{Reanalysis}\right)_i}; \qquad for\ i = 1, 2, \dots, 31, 32 \tag{2.3}$$

This operation would give a set of 32 correction factor numbers, one for every Froude number bins and with no distinction between the different cases of wind direction, speed and shear. Each of these correction factors will be multiplied by their respective frequency value

in the Reanalysis as shown in equation 2.4, in order to get a new set of frequencies for the Froude number bins of the Reanalysis.

$$\left(new\_FREQ_{Reanalysis}\right)_i = [Fcorr]_i \cdot \left(FREQ_{Reanalysis}\right)_i \quad (2.4)$$

With these correction factors, the frequency curve of the Reanalysis can change and match the frequency curve of the Radiosondes. These factors will augment or reduce the frequency curve where needed, and in turn, this will add or diminish the importance of certain Froude number (and their respective climate states as seen in section 2.3), such that the frequencies of stable and less stables cases are similar to the observations, and are well represented.

This procedure for the correction factor was done for Radiosonde stations located at 5 cities in the western mountainous region of Canada: Whitehorse, Port Hardy, Norman Wells, Prince George and Fort Nelson. The locations of these cities are shown in the Figure 2.2.

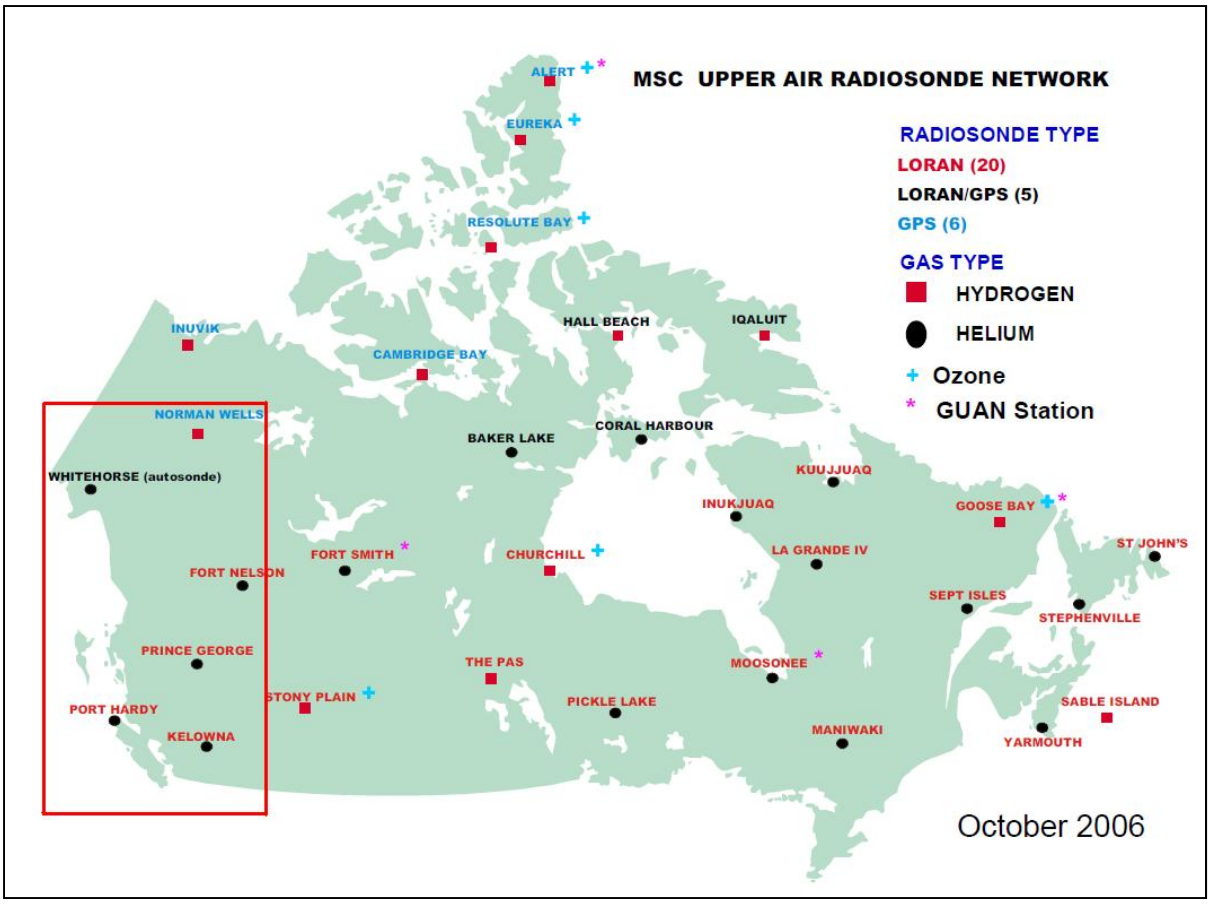

Figure 2.2 Map of the location and the type of the upper air Radiosondes network used in Canada
Taken from World Meteorological Organization (2006)

Using the respective Radiosondes and Reanalysis data of each city, the correction factors for Whitehorse is shown in Table 2.1, and the correction factors for all 5 cities are presented in Table-A III-1. The results of the Froude number frequency curve of the Radiosondes and the Reanalysis for Whitehorse are shown in Figure 2.3.

We see in Figure 2.3 that for the Reanalysis curve (dash-dotted line), the section with the highest frequency is around Fr = 0,4. However, from the data captured by the Radiosondes (dashed line), the section with the highest frequency should be more towards the left: in the lower Froude number section and the more stable part, at around Fr = 0,2. By using the correction factors derived for this specific region (Whitehorse), it is possible to modify the

frequency curve of the Reanalysis and obtain a new Reanalysis curve (solid line) more representative to the observations seen by the Radiosondes. The goal is to skew the curve to the left, and therefore switch the peak and bulk of the frequency to the lower Froude numbers and more stable stratification. Note that the new Reanalysis curve (solid line) should be directly on the Radiosonde curve (dashed line); however, it was offset by 5% for visual purposes.

Table 2.1 Correction factors of Whitehorse

Whitehorse			
xmesh	**fcorr**	**xmesh**	**fcorr**
0	21,151	**0,8258**	0,747
0,0516	7,177	**0,8774**	0,819
0,1032	3,406	**0,929**	0,916
0,1548	1,685	**0,9806**	1,034
0,2065	1,031	**1,0323**	1,17
0,2581	0,743	**1,0839**	1,246
0,3097	0,679	**1,1355**	1,161
0,3613	0,636	**1,1871**	1,216
0,4129	0,622	**1,2387**	1,608
0,4645	0,648	**1,2903**	1,734
0,5161	0,605	**1,3419**	1,723
0,5677	0,565	**1,3935**	1,718
0,6194	0,545	**1,4452**	1,755
0,671	0,589	**1,4968**	2,557
0,7226	0,693	**1,5484**	2,623
0,7742	0,719	**1,6**	0,986

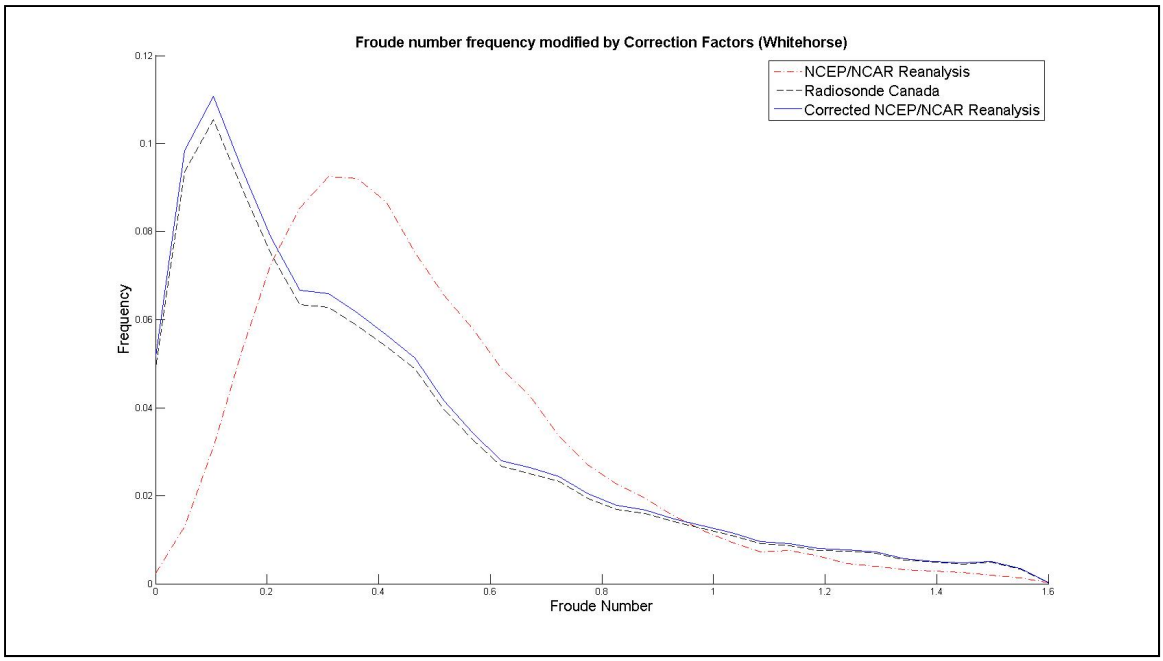

Figure 2.3 The Froude number frequency curve of Whitehorse modified by correction factors

Notice in Figure 2.3 that the frequency on the left side (from Fr≤ 0,2) of the corrected Reanalysis curve has been increased, and the section in the larger Froude number (0,2<Fr <1) has been slightly reduced; but the sum of frequencies for all curves still add up to one.

The same procedure has been done for the remaining 4 cities with their respective correction factors derived from their own Radiosondes and Reanalysis database. The curves for Fort Nelson, Norman Wells, Port Hardy and Prince George can be viewed in Figure-A IV-1, Figure-A IV-2, Figure-A IV-3 and Figure-A IV-4, respectively. Note that the points in the Reanalysis data are not always directly positioned at the same location as the Radiosondes; however, the closest one possible was used for this procedure.

An issue with the different set of correction factors for different cities is that they are only valid for their respective cities. However, by comparing all the Froude frequency curve of the Reanalysis and the Radiosondes (Figure 2.3, Figure-A IV-1, Figure-A IV-2, Figure-A IV-3 and Figure-A IV-4), some similarities are noticeable. All the Reanalysis curves share a common trend, where the frequency bell curve needs to be shifted to the left: towards the

more stable cases. Since all Reanalysis curves show this skewed effect for their Froude frequency curves, obtaining a generalized correction factor that could modify and improve the frequency curve was devised. To obtain a more generalized correction factor, all the correction factors of the 5 cities were tabulated, and the arithmetic average was calculated, as shown in the last column of Table-A III-1. The factors obtained from the merging of all the correction factors would be used to correct the Froude frequency curve of any city that is not among one of the five cities used to derive the merged factors.

In order to see the effectiveness of the merged correction factors, they were used on the Reanalysis frequency curve (dash-dotted line) of the 5 cities. Figure 2.4 shows the Froude frequency curve of Whitehorse with the corrected Reanalysis curve (solid line) modified by the merged factors. Even though the curve obtained is not exactly like the Radiosonde curve (dashed line), nonetheless, it is able to skew the curve towards the left and boost the frequency of low Froude number to a more representative value that follows the actual observations by the Radiosondes. The results of the other cities using the merged correction factors are in Figure-A V-1, Figure-A V-2, Figure-A V-3 and Figure-A V-4; and they display similar results. Even though these averaged correction factors seem relatively appropriate for the 5 cities used in this study, the extent of their use has not been studied, and using the factors outside of the west mountainous side of Canada should be used with caution.

These calculated correction factors were brought back to the classification scheme (the eighth step in the classification scheme algorithm in chapter 2.1), to modify the frequencies of the climate states obtained. By this point, the frequencies of the climate states have been divided by direction, speed, shear and Froude number. These climate state frequencies are then multiplied by the correction factors that match the Froude number bins of the climate state, to obtain the new and corrected frequencies as shown in equation 2.5.

$$freq^{corrected}_{dir,speed,shear,Froude} = fcorr_{Froude} \cdot freq_{dir,speed,shear,Froude} \qquad (2.5)$$

This means that as long as the Froude number bin of the frequency coincides with the Froude number bin of the correction factor, these two values will be multiplied together to obtain a new frequency, regardless of the other classification criteria.

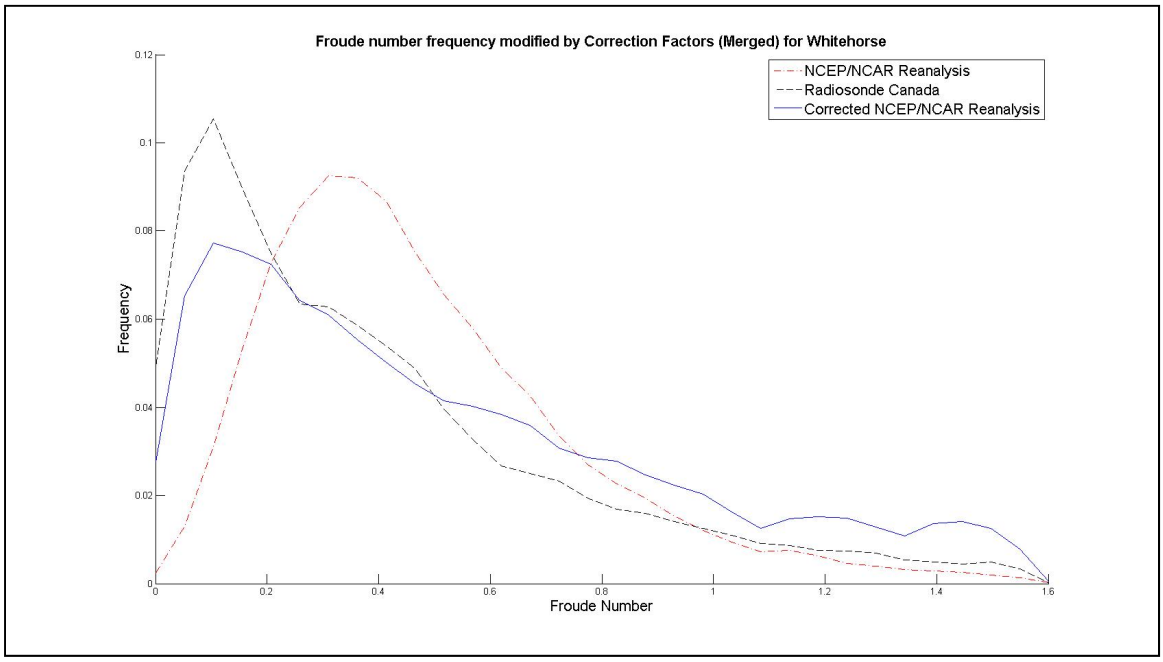

Figure 2.4 Froude number frequency curve of Whitehorse modified by merged correction factors

2.3 Climate States

After processing the Reanalysis data with the classification scheme, the climate state tables for each Reanalysis grid points are obtained. Each table contains their own respective list of climate states, and each climate state has its own frequency and its own values for uu/vv/tt for all 4 height levels.

In the new classification scheme, by combining the classification scheme with the correction factors, a new set of climate state tables and frequencies with a slightly modified nomenclature were obtained. The climate states originally followed the name format of "ANU1DdddCccS", where the "ANU1" indicates the classification scheme has used input data spanning all 12 months, and not a particular season; the "Dddd" specifies what is the

predominant direction of the climate states if the wind rose was divided into 16 equal sectors, where “D000” is north and the degrees are increasing clockwise; the “Ccc” indicates which speed class the geostrophic wind is for any climate state, and “S” indicates which shear bin any climate state belongs to (can be defined as M or P). In this study, the nomenclature for direction and magnitude of the geostrophic wind remain the same, but not for shear. Since shear bins now also incorporates Froude number bins, a new shear letter tag needs to be used. If the Froude number classification is used, the shear nomenclature is no longer defined by M and P, where M and P respectively represent a positive and negative shear; but the shear and the Froude numbers are combined and are defined by the letters A,B,C,D,M,N,O and P. The letters A to D are defined as positive shear; and the Froude number that defines the bins increases as the letter progress from A to D, where D is the highest Froude number. Similarly, the letters M to P are defined as negative shear; and the Froude number that defines the bins also increases as the letters progress alphabetically from M to P. Table 2.2 shows the limits of these bins for each letter.

Table 2.2 Limits for Froude bins

Letters	A and M	B and N	C and O	D and P
Froude number bins	[0, 0.3613)	[0.3613, 0.7742)	[0.7742, 1.1871)	[1.1871, 1.6+)

Since the classification scheme can have many settings to obtain climate states, Table 2.3 presents an overview of the different classification scheme variants used in this study, and the number of climate states obtained for each classification variant for NCEP/NCAR Reanalysis grid point 17\18 for the period of 1958-01-01 at 00:00 hour to 1999-12-31 at 18:00hour. The classification variants differ with one another based on which criteria are used to classify the Reanalysis data and if the correction factors are used. The “original classification” classifies the Reanalysis data by speed class, direction sectors and shear bins. This classification does not use any of the modifications implemented in this study, and

yields 306 climate states out of a maximum of 432 climate states for the NCEP/NCAR Reanalysis coordinate used in the region of Whitehorse (17\18). The climate states with frequencies < 0.02% are simply ignored.

The "classification variant 1" is the same as the original classification, except that the Froude number is an additional classifying criterion. By adding this new criterion, the number of climate states increases from 306 to 688 climate states for Whitehorse (17\18) out of a maximum of 1728 climate states. This significant increase in the number of climate states is due to the additional classification criterion of the Froude number that allows the classification scheme to distinguish different thermal stratification and produce 4 new types of climate states (i.e. 8 shear labels rather than 2).

The classification variant 2, with Froude and the correction factors distinguishes 736 climate states for the coordinate 17\18 near Whitehorse. The slight increase in the number of climate states between "classification variant 1" and "classification variant 2" is due to the correction factors increasing the frequency of certain climate states that were originally below the threshold, and consequently, were forced to merge into other climate states. This increase in frequency would allow certain climate states to become more important and appear in the list. Naturally, the opposite can also be true, where the factors decreases the frequencies and the climate states would go below a threshold and disappear (merging with other climate states).

In the case of "classification variant 3", the Froude classification scheme is activated, but the shear classification is deactivated. The negative shears are merged with the positive shears and only the set of letters A, B, C and D are used in the nomenclature. This case offers no distinction between positive and negative shear and 577 climate states are obtained in total, which is a reduction from 736 climate states when using the "classification variant 2". The reasons for classifying by Froude and deactivating the shear criterion is to reduce the number of climate states obtained, in order to make the simulations less intensive while still capturing the Froude bins.

Table 2.3 Description of different classification scheme and number of climate states

NAME	CLASSIFICATION CRITERIA					NUMBER OF CLIMATE STATES
	Speed Class	Direction Sector	Shear Bin	Froude Bin	Correction factor	
Original Classification	**X**	**X**	**X**			306
Classification Variant 1	**X**	**X**	**X**	**X**		688
Classification Variant 2	**X**	**X**	**X**	**X**	**X**	736
Classification Variant 3	**X**	**X**		**X**	**X**	577

2.4 Stable Climate States

In this section, we obtained some climate states after classifying the Reanalysis data by the Froude number ("classification variant 2"). These climate states are identified in terms of direction, magnitude, shear, and most importantly, by Froude number; and they are used as inputs to initialize the MC2 model. In order to see the effects of the difference in Froude number on the simulated results of MC2, two very similar climate states differing practically only in Froude number will be compared to one another. The climate states used for this comparison are ANU1D225C04A and ANU1D225C04D, which by the tag "D225C04" indicate a geostrophic wind coming from 225° (south-southwest) and a speed in the 4th wind speed class (approximately 6 m/s). Note that one is tagged with the letter A, which indicates a low Froude number and the other is tagged with the letter D, which indicates a high Froude number. The other climate states (ANU1D225C04B and ANU1D225C04C) could have been used as well, however the greatest contrast in results are with ANU1D225C04A and ANU1D225C04D. The Table 2.4 shows the specific variable values with numbers from 1 to 4 indicating the height levels of 0, 1500, 3000 and 5500m ASL for: the east and north component of the geostrophic wind, uu1/uu2/uu3/uu4 and vv1/vv2/vv3/vv4 in m/s, respectively; the temperature tt1/tt2/tt3/tt4 in Kelvin; and the magnitude and direction of the

wind at 0m ASL where north is 0° and increasing clockwise. In the "ANU1D225C04A" and "ANU1D225C04D" columns of Table 2.4, the values in the columns are not exactly identical; however, they are fairly similar in terms of direction, magnitude and shear, which allow them to be in the same direction sector, speed class and positive shear. The only exceptions are the values of tt, which gives them the characteristic of being in different Froude number bins (A and D). One can see an enormous difference at the level 0 and 1500 m ASL between "A" (isothermal) and "D" (lapse rate ≈ 7.5°/km, more than the standard atmosphere).

Table 2.4 Initialization variables for ANU1D225C04 climate states

		CLIMATE STATES ANUD225C04				
		A	**B**	**C**	**D**	**M**
Variables	**Direction of wind at level 1**	225,582	224,116	224,415	225,615	224,836
	Magnitude of wind at level 1	6,783	7,052	7,177	7,018	7,016
	uu1	4,845	4,909	5,023	5,016	4,947
	uu2	2,256	4,079	4,447	4,314	3,649
	uu3	1,403	4,181	3,972	3,653	3,282
	uu4	1,641	5,451	4,499	3,997	3,971
	vv1	4,748	5,063	5,126	4,909	4,975
	vv2	1,558	1,34	3,349	3,74	2,058
	vv3	-1,282	-1,715	1,438	2,057	-0,596
	vv4	-5,9	-6,35	-1,057	0,679	-4,485
	tt1	258,977	271,094	282,523	290,172	272,531
	tt2	259,641	266,773	273,883	278,867	267,758
	tt3	259,336	261,813	266,016	268,328	262,766
	tt4	243,609	247,117	250,82	253,188	247,688

The Figure 2.5 and Figure 2.6 show the direction and the horizontal wind vector[2] of the simulated wind at 40 m AGL in knots[3] for the region surrounding Whitehorse for climate state ANU1D225C04A and ANU1D225C04D respectively, using the MC2 configuration as in Table 2.6. For both these figures, the wind arrows are superimposed over the contours of the topography, and the arrows are colour coded according to the shown speed and color legend. The vector length is also proportional to speed. The figures specifically intends to display the wind flow going from the mountains on the bottom left (at coordinate [43.7, 43.7]) to the mountains on the other side of the valley (at coordinate [54.8, 56.7]). The idea is to observe if the wind flows down in the valley and accelerates, an issue highlighted in Pinard *et al.* (2009). Thus, we choose to examine the vertical component of the flow (WZ).

The Figure 2.7 and Figure 2.8 are cross-sectional cuts of the valley shown by the dashed lines in Figure 2.5 and Figure 2.6. They show the vertical velocity WZ of the wind in m/s for the climate states ANU1D225C04A and ANU1D225C04D, respectively. The results from Figure 2.7 and Figure 2.8 show a wind speed reaching a maximum of 0.04 m/s near the bottom of the valley for climate state ANU1D225C04A; and 0.17 m/s for climate state ANU1D225C04D, along with much larger extent of the vertical WZ cells. Furthermore, the results from Figure 2.7 indicate that there was a reduction of the wind speed in the lee and around the mountain when comparing the results between climate state ANU1D225C04D and ANU1D225C04A, as seen by the green colour and fewer contour lines in the figure. Isothermal lines of the cross-sections were also extracted; however, they did not bring further insights to the study and were omitted.

---

[2] The horizontal wind vector shown in this type of figure is the weighted average of all the x and y-component (U and V) for all climate states, and then combining these components to obtain the resultant vector $\sqrt{(\sum U)^2 + (\sum V)^2}$. It is different than the average magnitude of the wind (EU), where the resultant of x and y is computed, and then a weighted average for all climate states is obtained $\sum(\sqrt{U^2+V^2})$. Here, $\sum$ represents the weighted average operation.

[3] 1 knot is equivalent to 0.5144 m/s

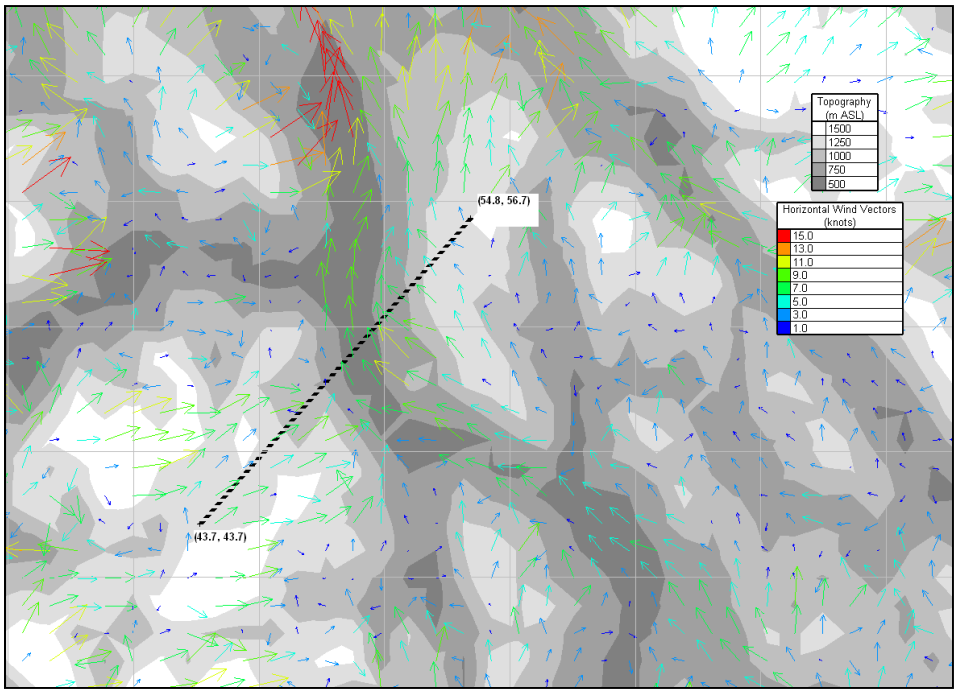

Figure 2.5 The simulated wind flow of climate state ANU1D225C04A at 40 m AGL

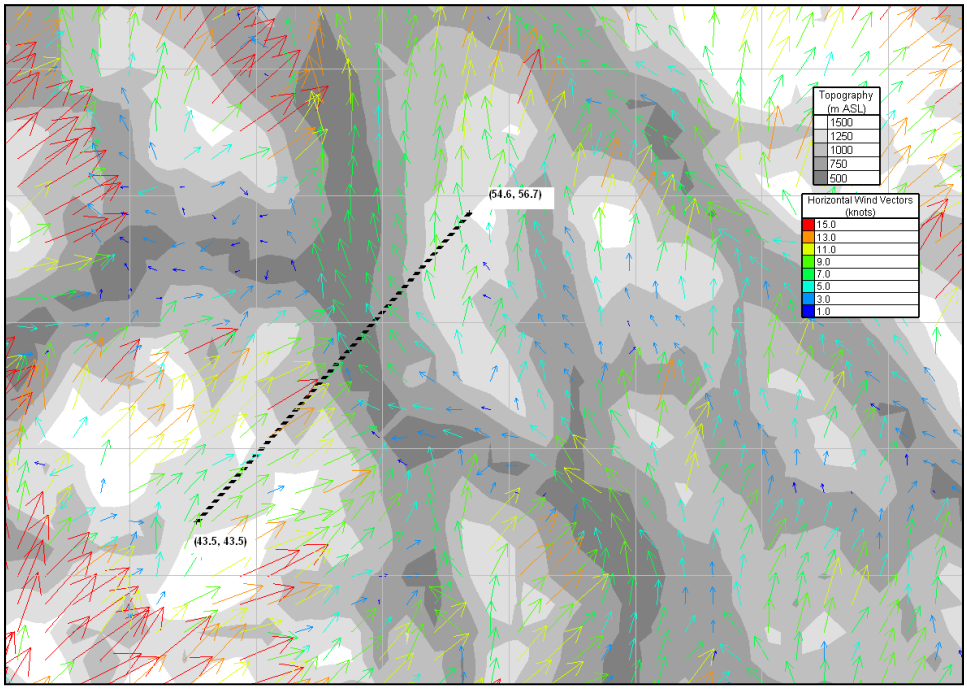

Figure 2.6 The simulated wind flow of climate state ANU1D225C04D at 40 m AGL

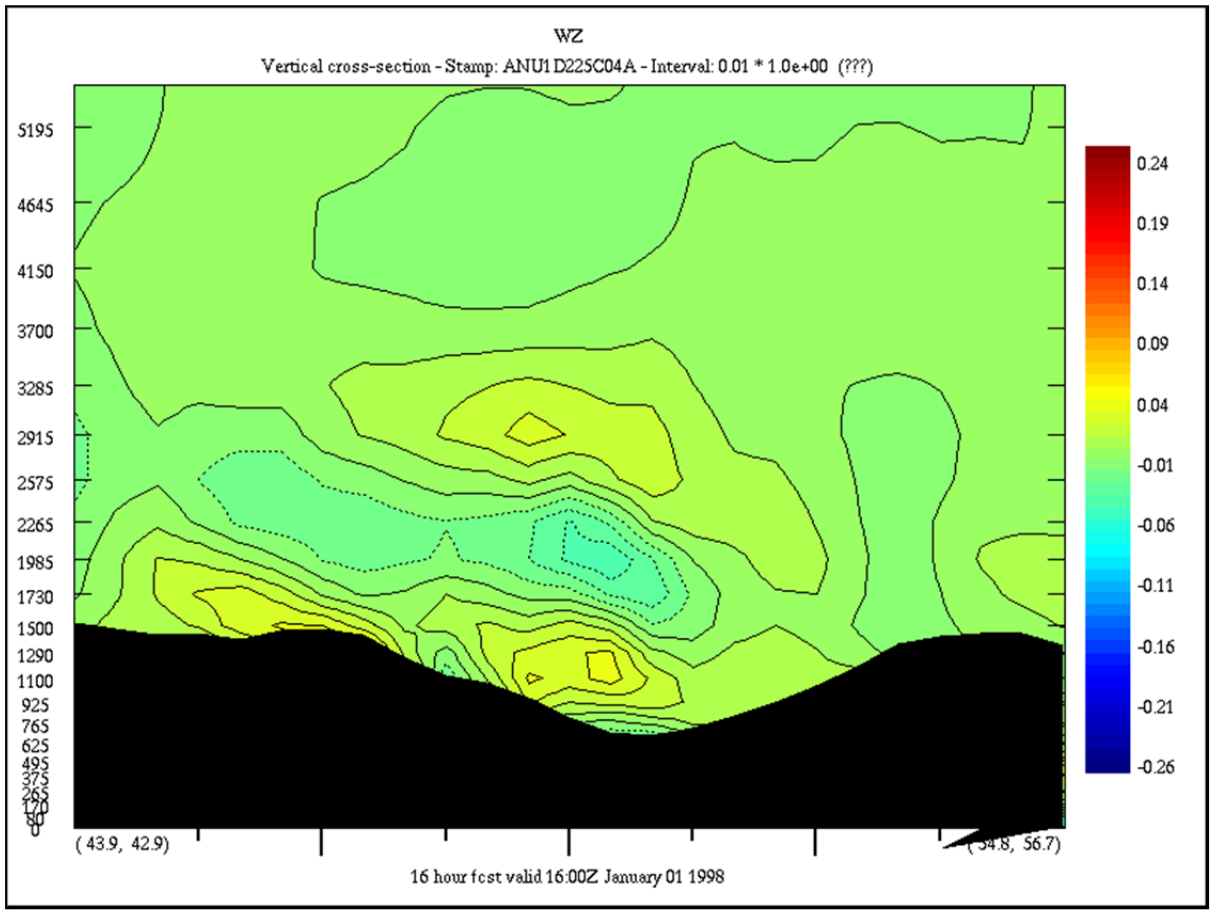

Figure 2.7 The vertical velocity of the cross-section of Whitehorse valley cross-section for ANU1D225C04A

Figure 2.9 shows the vertical variation in m ASL of the vertical velocity of the wind in m/s at the point where the maximum speed is reached in the cross-section of the valley (at coordinate [49, 50]) for climate states ANU1D225C04A (dotted line with circles), ANU1D225C04D (solid line with squares) and ANU1D225C04M (red solid line with diamonds), where the latter is the climate state equivalent when the original classification is used. From Figure 2.9, it is noticeable that there is much more vertical motion for the climate states with a high Froude number (ANU1D225C04D) compared to the climate states with a lower Froude number (ANU1D225C04A). Naturally, climate state ANU1D225C04M is in between the 2 extremes, since it is a climate state that includes both and two other cases.

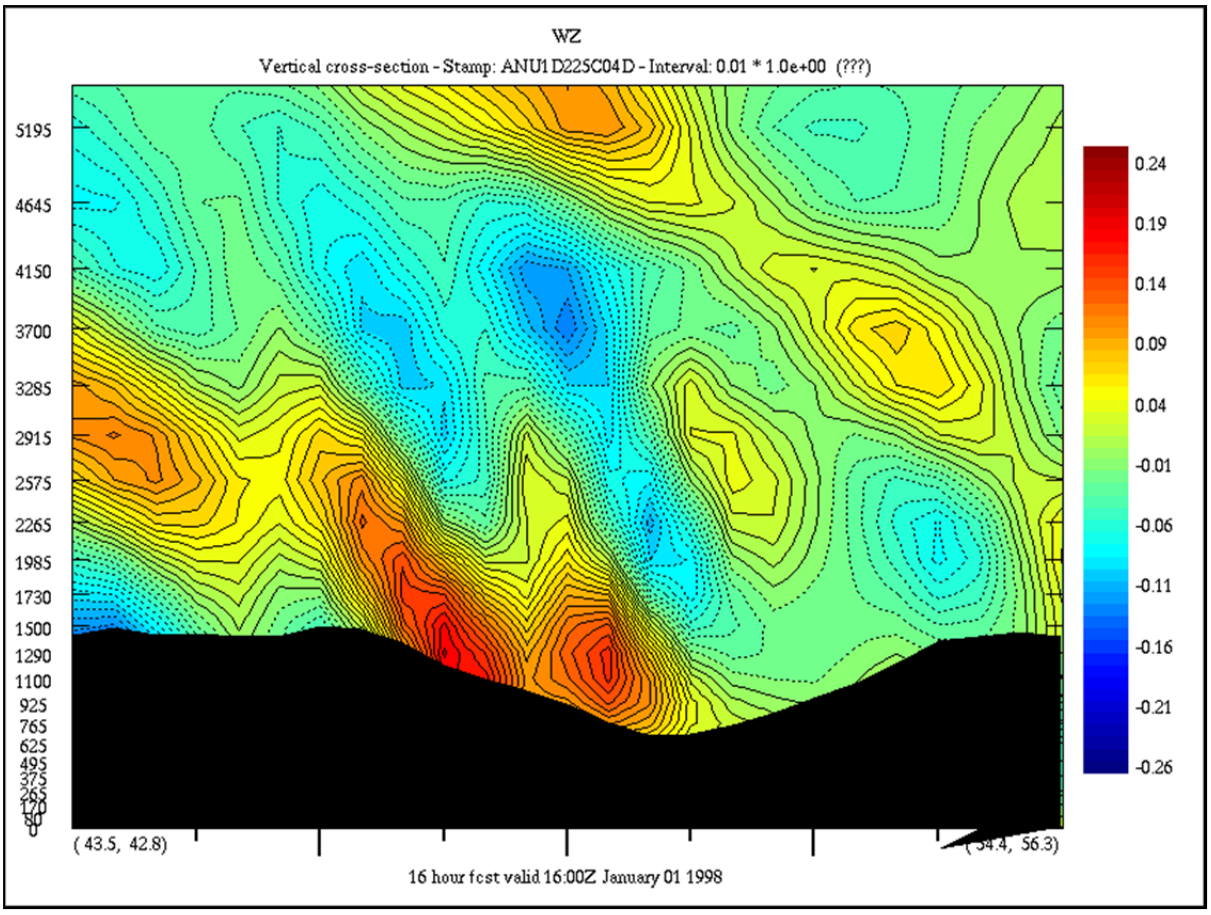

Figure 2.8 The vertical velocity of Whitehorse valley cross-section for ANU1D225C04D

From the results, it is clear that the velocities obtained from ANU1D225C0A are lower than those from ANU1D225C04D. For climate state ANU1D225C04D, the vertical component of the velocity (WZ) increases in the lee of the mountain until its maximum of 0.17 m/s at 1250 m ASL. For the same height, the climate state ANU1D225C04A reached only a maximum of 0.05 m/s. In addition, the vertical variation and amplitude of ANU1D225C04D in Figure 2.9 is much more prominent than ANU1D225C04A, which is also an indication of a less stable atmosphere. The reduction in velocity is caused by the difference in Froude number between these two climate states. Since the magnitude of the initialized winds are similar, and the wind speed (U_g) variable of the Froude number can be accounted as constant, the difference is deduced to be caused by the Brunt-Väisälä variable, N in equation 2.2. The Brunt-Väisälä values between data level 0m and 1500m ASL for the climate states are shown in Table 2.5.

The climate state ANU1D225C04A has the higher and most stable Brunt-Väisälä frequency value of 0.0171, and the Brunt-Väisälä frequency values decrease progressively as we reach climate state ANU1D225C04D with the lowest and least stable Brunt-Väisälä frequency of 0.0071.

We pushed further, and the mean value of the Brunt-Väisälä frequency was calculated for all the climate states grouped in their respective Froude number bin for classification variant 2 (736 climate states). Again, we see from Table 2.5 that the average value for all the climate states with ending A&M have one of highest Brunt-Väisälä frequency, and the climate states with ending D&P have the lowest Brunt-Väisälä frequency. However, notice that the "all climate states B&N" has a higher Brunt-Väisälä frequency than the "all climate states A&M", with a value of 0.0129 and 0.0122 respectively. If this is the case, we might ask why these climate states do not move to the more stable categories. The answer lies with the Froude number. The Froude number from equation 1.1 is dependent on Brunt-Väisälä, but also on the mean wind speed. The "all climate states B&N" may have a stronger thermal stratification than the "all climate state A&M", but its mean wind speed is also higher, which gives it a higher Froude number. Physically speaking, if the wind is faster, it may have enough energy to go up the topography and overcome the stratification, instead of going around the topography.

Table 2.5 Brunt-Väisälä frequency of Climate states for 0 and 1500 m

	ANU1D225C04-				ALL CLIMATE STATES			
	A	B	C	D	A&M	B&N	C&O	D&P
Brunt-Väisälä frequency	0,0171	0,0119	0,0105	0,0071	0,0122	0,0129	0,0120	0,0100

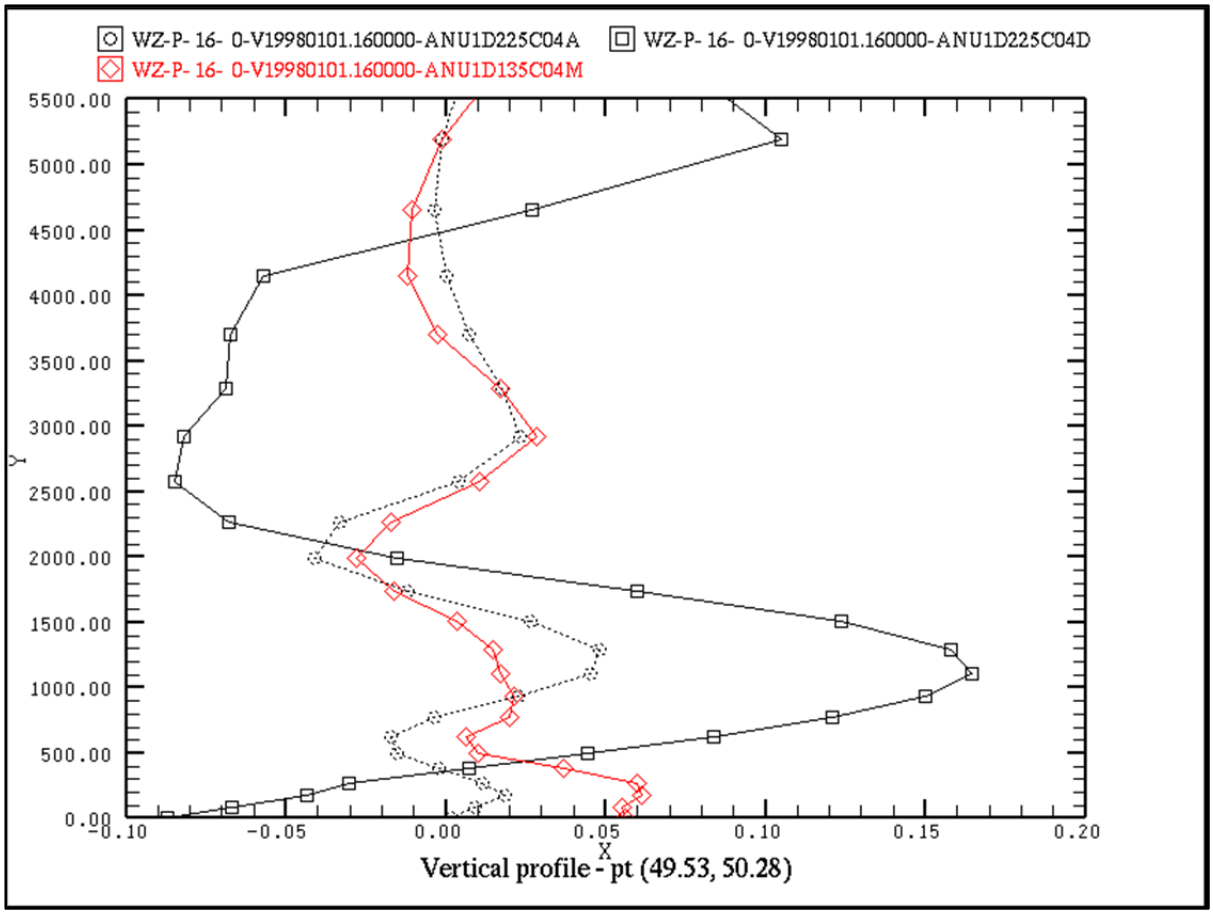

Figure 2.9 The vertical profile of the vertical velocity WZ for climate state ANU1D225C04-

A crucial variable affecting the Brunt-Väisälä frequency is the temperature profile; and the differences seen with climate states ANU1D225C04A and ANU1D225C04D is caused by the difference in said temperature profiles used in the initialization. As seen previously in Table 2.4, the largest differences between A and D are the 4 temperatures (t1, t2, t3 and t4) used to initialize the model. Figure 2.10 shows the temperature profile of the cases mentioned. Climate state ANU1D225C04A shows a temperature profile significantly more stable than climate state ANU1D225C04D, with an environmental lapse rate of 0.43°C/km for the former and -7.54°C/km for the latter. For the height of 0 and 1500m, the curve for ANU1D225C04A is practically vertical, which signifies a more stable temperature profile. These temperature profiles were also compared with their same climate state counterpart that was not classified by Froude number: ANU1D225C04M. Figure 2.10 shows that the

ANU1D225C04M temperature profile, and the values of u1/u2/u3/u4 and v1/v2/v3/v4 are somewhere between the mix of the climate states ANU1D225C04A, ANU1D225C04B, ANU1D225C04C and ANU1D225C04D. This is congruent, since ANU1D225C04M was the original climate state before it was classified into different Froude number and split into 4 climate states.

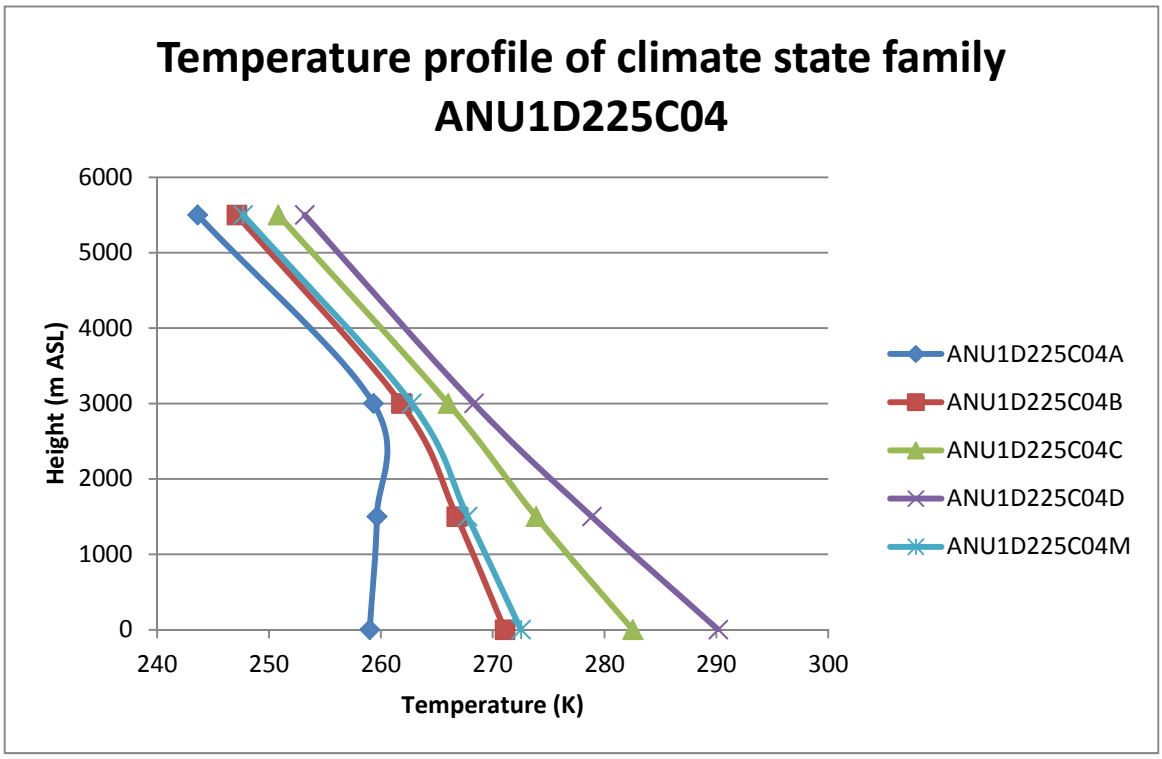

Figure 2.10 The temperature profile of climate state ANU1D225C04-

The results suggest that by using the classification by Froude number, it was possible to separate the stable and less stable cases, and inherently, do separate simulations in order to obtain results from stable climate states and less stable climate states. This would consequently affect the vertical flow and the interaction between the atmosphere and the valley. Similar effects to the Figure 2.7, Figure 2.8 and Figure 2.9 were obtained in Vosper (2004), where vertical mountain waves were modelled by changing Froude numbers to observe the sensitivity of the flow with respect to the inversion strength. In addition, by combining this capability with the correction factors that increase or decrease the frequency

of the climate states, it is possible to put more importance to key climate states that resemble the stratification climatology of Whitehorse.

2.5 Results

As described in Table 2.3, there are 4 different classification variants. All classification variants have their own tables containing their specific climate states. Each climate state in a climate state table would be used as input to initialize the MC2 model, and consequently, each climate state would yield its specific results. The same model settings have been used for all the classification cases, and these settings were set to match exactly those of Pinard *et al.* (2009), in order to make the results comparable with one another. The Table 2.6 shows the values of these model settings.

Table 2.6 Parameters used in the MC2 simulation

Parameter description	Values	Units
Horizontal resolution	4400	m
Horizontal grid	100x100	grid cells
Height model grid	20000	m
Number of vertical levels	35	
Number of vertical levels in 1500m boundary layer	12	
Blending zone linking terrain and flat plane	3	grid cells
Width of flat plane around model	5	grid cells
Time step	60	s
Total steps	960	
Total model time	16	hours
Number of time steps for mountain growth	250	
Height of first momentum level	40	m

The Courant number for these settings is ≈ 0.41, which indicates that the model will not be noisy. Once all the results of each climate state are obtained, statistical analyses involving all the climate state results are performed. All climate state results are multiplied by the frequency (depending on the cases, the frequency might have been modified by the correction factors discussed in the previous sections) of the climate state in the table, and then they are added together to obtain a weighted average. The WESTATS module, a component of the WEST software, was used to obtain these weighted averages. In order to keep this chapter concise, only the results from the original classification, and the classification variant 1 and 2 (without and with Froude) will be discussed here. As for the results from the classification variant 3 (involving the Froude with no shear), they can be found in annex VI, as they are not central to this study.

The simulated average results of all climate states using the original classification are shown in Figure 2.11 and Figure-A III. Figure 2.11 mainly shows the direction and to some extent, the magnitude of the winds, and Figure-A III shows through contours lines, the magnitude of the winds over the region of Whitehorse. The wind in the valley of Whitehorse (point #1) is northward with speeds around 1-3 knots; the wind in the Takhini valley (point #11) is eastward with speeds around 3-5 knots; and most wind on higher altitudes (point #5) flows in the north-eastward direction with speeds that can reach 7-9 knots.

The same type of results have been obtained for classification variant 1 and are displayed in Figure 2.12, where the arrows show the direction of the wind and the colour and size show the horizontal vector of the wind. The wind directions in Figure 2.12 are the same throughout the region as the wind results in Figure 2.11, and the magnitude of the horizontal vectors are within the same range as Figure 2.11, albeit, slightly faster.

As for the simulated results from the climate states obtained from classification variant 2, they are shown in Figure 2.13 and Figure-A V. Figure 2.13 shows the horizontal wind vector and direction of the wind, and Figure-A V shows the contour lines of the wind speed. The

wind is northward in the Whitehorse valley with horizontal speed vector of 1-3 knots; the wind is eastward in the Takhini valley with speeds of 1-3 knots; and the general wind in the high mountains are north-eastward with speeds between 5-7 knots.

From Figure 2.11, Figure 2.12, and Figure 2.13, we can quickly assess that the simulated wind directions for all 3 experiments are all similar. Only the simulated wind speeds have changed between the 3 different experiments. But the most drastic change in wind speed is with the result of Variant 2, where the correction factors have been inserted. It seems that correction factors are required to put more importance in stratified climate states with low Froude number, because even though those climate states are more realistic, they do not influence the mean wind speed by a significant amount.

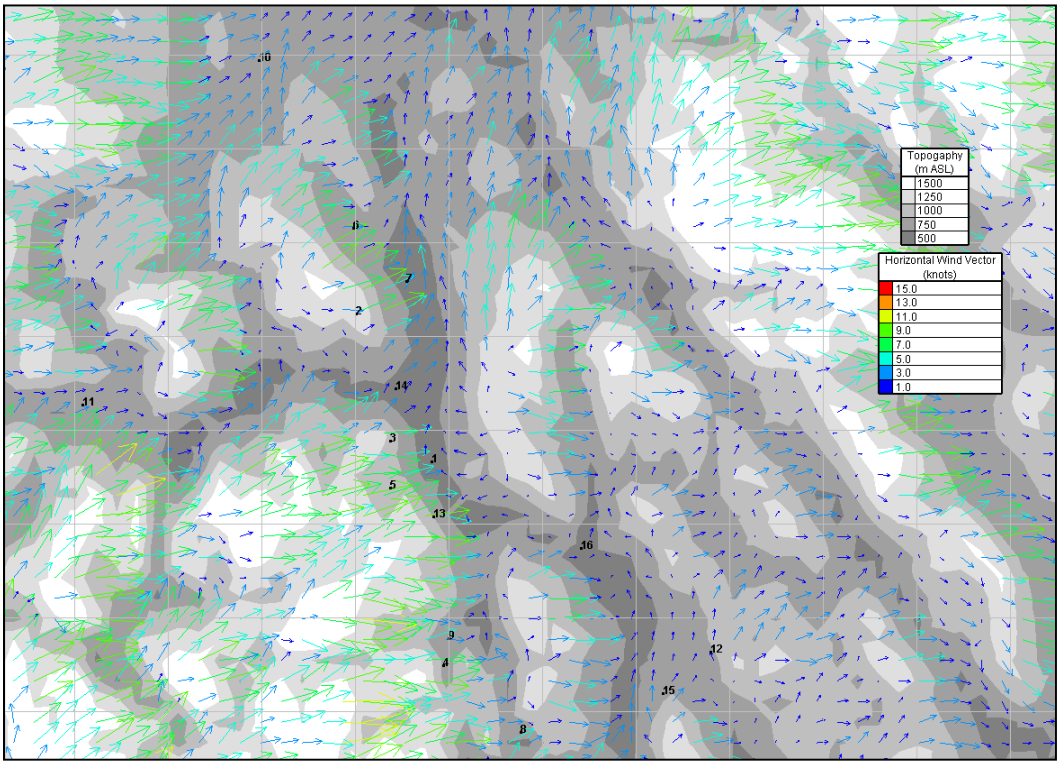

Figure 2.11 The simulated wind flow for original classification

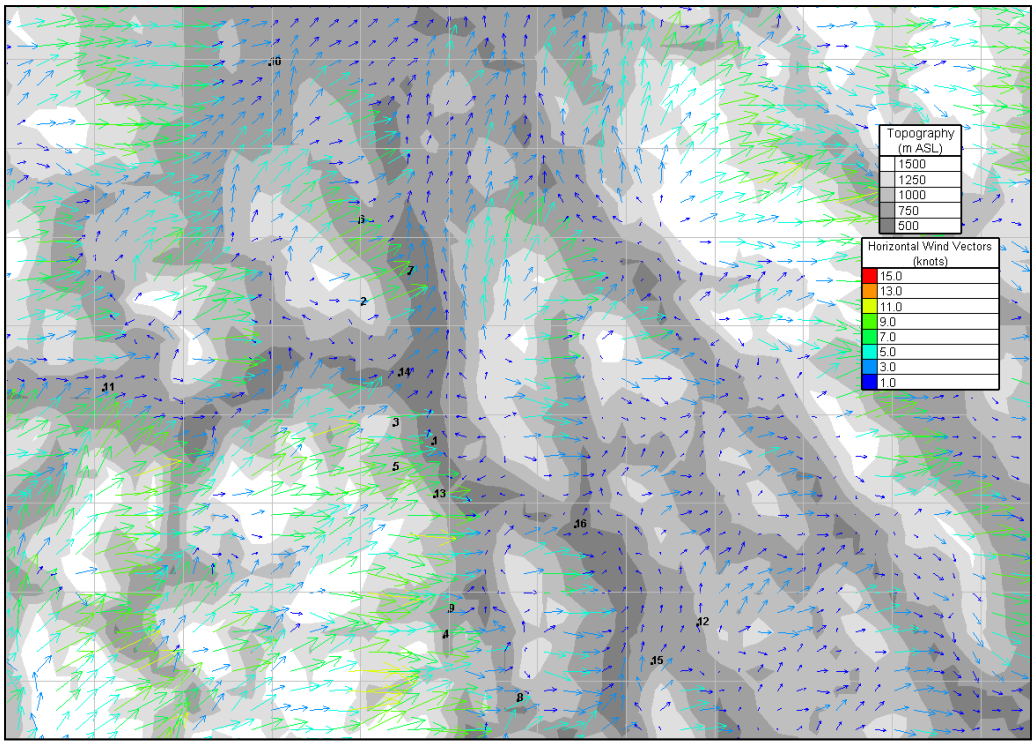

Figure 2.12 The simulated wind flow for classification variant 1

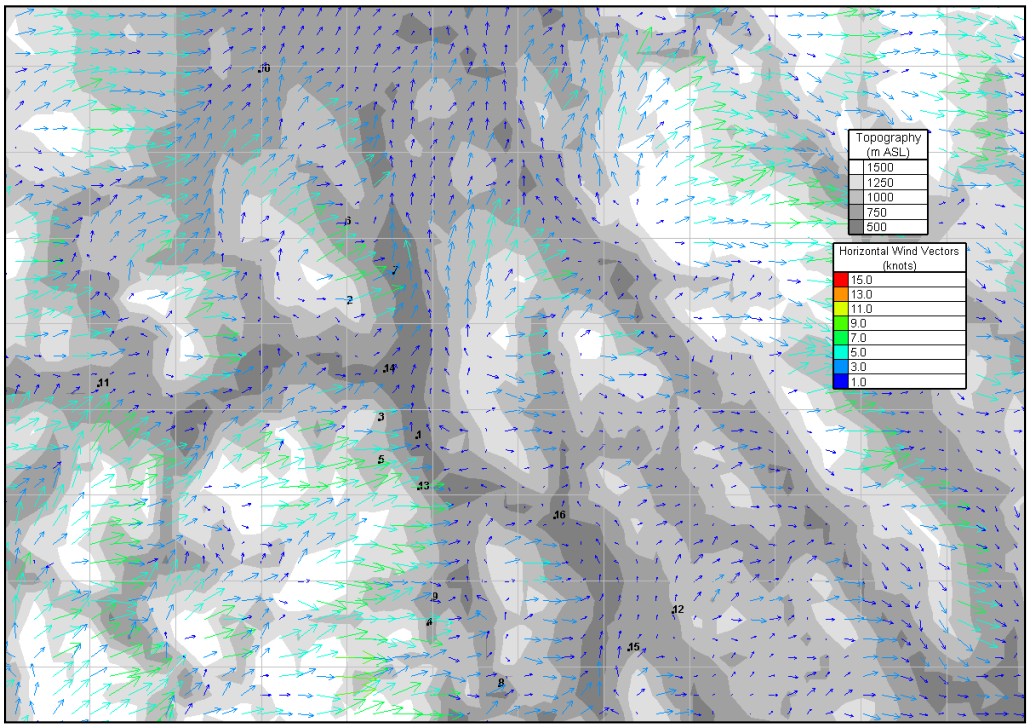

Figure 2.13 The Simulated wind flow for classification variant 2

CHAPTER 3

INITIAL REFERENCE TOPOGRAPHY

3.1 Method

It was suggested in Pinard *et al*. (2009) to raise the initial plane reference topography level. Formerly, in the standard WEST, the actual topography is built upon a reference topography at sea-level during the early steps of the simulation process. In this study, instead of the initial reference topography being a plane at sea-level, the plane would be raised at a higher level appropriate to the topography of the simulated region defined by the user. It is believed that with the insertion of the topography, it would create steep cliffs all around the model domain as the topography would return to the sea-level initial reference topography and this might affect the flow of the simulated winds by causing a spurious drainage flow, caused by the general stable stratification. The Figure 3.1 and Figure 3.2 are vertical cross-section of a domain, and show an example of these effects for the region of Regina in the province of Saskatchewan. On each side of Figure 3.1, the topography is transitioning from the 600-800m terrain level to the reference initial topography at sea-level. Since the topography has to transition to reach the sea-level, it creates a cliff, and the whole region resembles an elevated plateau. The proposed modification would raise this initial reference topography to a higher height, and thus, reduce the steep slopes between the actual topography and the outside border.

An additional key was added to the mc2_settings.nml file: init_topo. This key would control the height of the initial reference topography. Figure 3.2 shows the effect of init_topo having a value of 500 for the region of Regina on the model and its topography.

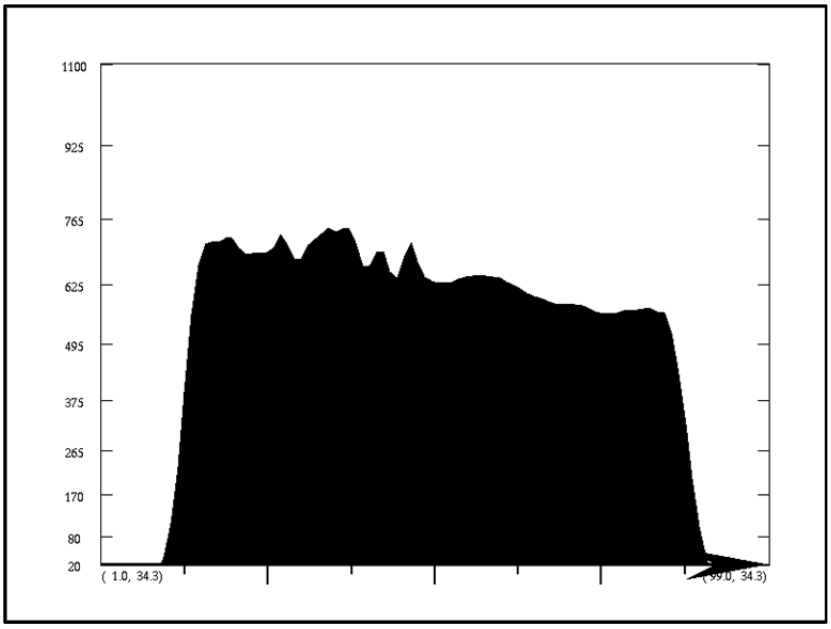

Figure 3.1 The vertical cross-section of topography for entire domain for the region of Regina (Saskatchewan) in m ASL

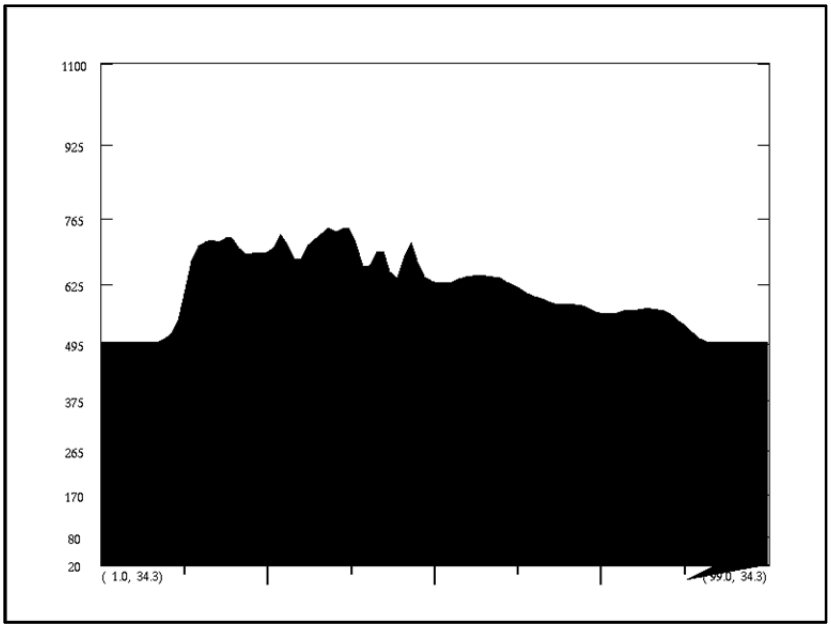

Figure 3.2 The vertical cross-section of topography for entire domain for the region of Regina (Saskatchewan), with initial reference topography set at 500m ASL

3.2 Theoretical Topography

In order to see the effect of raising the initial reference topography on the simulated winds, a theoretical topography was created. This topography is an elevated plain of 500m ASL, and the init_topo key was set to 0.0 and 500.0, as shown in Figure 3.3 and Figure 3.4, respectively.

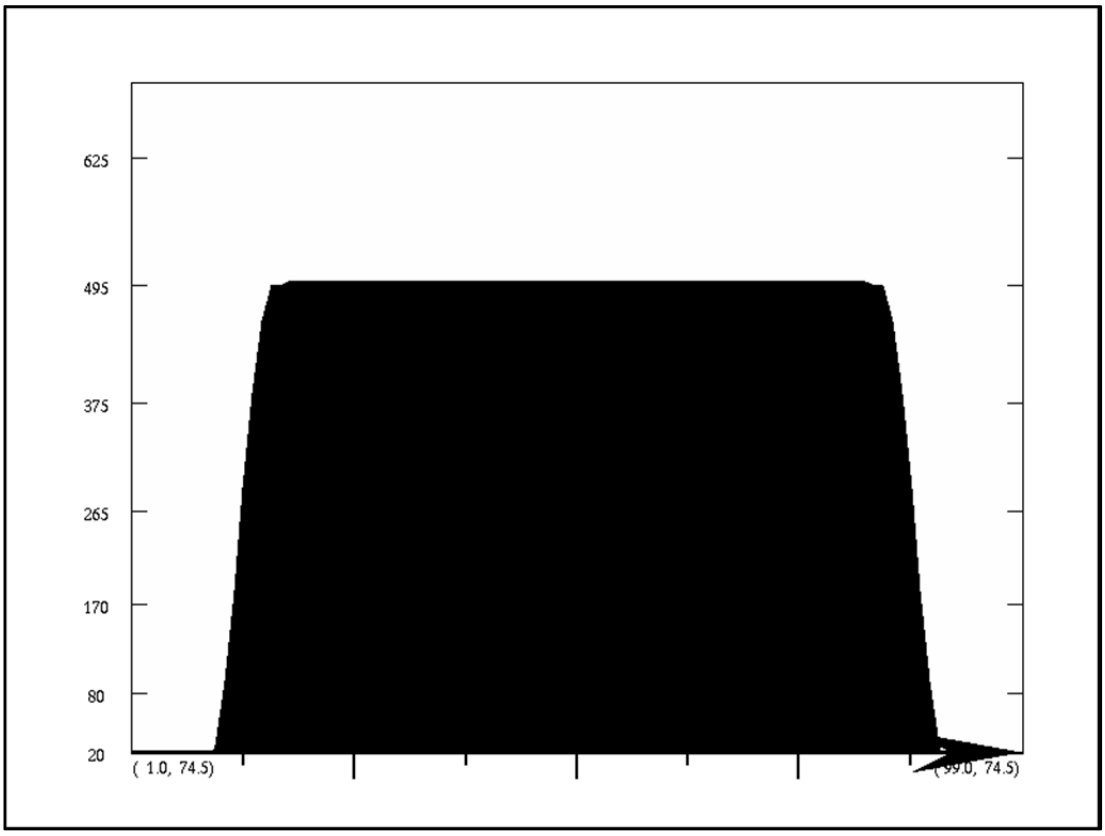

Figure 3.3 The cross-section of theoretical topography
with initial reference topography at 0m

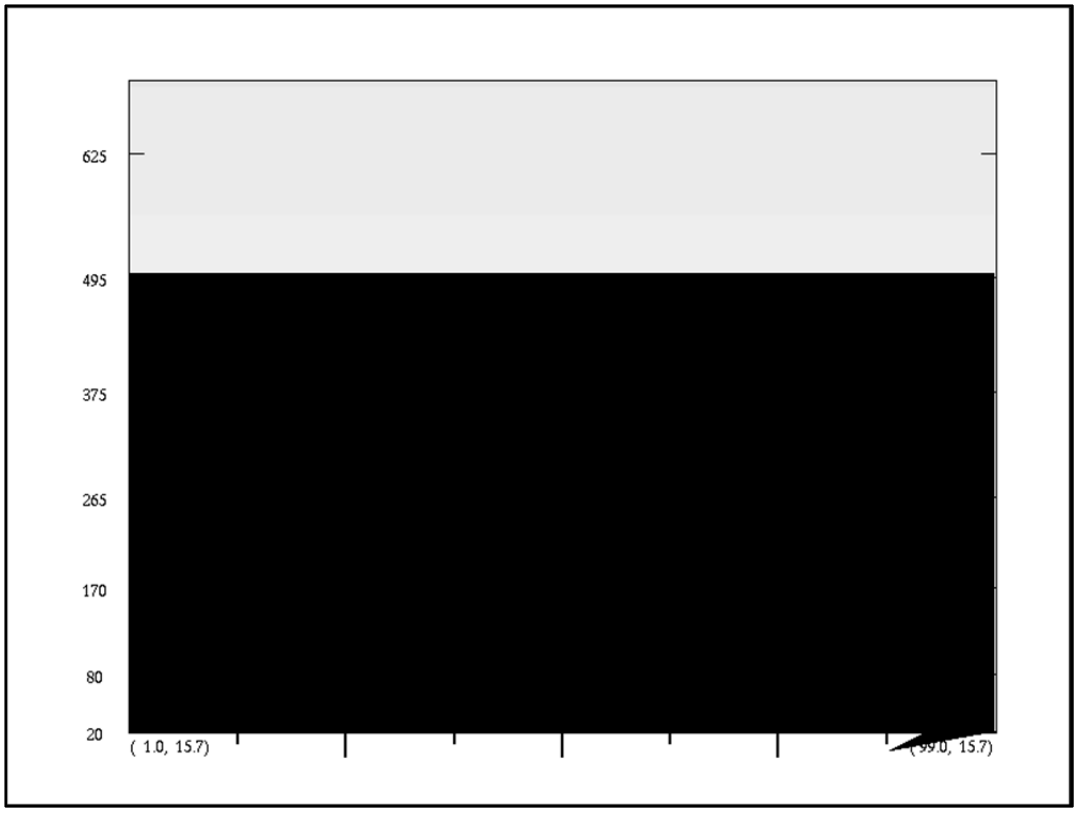

Figure 3.4 The cross-section of theoretical topography
with initial reference topography at 500m

Runs on MC2 were performed for both of these topography settings. A simple theoretical uu/vv/tt profile was used to initialize the model are shown in Table 3.1, and the model settings for the MC2 model remain the same as in Table 2.6. The results of the simulated runs with init_topo = 0.0 and init_topo = 500.0 are shown in Figure 3.5. The red arrows represent the results with init_topo at 500m ASL. The black arrows represent the results with init_topo at 0m ASL Some slight differences in magnitude and direction of the winds can be observed in the central part of the domain, and major differences can be seen on the outside of the domain. By taking the vector differences of the simulated winds for the run with init_topo at 0.0 and the run with init_topo at 500.0 (results from init_topo = 0 subtracted by results from init_topo = 500), we obtain Figure 3.6.

Table 3.1 Initialization profile of theoretical topography

Variables	u (m/s)				v(m/s)				Temperature(K)			
Height levels	1	2	3	4	1	2	3	4	1	2	3	4
Theoretical Topography	8,0	8,0	8,0	8,0	0,0	0,0	0,0	0,0	278,0	278,0	278,0	278,0

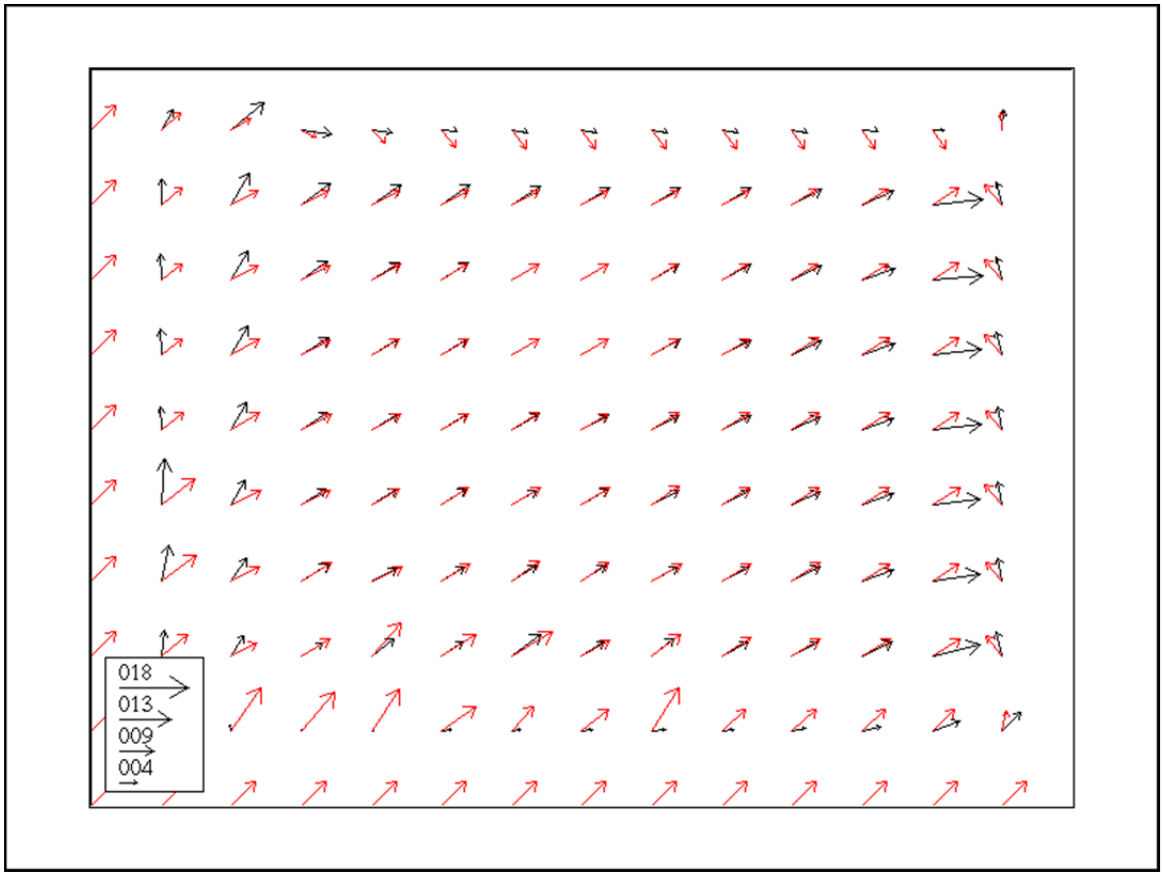

Figure 3.5 The superposition of the wind flow over theoretical topography with init_topo at 0 and 500m ASL

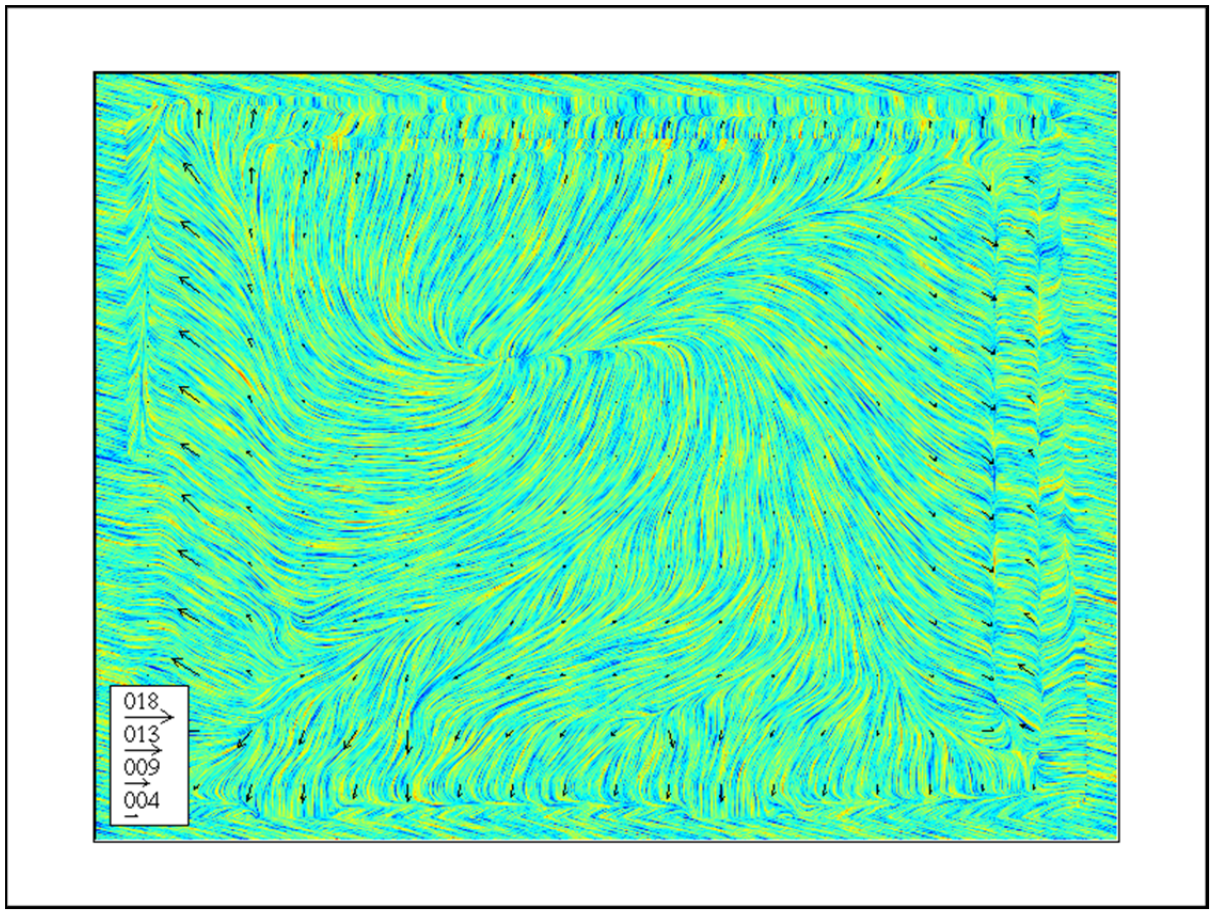

Figure 3.6 The vector difference between initial reference topography at 0m ASL and 500m ASL

We see in Figure 3.6 streamlines that represent the flow resulting from the difference of the two init_topo values, and there is an outflow of the wind towards the outside of the simulated region. The outflow starts small in the center of the domain, and slowly increases as it moves towards the outside of the domain. Also, the “drainage” of the flow is deflected by coriolis acceleration, which veers the flow to its right. Note that the MC2 settings used in the WEST context cause the lateral boundary flow to be fixed with time. This flow’s behaviour leads us to believe that the “draining” of the flow is due to the initial reference topography at sea-level creating steep cliffs on the border of the topography, which forces and diverges part of the simulated wind. This outward flow effect can be an influence on the simulated results of any region where the topography is much higher than the sea-level. Since this study is located in

Whitehorse at over 600m ASL, it is reasonable to suggest that part of the results obtained are affected by it.

3.3 Results

The principle of raising the initial reference topography has been applied to the region of Whitehorse and the climate states obtained with classification variant 2 are used as input, since they offer a better representation of the Whitehorse climatology than any other set of climate states (as discussed in chapter 2). The height chosen for init_topo is usually to the user's discretion. In this study, the value of 600.0 m was chosen, as it seems low enough not to overwhelm the orography and valleys of the region; and high enough to reduce the steep cliffs that can be seen on the sides of the simulated region and the low-level wind flow divergence that may result from it. Using the same model settings as described in Table 2.6, wind vectors were obtained for both init_topo = 0 and init_topo= 600 with the climate states from classification variant 2. The Figure 3.7 shows the vector difference of these wind flows, where the wind of the simulations with init_topo = 600 were subtracted by the wind simulations with init_topo = 0.

Even though clear effects of the change in the flow are seen in the simple theoretical case when the initial topography is raised in Figure 3.5, the results for the region of Whitehorse are not as apparent, as shown in Figure 3.7; where the vector difference does not seem to go over 0.5 m/s and the directions are very similar to one another for the centre of the domain. One of the speculated reasons is that the terrain in the center of the grid is much more complex than a simple plateau as seen in chapter 3.2, and the topography weighs more to the results than the simple effect of elevating the initial topography. The flow is forced through channels and valleys, and therefore, will mostly flow in one set directions. There are larger differences on the edge of the domain; however, it is outside the region of interest, which is the center. The improvement to the height around the perimeter of the grid has little effect on the flow compared to the strong effects by the topography in the middle of the grid, which suggests that this modification might not bring much improvement to the results.

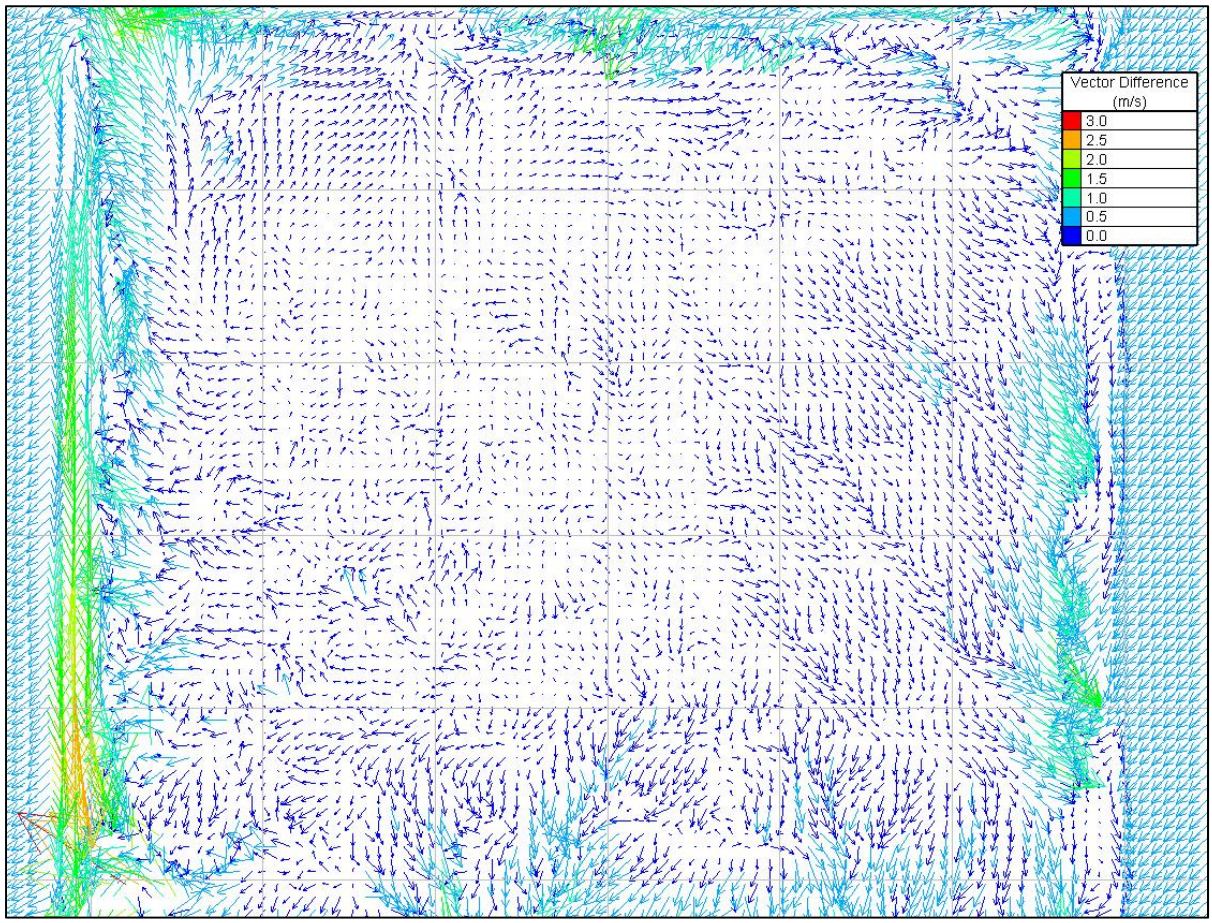

Figure 3.7 Vector difference of the simulated wind flow for the cases of "classification variant 2"with initial reference topography at 0m ASL and initial reference topography" at 600m ASL

CHAPTER 4

LOW LEVEL PROFILES

4.1 Profile Modifications

In Pinard, *et al.* (2009), it was proposed that the input data below the topography should not be used to initialize the model. It was argued that the south-east surface (i.e. z=0 m ASL) direction of the geostrophic wind for Whitehorse's Reanalysis grid point were erroneous, as they were largely affected by the topography and not representative of the actual geostrophic wind direction needed to initialize the model. Indeed, the Reanalysis grid point for this region gets its source from the Whitehorse Radiosondes that is within the Whitehorse valley. This valley axis being in the south-east/north-west direction would naturally indicate a south-east geostrophic wind direction for low Reanalysis data level. And consequently, the initialization of the pressure gradient would be different from the observations, that require a geostrophic wind coming from the south-west (based on the climatology studies in Pinard 2007). Figure 4.1 shows a comparison of the direction on different height for Reanalysis and Radiosondes. The wind energy frequency roses[4] have the Reanalysis (shaded) and Whitehorse Radiosondes (outlines) superimposed for the height 0 (714m ASL for the Radiosondes), 1500, 3000, and 5500m ASL. Both analyses are from period 1958-2000, and the Reanalysis roses are from node 61/90 used in Pinard *et al.* (2009), with node 17\18 being the equivalent in this study.

[4] The wind energy-frequency is calculated as the product of the percentage frequency and the cube of the mean wind for each direction, divided by the sum of those products in all directions.

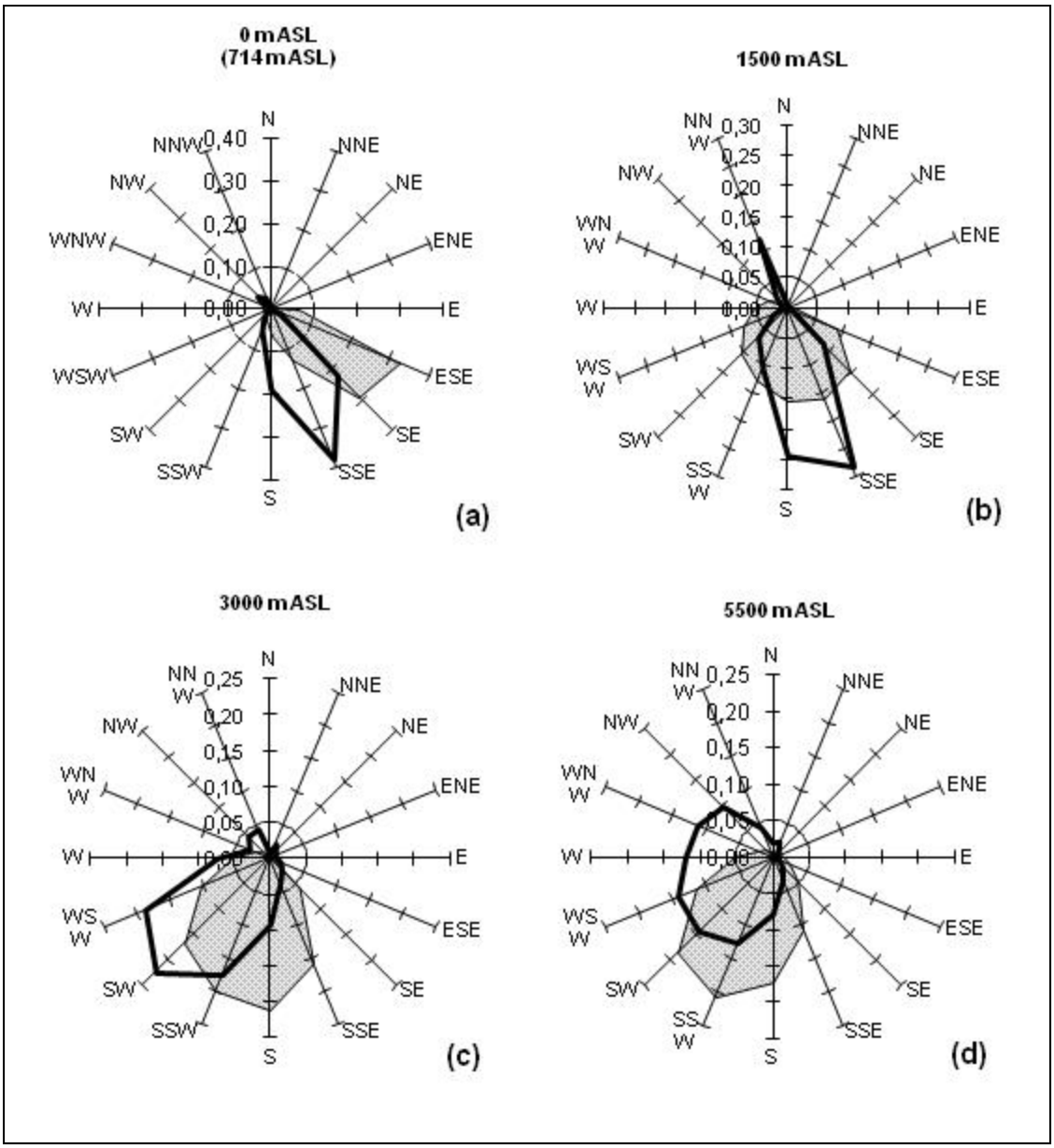

Figure 4.1 The wind energy frequency roses of Reanalysis (shaded) and Radiosondes (outlined) for Whitehorse

Taken from Pinard *et al.* (2009, p. 63)

To further illustrate the difference in direction of the geostrophic wind of the Reanalysis, Figure 4.2 shows the average geopotential heights (in decametres) obtained from the Reanalysis for the period of 1958-2000 over the Yukon at pressure levels of 1000, 850, 700 and 500 mb. At level 1000 mb (a), the pressure gradient is from the top right corner to the

bottom left corner, which indicates a geostrophic wind along the isobars, and going in the north-west direction above the Yukon. As we move up, at level 850 mb (b) and higher (700 and 500 mb), the pressure gradient has changed direction to the north-west, which signifies a geostrophic wind above Whitehorse in the north-east.

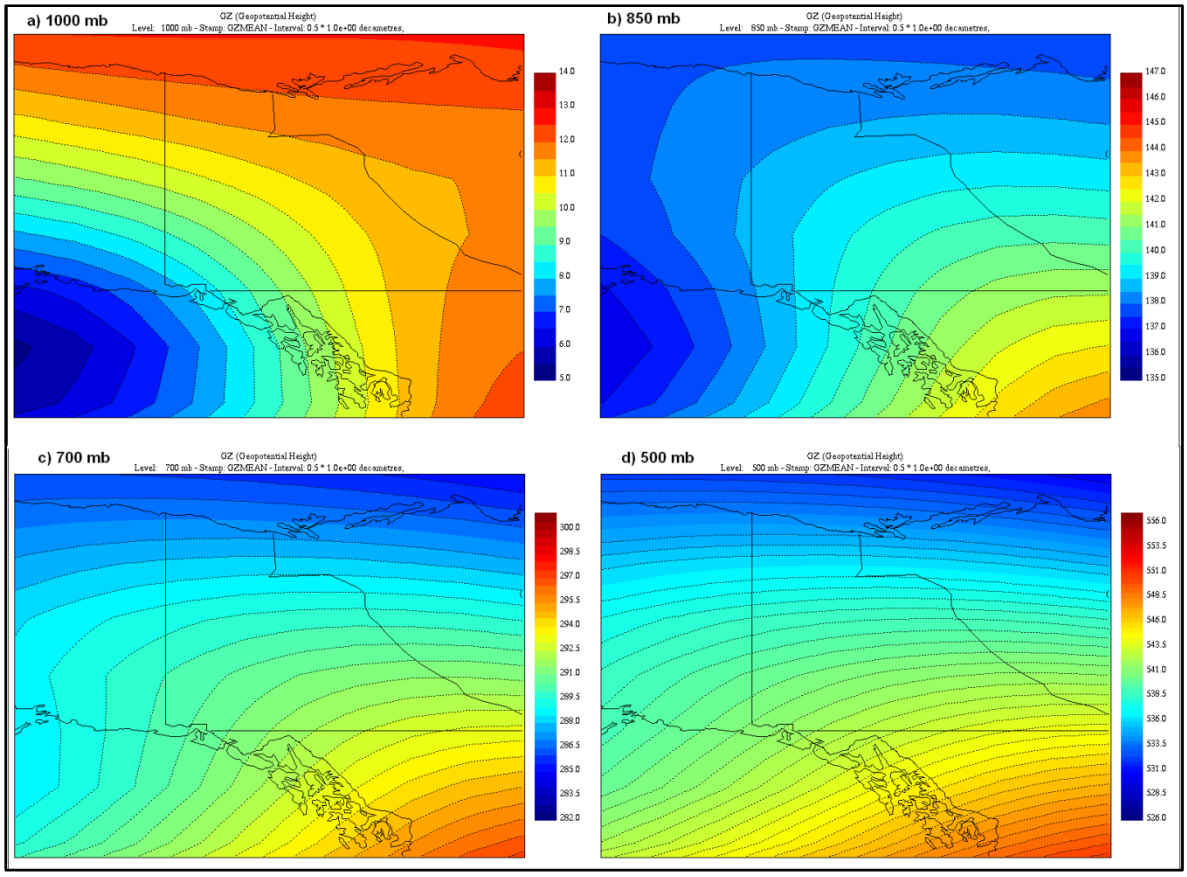

Figure 4.2 Geopotential heights of Reanalysis over the Yukon

This difference in surface level geostrophic wind direction at the initialization would cause erroneous forced channelling and pressure-driven channelling (Bergstrom *et al.* 2006) for the key regions of the simulated map by MC2. Instead of using the values below the surface to initialize, values above the topography should be used, since the directions are more appropriate for initialization according to the observations. The initialization process of MC2 uses 4 data levels: 0, 1500, 3000 and 5500m ASL. Each of these 4 levels contains their values of uu/vv/tt, and they are used to extrapolate the uu/vv/tt values of any other levels in

between. In this case, the initialization process has been modified, such that the lowest uu and vv component of the geostrophic wind data level (0m ASL) would be ignored. The uu/vv values at a higher level would be brought down through the thermal wind equation to replace these surface data levels. It is worth mentioning that the original tt values at the surface level remains untouched, as these values are required to allow an accurate and proper temperature profile of the atmosphere. The thermal wind relation is used since it is one of the fundamental principles that relate the change in horizontal geostrophic wind at different height with temperature. By combining the x and y geostrophic equations 4.1 and 4.2; the hydrostatic balance 4.3; the equation of state 4.4.

$$u_g = \frac{-1}{\rho f}\frac{\partial p}{\partial y} \tag{4.1}$$

$$v_g = \frac{1}{\rho f}\frac{\partial p}{\partial x} \tag{4.2}$$

$$\frac{\partial p}{\partial z} = -\rho g \tag{4.3}$$

$$p = \rho R T \tag{4.4}$$

And taking the derivative of the geostrophic wind with respect to height, we obtain:

$$\frac{\partial \overrightarrow{V_g}}{\partial z} = \frac{g}{fT}\hat{k} \times \overrightarrow{\nabla_H T} + \frac{1}{T}\frac{\partial T}{\partial z}\overrightarrow{V_g} \tag{4.5}$$

By scaling analysis, we see that the second term on the right hand side of equation 4.5 is much smaller than the first term, which would give the thermal wind equation 4.6:

$$\boxed{\overrightarrow{V_T} = \frac{\partial \overrightarrow{V_g}}{\partial z} = \frac{g}{fT}\overrightarrow{\nabla_H T} \times \hat{k}} \tag{4.6}$$

Where T is the temperature in Kelvin, g is gravitational acceleration (9.8 m/s^2), f is the coriolis parameter ($f = 2\Omega\sin\Phi$, with Ω being the angular velocity of the earth's rotation, and Φ the latitude), V_g is the geostrophic wind in m/s, and V_T is the thermal wind in m/s. Equation 4.6 shows the dependence of the vertical shear of the geostrophic wind on the horizontal temperature gradient of the atmosphere. Depending on the direction of the horizontal temperature gradient with respect to the direction of the geostrophic wind, the geostrophic wind at higher levels may increase, decrease, and change directions. In this study, the horizontal temperature gradient was taken from the average temperature values of the neighbouring grid points of the Reanalysis dataset surrounding the grid point of Whitehorse at i = 18, j = 17 for the period of January 1st 1958 to December 31st 1999, as presented in Table 4.1. Also, Figure 4.3 illustrates the average temperature field (in degree Celsius) of the pressure level at 1000 mb, over the Yukon for the mentioned data period. Combining this horizontal temperature gradient with the vertical temperature profile and the geostrophic wind in the *mc2_settings* files, we obtain the thermal wind used to change the wind profile in the initialization for each climate states.

Table 4.1 Horizontal temperature gradient of Whitehorse Reanalaysis grid point

	Adjacent grid points			
	i = 17; j = 17	**i = 19; j = 17**	**i = 18; j = 16**	**i = 18; j = 18**
Temp at level 1 (K)	275,8918	274,4554	277,501	271,5823
Temp at level 2 (K)	267,8227	267,9538	267,1223	266,8575
Temp at level 3 (K)	261,4665	261,452	262,3632	260,349
Temp at level 4 (K)	245,5557	245,6435	246,6106	244,5837

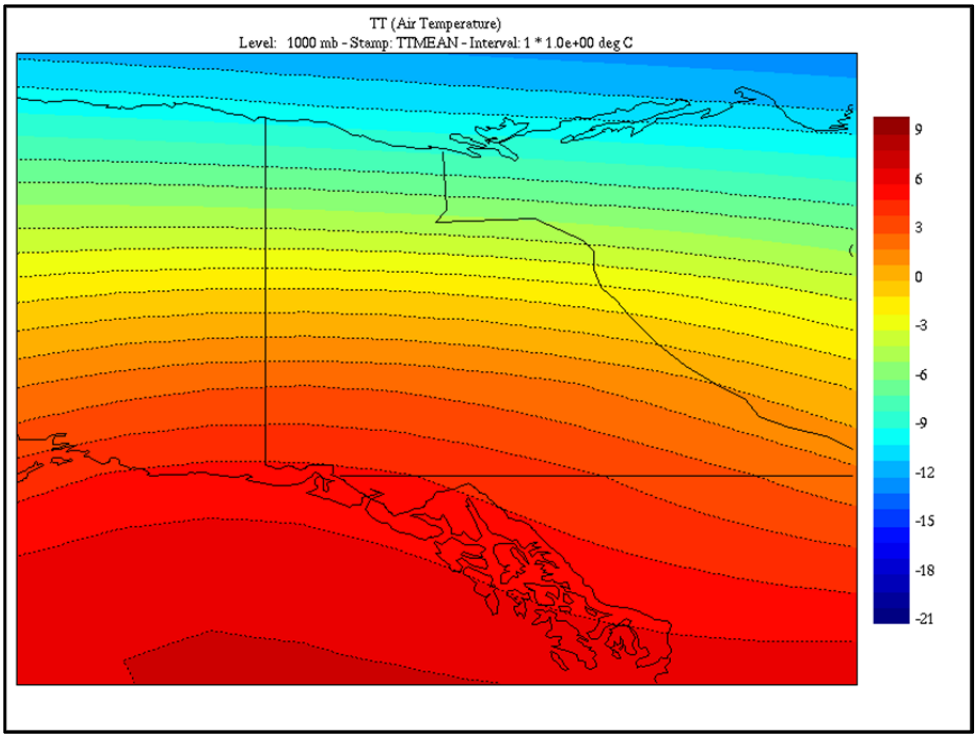

Figure 4.3 Average temperature field of Reanalysis over the Yukon

4.2 Results

The module to ignore the lower data levels during initialization, also referred as “kdrop”, has been implemented in the MC2 model. The key used to control this feature in mc2_settings is named: “kncep_drop”. For the region of Whitehorse, since most of the topography is well above the sea-level, the “kncep_drop” key was set to 1 (key also set to 2, but not shown as they yielded similar results), meaning the data level profile of uu and vv at 0m ASL will be ignored and it will be replaced by values extrapolated from the 1500m level through the thermal wind equation 4.6. The climate states of the classification variant 2 (with Froude and the correction factors discussed in the chapter 2.3) were used, and initialized in MC2, while ignoring the bottom data level during the initialization of each run. A more detailed explanation on how to use this modification can be found in the annex XI.

The Figure 4.4 shows the wind vectors of the simulation with the kdrop module set to 1 (red arrows), and the simulation without the use of the kdrop module (black arrows). The arrows’

direction between both cases differ minimally, which seems to indicate that for the set of climate state used in this experiment, no apparent correction in simulated wind directions were obtained by initializing with a geostrophic wind taken at a higher level. These results suggest that for the set of climate states used here, the kdrop module does not improve or change the direction of the simulated wind flow. In order to see a difference, the geostrophic wind of the climate states used to initialize would need to be of a different direction for both 0 and 1500m ASL levels (also for 3000m). This difference in directions would require a different set of climate states, which can only stem from a different classification scheme, or different Reanalysis input (this will be tackled in chapter 5.2.4).

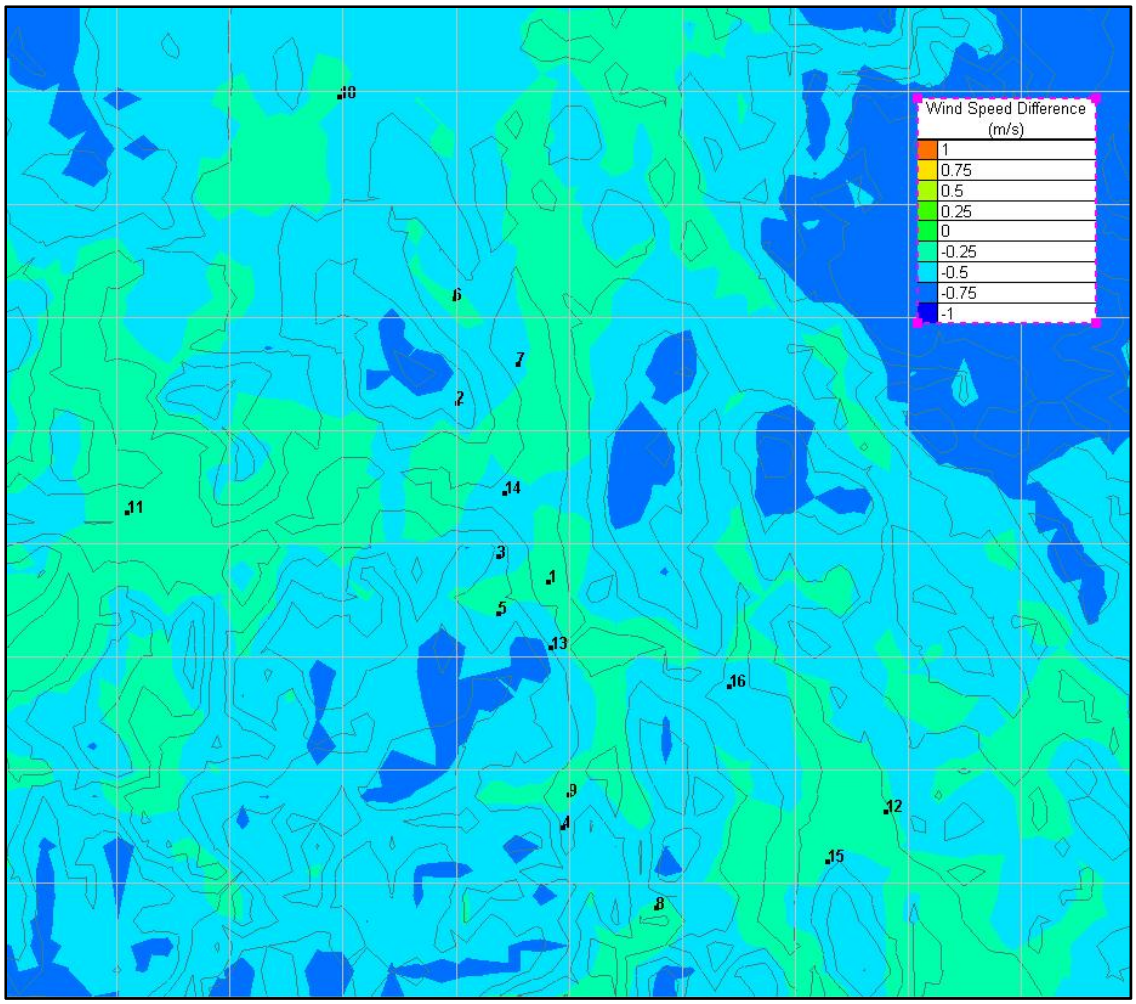

Figure 4.4 The simulated wind flow for classification variant 2 with module kdrop

CHAPTER 5

COMPARISON OF RESULTS

5.1 Wind Stations

The simulated results obtained throughout this study (chapter 2, chapter 3, chapter 4) will be compared with observation values recorded throughout the region of Whitehorse. There are 16 surface wind monitoring stations that were used in this study; the majority of them are located in valley bottoms. The observation data are extracted from Figure 5.1, which were originally obtained through a combination of programs: the Yukon Government (YG), the Boreal Alternative Energy Centre (BAEC), and the Meteorological Service of Canada (MSC). Depending on the wind stations, the wind was measured at 10, 20, or 30 m AGL, and the mean wind speed for each site was projected to 30m AGL using a simple logarithmic law and estimates of local surface roughness. Pinard *et al.* (2005) and Pinard (2007) presents a more detailed explanation of these monitoring stations and Table 5.1 has tabulated the results extracted from these sources for the wind stations pertinent in the region of Whitehorse, and they will be used as a basis of comparison for the direction and magnitude of the simulated wind.

There are 16 wind monitoring stations, and Table 5.1 shows the name of the stations; their latitude and longitude; their elevation in m ASL; their mean wind speed in m/s; their MC2 coordinate points that are most representative of their location for the grid used in the simulations by comparing the latitude, longitude and the geographical terrain; their assigned station number used to identify them in this study; their mean wind speed (m/s) for each station's period of observation; and their uncertainty-on-average[5] for wind speed obtained from Pinard *et al.* (2005). The mean wind speed varies from 2.2 m/s in valleys to 8.4 m/s up in the mountains, and the variability of the mean wind speed can range from 6% to 40%,

[5] Variability of mean wind speeds based on the period length of observations.

depending on the length of the period of observation by the wind station (Pinard *et al.* 2005). This is included to facilitate comparison with WEST results based on 50 years statistics. A more descriptive table with period of record for each station can be found in the annex XII, which also includes the period length of the recorded data and the surface roughness at the stations. Figure 5.1 shows the location of each of these observation points listed in Table 5.1 with respect to the grid used by the simulations.

Table 5.1 Description of wind stations and wind measured wind speeds

Station Name	Station #	Latitude (°)	Longitude (°)	Elevation (m)	Grid coordinates		Average Wind Magnitude (m/s)	Uncertainty on average wind speed (%)
					I	J		
Whitehorse A	1	60,710	-135,067	706	50	49	4,6	6
Flat Mtn	2	60,994	-135,370	1930	46	58	8,4	40
Haeckel Hill	3	60,749	-135,231	1430	48	51	6,9	8
Annie	4	60,319	-135,020	876	51	39	3	12
Fish	5	60,659	-135,230	1175	48	48	4,1	9
Fox Lake	6	61,160	-135,380	793	47	61	2,7	12
Laberge	7	61,057	-135,170	645	49	58	4,5	12
Watson	8	60,190	-134,720	702	54	36	4,1	12
Wheaten	9	60,370	-135,000	783	52	41	2,2	12
Braeburn	10	61,481	-135,770	725	41	69	3,1	9
Champagne	11	60,811	-136,448	732	33	51	2,9	9
Jakes	12	60,339	-133,980	814	64	40	2,5	13
Mt Sima	13	60,604	-135,060	939	50	46	5,1	13
Nursery	14	60,851	-135,210	674	49	53	3,5	13
Jubilee Mtn	15	60,262	-134,170	1280	62	38	4,5	12
Marsh Lake	16	60,542	-134,480	656	57	45	3	12

Figure 5.2 was extracted from Pinard *et al.* (2005) and displays the 16 wind stations tabulated in Table 5.1 with their respective wind energy frequency, mean wind speeds, and elevation. The roses represent the relative amount of wind energy that occurs in each direction. This type of rose gives a better measure of direction for wind energy purposes than the simple wind direction frequency rose (Pinard *et al.* 2005). The wind stations in Figure 5.2 show a predominance of wind in the Whitehorse Valley to flow northward (#6Fox, #7Laberge,

#14Nursery, #1Whitehorse, #9Wheaten, #4Annie, #16Marsh Lake), and the wind in the Takhini Valley to flow eastward (#11Champagne). At higher altitudes and in the mountains, the wind has a tendency to flow north-eastward (#2Flat Mtn, #5Fish, #13Mt. Sima). This is also supported by the Whitehorse Upper-air station measurements that indicate the wind flowing to the north at 714m ASL, and changing to north-east direction at 1900m ASL.

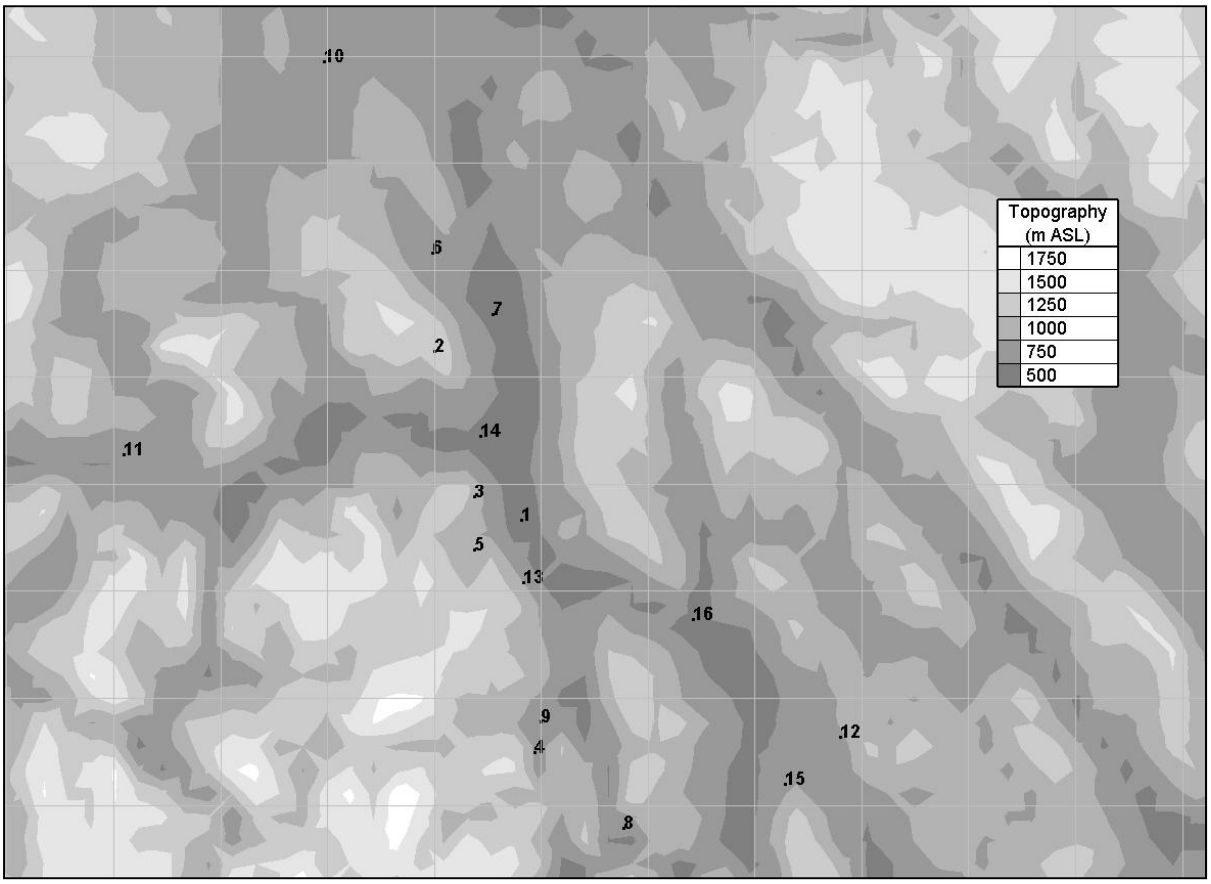

Figure 5.1 The topography and location of the 16 wind stations

Figure 5.2 Map of Whitehorse area and wind energy frequency of the 16 wind stations and the upper-air Radiosondes (plus Mt.Sumanik)

Taken from Pinard, Benoit *et al.* (2009, p. 63)

5.2 Modeled Results

The modeled wind obtained using the various methods described in chapter 2, 3 and 4, are compared with the observed wind data from the 16 wind stations for the region of Whitehorse. The cases that will be analyzed in this chapter are the results of:

- Original classification (from chapter 2.5);
- Classification variant 1 (from chapter 2.5);
- Classification variant 2 (from chapter 2.5);
- Classification variant 2 with the initial reference topography (from chapter 3.1);
- Classification variant 2 with the module to drop the lower data levels (from chapter 4.1).

The Table-A XIII-1 gathers the measured wind speeds of the wind stations and the modeled wind speeds at the grid points of the 16 Wind Stations of the various cases that were run. Table-A XIV-1 shows the difference of the simulated results with respect to the observed wind speeds, as well as the mean and standard deviation of the difference of the 16 wind stations for each simulated cases.

5.2.1 Classification Variants

The results from the original classification, the classification variant 1 and classification variant 2 are respectively shown in the first, second and third column of the "simulations" section of Table-A XIII-1. For the original classification (1st column), which could be considered the starting point and base for the other subsequent simulated cases, gives a correlation coefficient of 0.750 when its modeled wind speeds are compared with the observation as presented in Figure 5.3. Some similarities can be seen, however not strong.

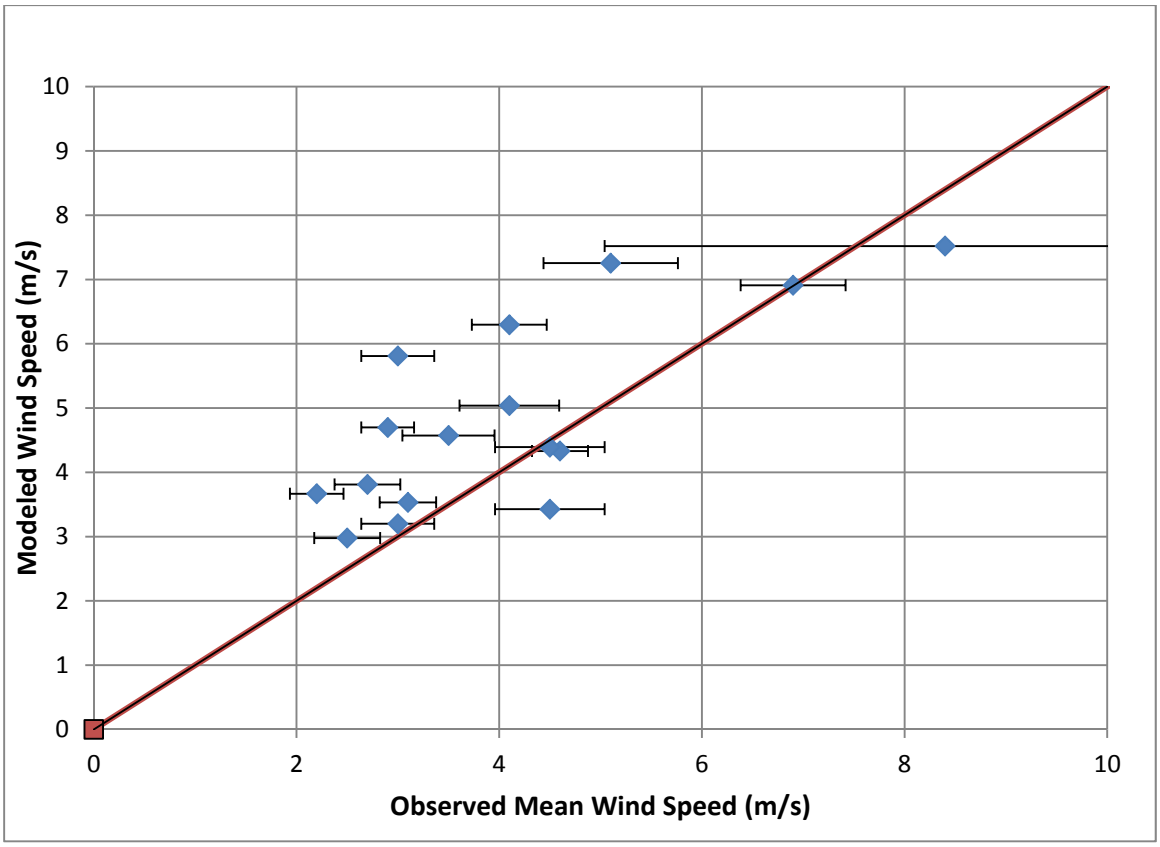

Figure 5.3 The comparison of the wind speed in m/s of the observations and the "original classification" (not using Froude) for the 16 wind stations

The majority of the modeled wind speed results in Figure 5.3 give an overestimation compared to the actual wind; the points are quite staggered and most are above the 1:1 diagonal. From Table-A XIV-1, a mean wind speed difference with the observations of 0.8 m/s and a standard deviation of 1.1 m/s is obtained.

By introducing the Froude number in the classification, as in classification variant 1 (2nd column), we obtained a correlation coefficient of 0.743 and the plotted points of the 16 wind stations for the modeled and observed wind speeds are shown in Figure 5.4. For this case, the mean wind speed difference has increased to 1.0 m/s, which indicates that for most of the stations, there has been an increase in simulated wind speeds.

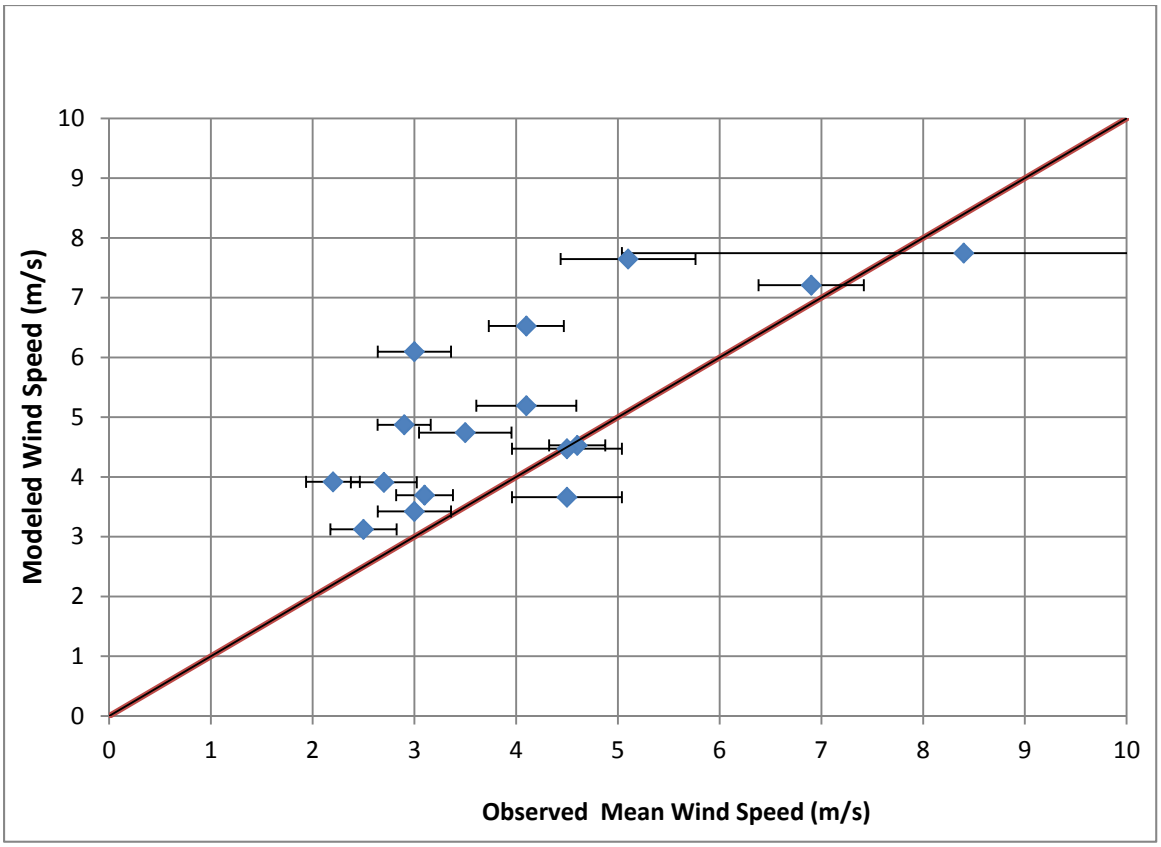

Figure 5.4 The comparison of the wind speed in m/s of the observations and the "classification variant 1 (without correction factors) for the 16 wind stations

Practically speaking, there has been no improvement of the wind speeds between classification variant 1 and the original classification when comparing with the observed wind measurements. Most points are still above the 1:1 diagonal, which indicates an overestimation of the modeled winds. As a matter of fact, when calculating the wind speed difference of all the stations between the variant 1 and the original classification as presented in Table 5.2, we see an average mean wind speed increase of 0.21 m/s with a standard deviation of 0.08 m/s. Meaning for most wind stations, the results have gotten worse, except for wind stations Whitehorse(#1), FlatMtn(#2) and JubileeMtn(#15); where the wind speeds were already underestimated, and this increase in wind speeds bring them closer to observed values. This suggests that even with the Froude number as a classifying criterion, which allows for more distinct climate states with more diverse atmospheric conditions to initialize, the overall results when averaged yield practically the same results as the original. This

means the Froude number criterion by itself, does not improve the results and does not make the wind speeds approach the values of the observations. The reason was seen in chapter 2.5, where it was mentioned that despite being able to capture the stable climate states, their frequencies of the stable climate states were not high enough compared to the other climate states to have a significant effect on the results. The method to remedy this issue is by adding the correction factors, as seen in classification variant 2.

Table 5.2 Wind speed difference between Original and Variant 1

Station Name	Station #	Reference	Simulations	Difference (m/s)
		Original	Variant 1	
Whitehorse A	1	4,33	4,53	0,20
Flat Mtn	2	7,52	7,74	0,22
Haeckel Hill	3	6,91	7,21	0,30
Annie	4	5,81	6,10	0,29
Fish	5	6,30	6,53	0,23
Fox Lake	6	3,81	3,91	0,10
Laberge	7	4,39	4,47	0,08
Watson	8	5,04	5,19	0,15
Wheaten	9	3,67	3,92	0,25
Braeburn	10	3,53	3,69	0,16
Champagne	11	4,70	4,87	0,17
Jakes	12	2,98	3,12	0,15
Mt Sima	13	7,26	7,65	0,39
Nursery	14	4,57	4,74	0,17
Jubilee Mtn	15	3,43	3,66	0,23
Marsh Lake	16	3,20	3,42	0,22
Mean Difference (m/s)				0,21
Standard Deviation (m/s)				0,08

In the case of the classification variant 2 (3rd column), a correlation coefficient of 0.782 and a mean wind speed difference of -0.1 m/s is obtained when compared with the observations. It is an improvement over the previous cases, and this improvement can be better viewed when plotting the modeled wind speeds points with the observation values, as shown in Figure 5.5.

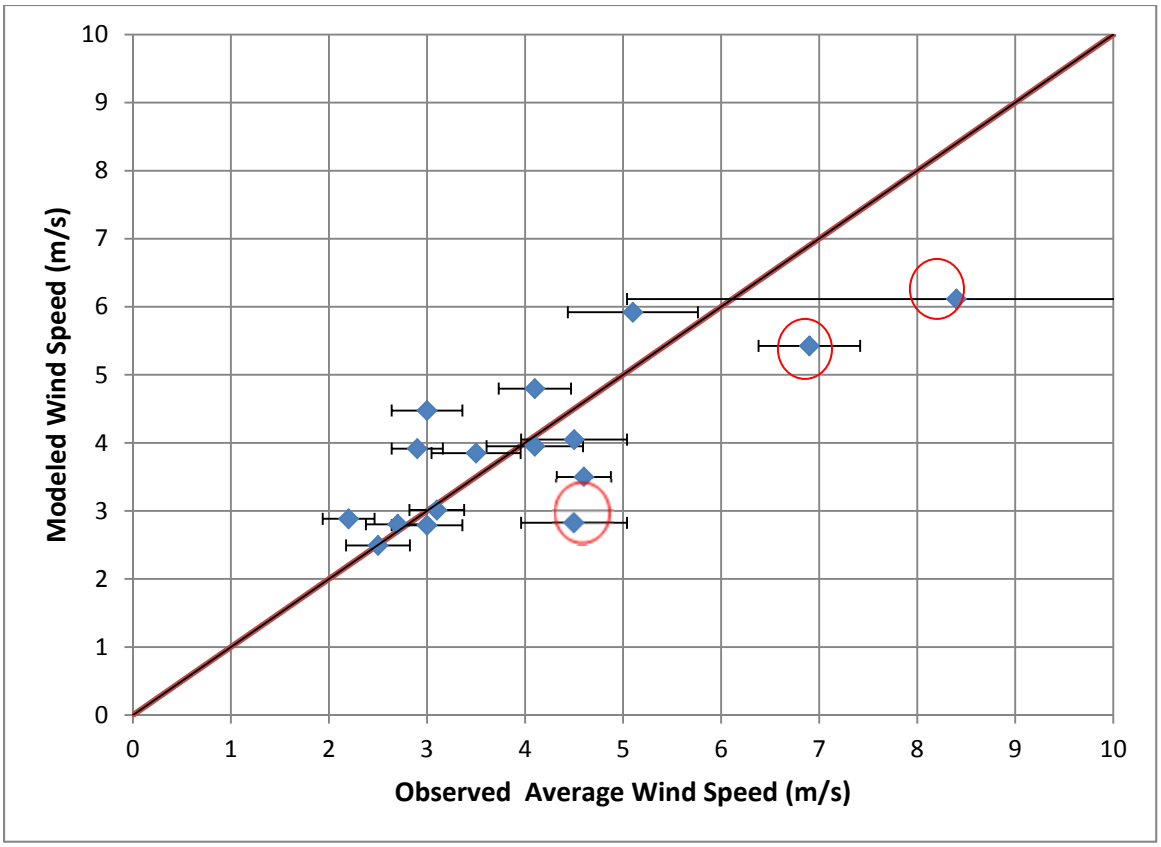

Figure 5.5 The comparison of the wind speed in m/s of the observations and the "classification variant 2" (using correction factors) for the 16 wind stations

Figure 5.5 shows that all modeled wind speeds have shifted down, and most points are now closer to the 1:1 diagonal, and thus, the overall results are closer to the observed wind speeds. The difference between classification variant 1 and 2 were calculated in Table 5.3, where the mean wind speed difference for the 16 wind stations was found to be -1.12 m/s, and a standard deviation of 0.45 m/s. All the simulated wind speeds have lowered; however, we can observe in Figure 5.5 that a few points are quite distant from the diagonal: two points on the right hand side of the graphs and one point on the bottom middle of the graph (circled in Figure 5.5). Coincidently, these three points are from the wind stations Flat Mtn(#2), Haeckell Hill(#3) and Jubilee Mtn(#15); three stations situated in the mountains at a high elevation: 1930, 1430, 1280 m ASL, respectively. Since the three wind stations mentioned above were already near the 1:1 diagonal, introducing the correction factors would naturally offset them to be lower and further from the observed values.

The overall wind speed reduction seen throughout the domain can be attributed to the correction factors. In Figure 5.6, all the climate state frequencies with the same wind speed class were added together, regardless of their direction sector, shear and Froude number bins; and the frequencies without correction factors (solid line) and the frequencies with the use of the correction factors (dashed) were plotted with respect to the 14 wind speed classes. We can see that with the use of the correction factors, the total frequency of the lower speed classes (i.e. low wind speeds) have vastly increased, and a reduction of the total frequency at higher speed classes is observed. This means that climate states with low wind speed as their initialization profile are more numerous; consequently, this will yield a higher number of low simulated wind speed, which will bring down the overall simulated wind speeds.

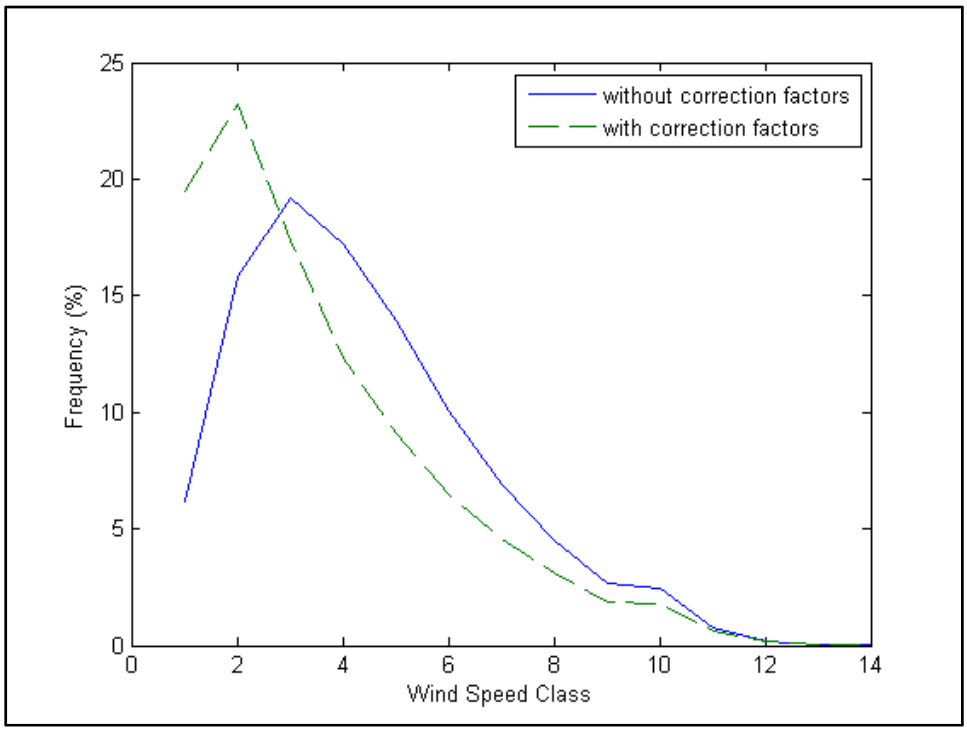

Figure 5.6 Total frequencies of climate states in same speed class with and without correction factors

Table 5.3 Wind speed difference between Variant 1 and Variant 2

Station Name	Station #	Reference	Simulations	Difference (m/s)
		Variant 1	Variant 2	
Whitehorse A	1	4,528	3,498	-1,03
Flat Mtn	2	7,745	6,113	-1,63
Haeckel Hill	3	7,208	5,425	-1,78
Annie	4	6,097	4,475	-1,62
Fish	5	6,525	4,797	-1,73
Fox Lake	6	3,910	2,803	-1,11
Laberge	7	4,472	4,048	-0,42
Watson	8	5,191	3,950	-1,24
Wheaten	9	3,918	2,884	-1,03
Braeburn	10	3,695	3,014	-0,68
Champagne	11	4,873	3,915	-0,96
Jakes	12	3,123	2,492	-0,63
Mt Sima	13	7,647	5,920	-1,73
Nursery	14	4,741	3,849	-0,89
Jubilee Mtn	15	3,660	2,825	-0,84
Marsh Lake	16	3,422	2,789	-0,63
Mean Difference (m/s)				-1,12
Standard Deviation (m/s)				0,45

In order to compare the changes between the simulated results and the observations, the wind speed differences with respect to the observations were calculated for each of the simulated cases and are presented in Table-A XIV-1. The mean wind speed average and standard deviation of the 16 stations was also obtained. From Table-A XIV-1, the mean wind speed difference of the original classification is 0.8 m/s with a standard deviation of 1.1 m/s. With the addition of the classification with Froude in the classification variant 1, the mean wind speed difference rises to 1.0 m/s with a standard deviation of 1.1 m/s. However, by also introducing the Froude classification with the correction factors, the mean wind speed difference with the observed values reduces to -0.1 m/s with a standard deviation of 1.0 m/s. These numbers suggest that using the new classifications scheme coupled with the corrected frequencies, it is possible to obtain wind speed results that are closer to the observations. The

classification allows certain climate states that give low wind speeds to appear, and the correction factors give more weight on these climate states in order to reduce the overall average speed of all the climate states.

5.2.2 Initial Reference Topography

In this second part, the results of the introduction of the initial reference topography are discussed. In chapter 3.1, the theoretical case found that with the introduction of init_topo, the flow would be reduced due to the lack of "drainage" and outflow, and we expected a similar outcome in this chapter. The Figure 5.7 shows the simulated wind speeds for each wind stations compared with their respective observations, for the case of the new classification with corrected frequencies and initial topography raised at 600 m ASL.

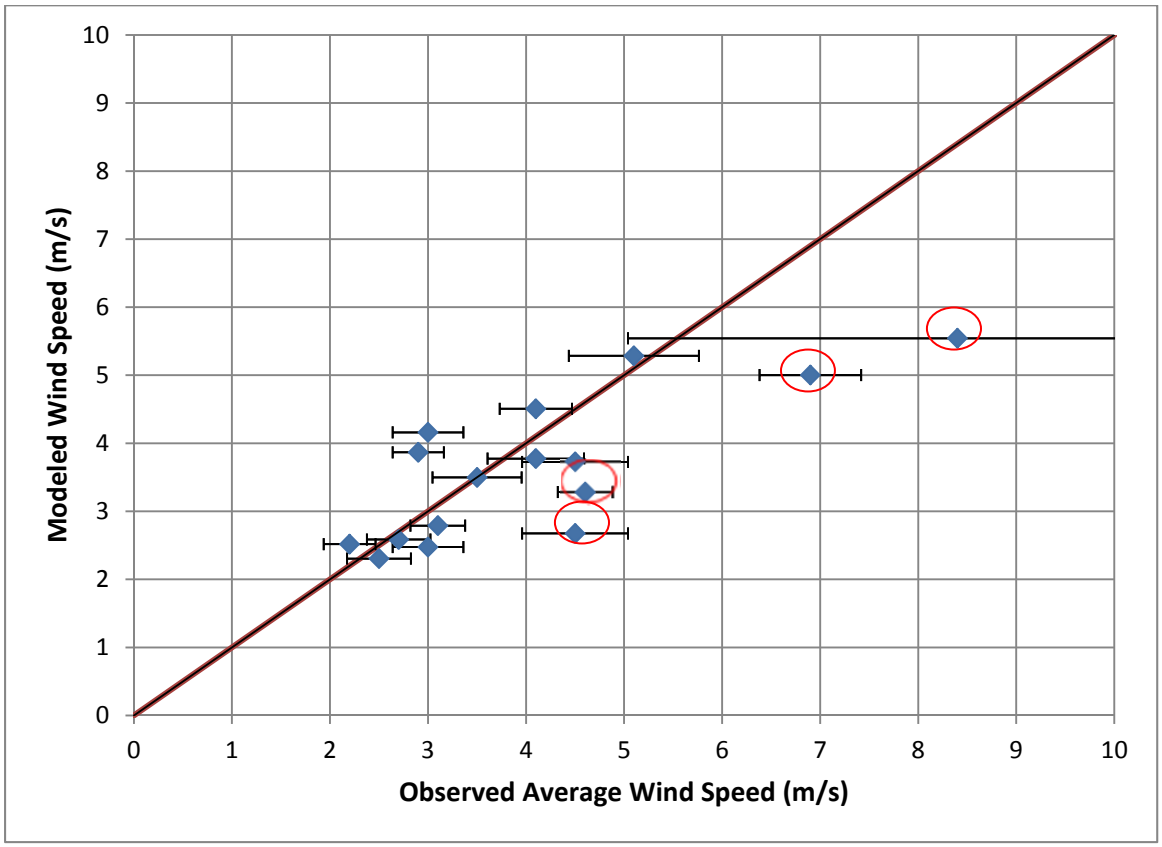

Figure 5.7 The comparison of wind speeds in m/s of the observations and the "classification variant 2 with initial reference topography" for the 16 wind stations

The data points are somewhat close to the observations, with a correlation coefficient of 0.7730 and a mean wind speed difference of -0.4 m/s; however, it is still possible to catch a few points that are far from the 1:1 ratio diagonal that mostly correspond to the wind stations FlatMtn(#2), HaeckelHill(#3) and JubileeMtn(#15). Again, these three stations were already quite below the diagonal, and there has been no improvements for them. In fact, the distribution of the data points is very similar to the simulations of classification variant 2. When the wind speed differences of the results for this simulation are compared with the simulations of classification variant 2, Table 5.4 is obtained.

Table 5.4 Wind speed difference between Variant 2 and Variant 2 with init_topo

Station Name	Station #	Reference	Simulations	Difference (m/s)
		Variant 2	Variant 2 topo	
Whitehorse A	1	3,498	3,284	-0,21
Flat Mtn	2	6,113	5,542	-0,57
Haeckel Hill	3	5,425	5,001	-0,42
Annie	4	4,475	4,159	-0,32
Fish	5	4,797	4,507	-0,29
Fox Lake	6	2,803	2,585	-0,22
Laberge	7	4,048	3,725	-0,32
Watson	8	3,950	3,775	-0,18
Wheaten	9	2,884	2,518	-0,37
Braeburn	10	3,014	2,789	-0,22
Champagne	11	3,915	3,867	-0,05
Jakes	12	2,492	2,305	-0,19
Mt Sima	13	5,920	5,286	-0,63
Nursery	14	3,849	3,498	-0,35
Jubilee Mtn	15	2,825	2,675	-0,15
Marsh Lake	16	2,789	2,475	-0,31
Mean Difference (m/s)				-0,30
Standard Deviation (m/s)				0,15

Table 5.4 shows that for the case with the added initial reference topography at 600m, there has been a mean wind speed reduction of -0.30 m/s, with a standard deviation of 0,15 m/s. As a matter of fact, all the wind stations' wind speeds have been reduced, as demonstrated by the negative signs.

One of the speculated reasons for this is that the terrain in the center of the grid is much more complex than a simple plateau as seen in section 3.2, and the topography weighs more to the results than the simple effect of elevating the initial topography. The flow is forced through channels and valleys, and therefore, will mostly flow in one set directions. The improvement to the height around the perimeter of the grid has little effect on the flow compared to the strong effects by the topography in the middle of the grid. Nonetheless, it is still possible to see an overall reduction of the wind speeds created by the higher reference topography as shown by the speed reduction for all stations in Table 5.4 and in Figure 5.8; which shows the speed reduction throughout the simulated region, especially around the elevation of the initial reference topography. The topography is represented as the contour lines, and the wind speed difference is represented as the filled contours.

This reduction in wind speed is believed to be explained by a reduction of the flow drainage from the elevated initial topography. By raising the initial reference topography, the cliffs on the edges of the simulated region are not as high. Since these cliffs are not as deep, the forcing of the flow outward is not as prominent, and in turn, the flow in the model is not sped up by it and all wind stations slow down due to reduced drainage. Naturally, this makes the overestimated simulated wind speeds to be lower and closer to the observations; and the underestimated wind speeds to be even lower and further from the observations. With a mean wind speed difference of -0.4 m/s, a decrease of 0.03 m/s from the case of classification variant 2, the added feature does not necessarily provide better results for this specific experiment when compared with the 16 wind stations.

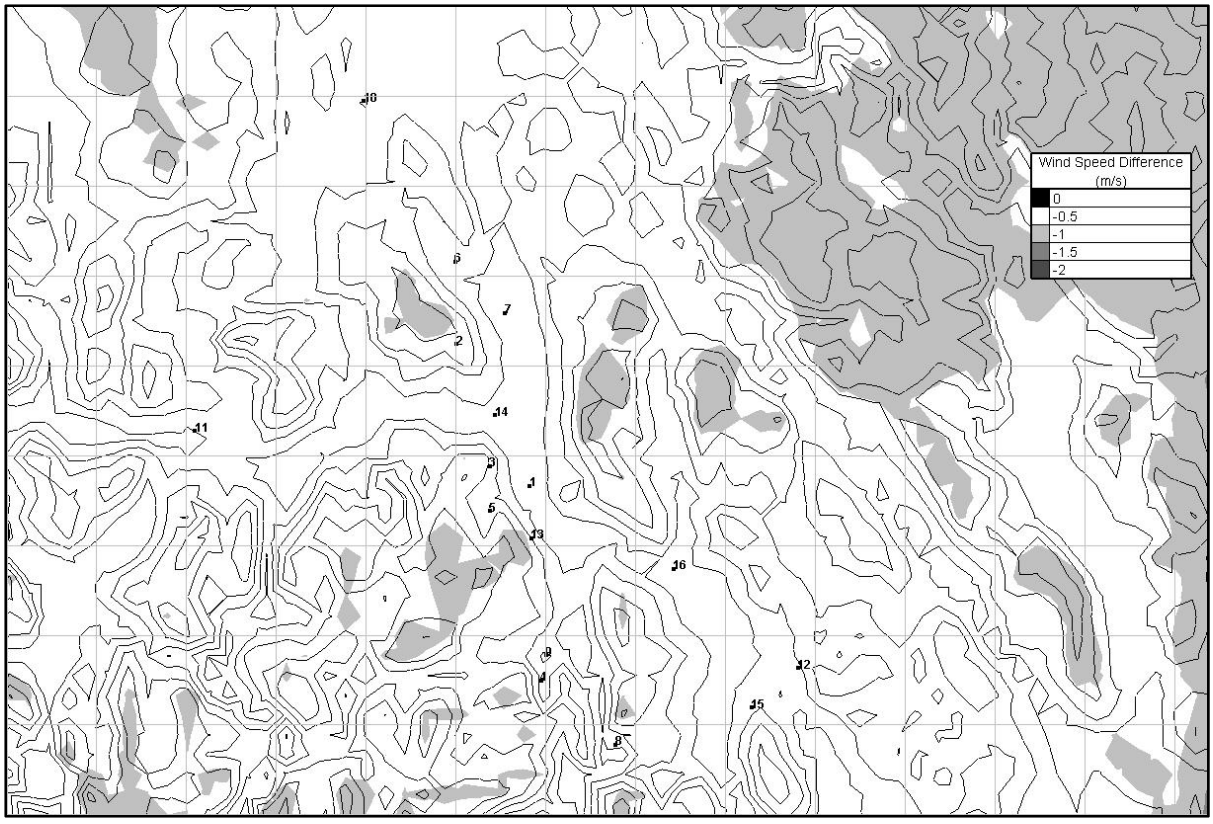

Figure 5.8 Map of wind speed difference of the classification variant 2 with respect to the classification variant 2 with init_topo at 600m

5.2.3 Low level profiles

The third part involves the introduction of the module that ignores data levels below the topography during the initialization process, also referred as kdrop. This was added to correct the possible initialization error of the geostrophic wind. The module was first added to the case of classification variant 2 and it was compared with the simulation of classification variant 2 without the module. The differences of this comparison for the wind stations are shown in Table 5.5.

For the simulation with the module, the wind speeds are found to be above, as well as below the simulation without the module for the various wind stations. The mean wind speed difference obtained was -0.08 m/s, with a standard deviation of 0.19 m/s. There are small

changes in wind speeds; however, distinguishing a pattern for these specific changes was not successful.

The wind speed results for this simulation are compared to their respective observation data points in Figure 5.10. The winds at the data points' positions are fairly similar to the previous cases (Figure 5.5 and Figure 5.7), with values from wind stations FlatMtn(#2), HaeckelHill(#3) and JubileeMtn(#15) being once again, quite below the observed wind speeds and even lower than for variant 2. This particular effect is traced back to the results of classification variant 2, where the effect of correction factors reduced the modeled wind speeds of these points.

One of the main reasons for implementing the kdrop key is to initialize the wind with the right values, especially in terms of direction. The classification tables and climate states that were used to bring up this issue in Pinard *et al.* (2009) are different than the ones used in this study[6]. In Pinard *et al.* (2009), the climate states showed a predominance of the wind coming from the south-east direction, which would result in erroneous wind directions. In this study, despite using the same Reanalysis point for the classification scheme, a different set of climate states were obtained. The set of climate states use in the study coincidently yielded an appropriate predominance of the wind from the south-west and this would result in good overall wind directions, similar to the observations. There was no modifications done to the code that classifies by direction in this study, and it can be seen (from Figure 2.11, Figure 2.12 and Figure 2.13) that good wind directions were obtained from the start with the Original Classification. Further investigations were done and it was concluded that certain undocumented changes to the code of the classification had been done between the classification scheme used to obtain the climate states for Anemoscope and the new classification scheme used in this study. Understanding what was just discussed, it is clear that the kdrop key used to obtain the results in Figure 4.4 does not yield any improvements in overall wind directions, since the climate states did not need to be fixed and already had the

[6] It was impossible for use to reproduce these climate states with the classification code we had.

appropriate wind direction for initialization, as shown in Figure 5.9. The roses already have wind directions coming from the West, which forces the proper wind direction initialization.

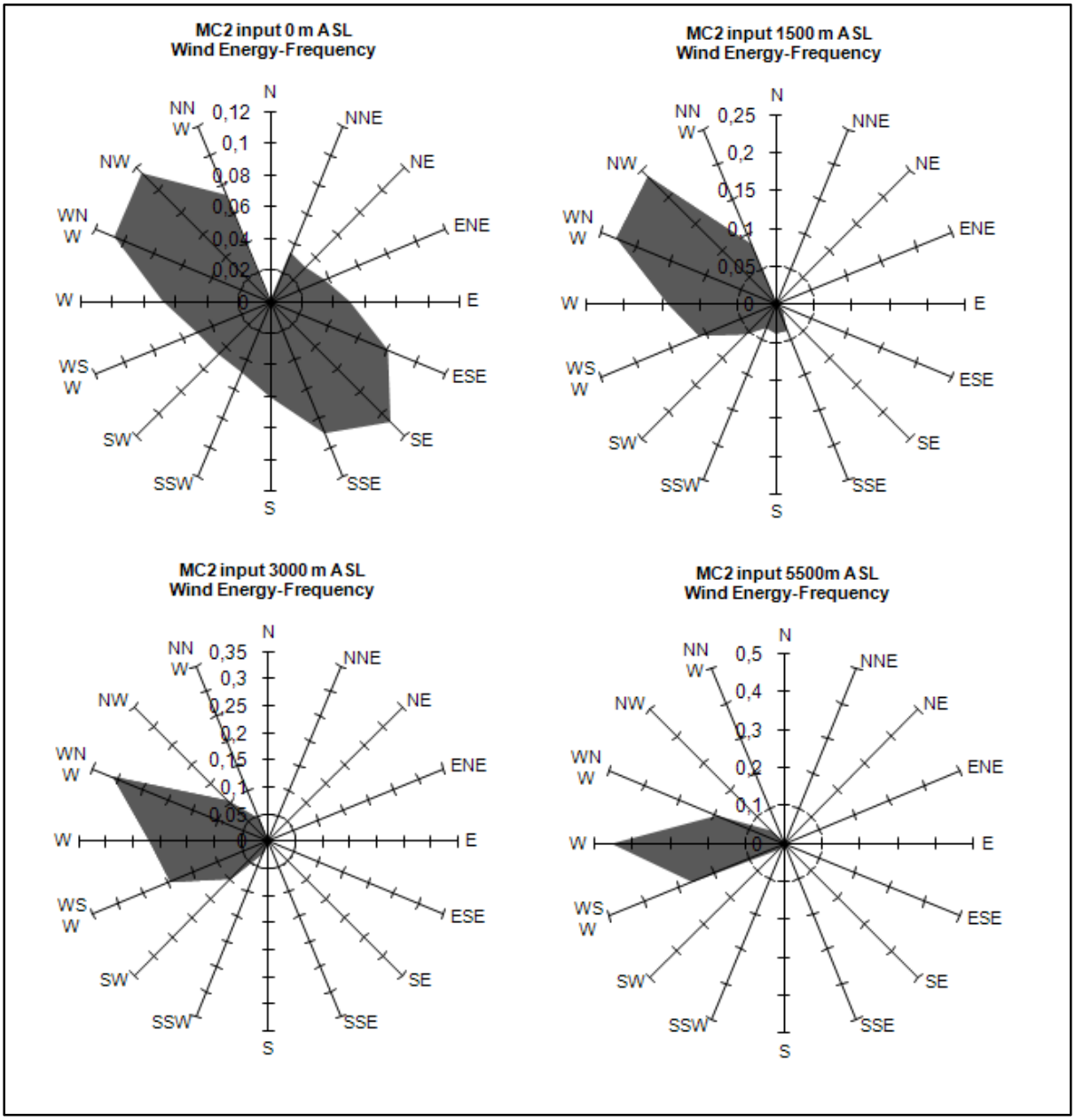

Figure 5.9 The wind energy frequency roses of Reanalysis from Original Classification

Table 5.5 Difference between Variant 2
and Variant 2 with kdrop

Station Name	Station #	Reference	Simulations	Difference (m/s)
		Variant 2	Variant 2 kdrop	
Whitehorse A	1	3,498	3,413	-0,08
Flat Mtn	2	6,113	6,027	-0,09
Haeckel Hill	3	5,425	5,103	-0,32
Annie	4	4,475	4,485	0,01
Fish	5	4,797	4,857	0,06
Fox Lake	6	2,803	2,832	0,03
Laberge	7	4,048	4,163	0,12
Watson	8	3,950	4,099	0,15
Wheaten	9	2,884	2,647	-0,24
Braeburn	10	3,014	3,159	0,15
Champagne	11	3,915	4,118	0,20
Jakes	12	2,492	2,171	-0,32
Mt Sima	13	5,920	5,839	-0,08
Nursery	14	3,849	3,467	-0,38
Jubilee Mtn	15	2,825	2,548	-0,28
Marsh Lake	16	2,789	2,547	-0,24
Mean Difference (m/s)				-0,08
Standard Deviation (m/s)				0,19

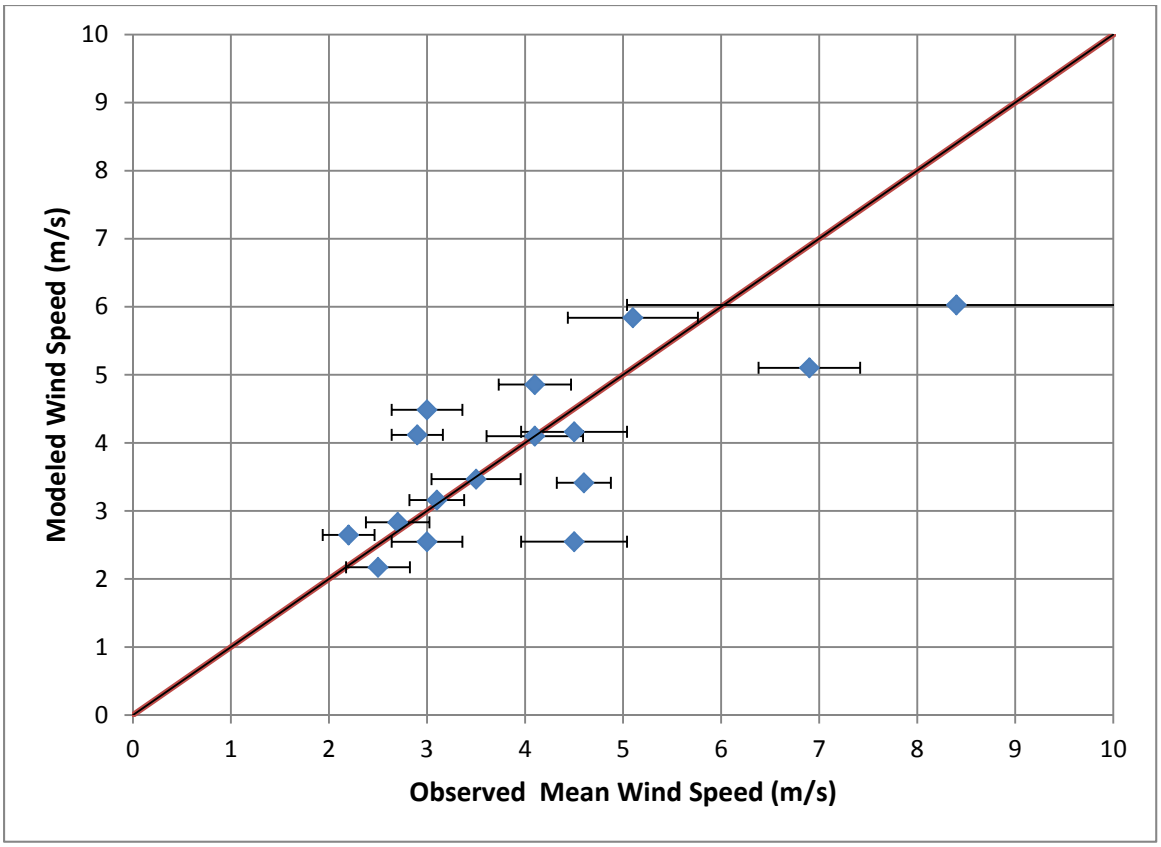

Figure 5.10 Comparison of wind speeds in m/s of the observations and the "classification variant 2 with kdrop" for the 16 wind stations

5.2.4 Effects on Past Studies

To show the effect of the kdrop module, a simulation was performed using the exact climate state tables from the past studies (with the wrong lower level wind directions) without the module, and a simulation using said climate states with the kdrop module. The Reanalysis point used is 61/90, which is the equivalent of the Reanalysis point 17\18 of this study. Figure 5.11 shows the overall wind flow of the experiment without the module for the region of Whitehorse. The wind in the Whitehorse valley flows correctly in the northward direction; however, the wind in the Takhini Valley flows in the westward, which is the opposite direction of what is observed. In addition, the winds in higher altitude also flow in the northward direction, while they are supposed to flow in the north-eastward direction. As for the experiments with the kdrop module, the "kncep_drop" key was set to a value of two.

According to Figure 4.1, a value of two is appropriate, since the wind directions at 3000m ASL for the Reanalysis indicate the proper direction to initialize the model. Figure 5.12 shows the wind flow of the experiment with the kdrop module. The wind in the Whitehorse Valley is still northward; however the wind in Takhini valley is no longer westward and has been corrected to the east. Furthermore, the wind in high altitudes has also been corrected to be going in the north-eastward directions.

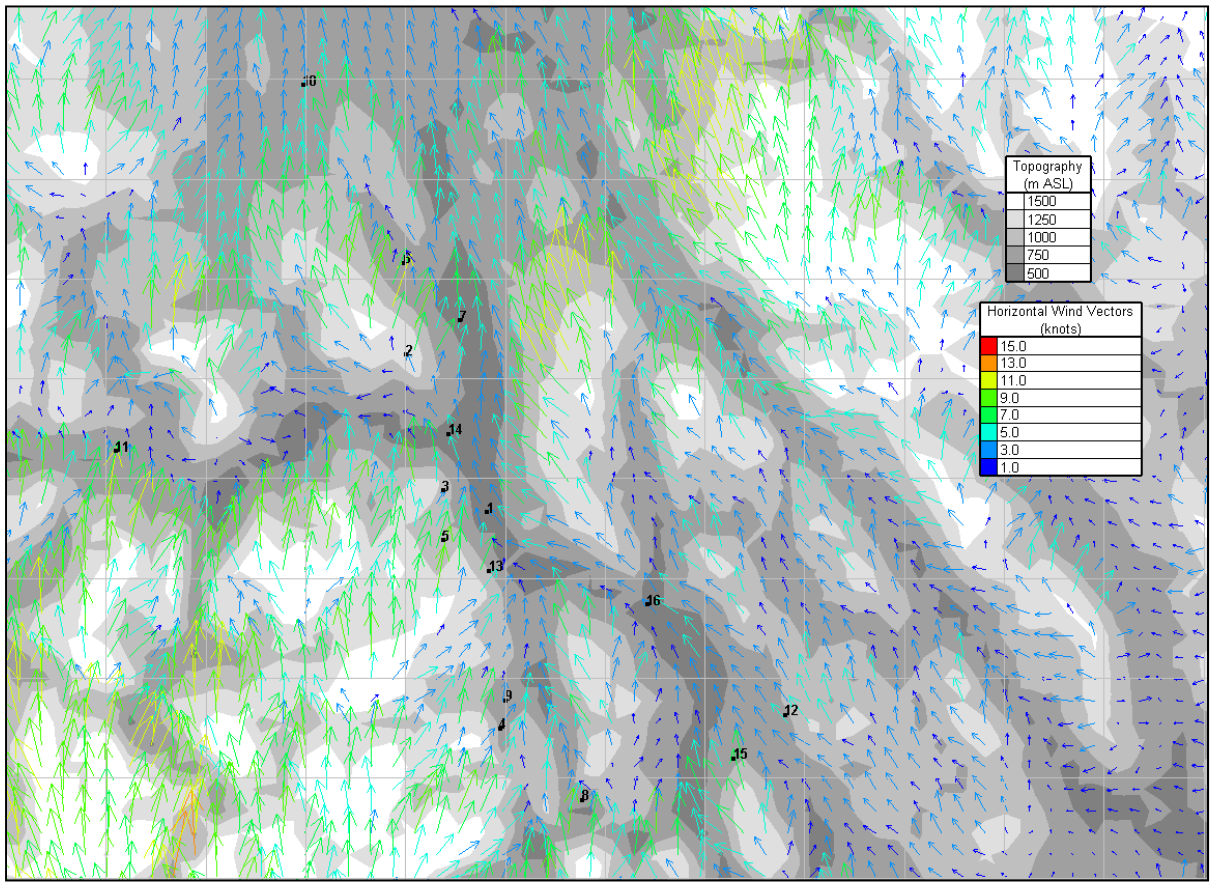

Figure 5.11 The simulated wind flow of the climate states from WEST database and used in Pinard *et al.* (2009)

The kdrop module with "kncep_drop" set to two was successful due to the wind direction at the third level being in the proper direction. With the wind going to the northeast, not only does this direction give proper high altitude with directions, but the east component of this geostrophic wind allows the wind in the Takhini valley to flow eastward. If the simulations

had used the first level to initialize, with the north-westward wind, it would have created a pressure gradient in the south-westward direction, and the west component of that pressure gradient would have forced the wind in the Takhini valley to flow in the westward direction. This shows that if the climate states directions at the lower levels are erroneous, but the direction on the higher levels are correct and appropriate to initialize, the kdrop key can be used in order to obtain a better initialization.

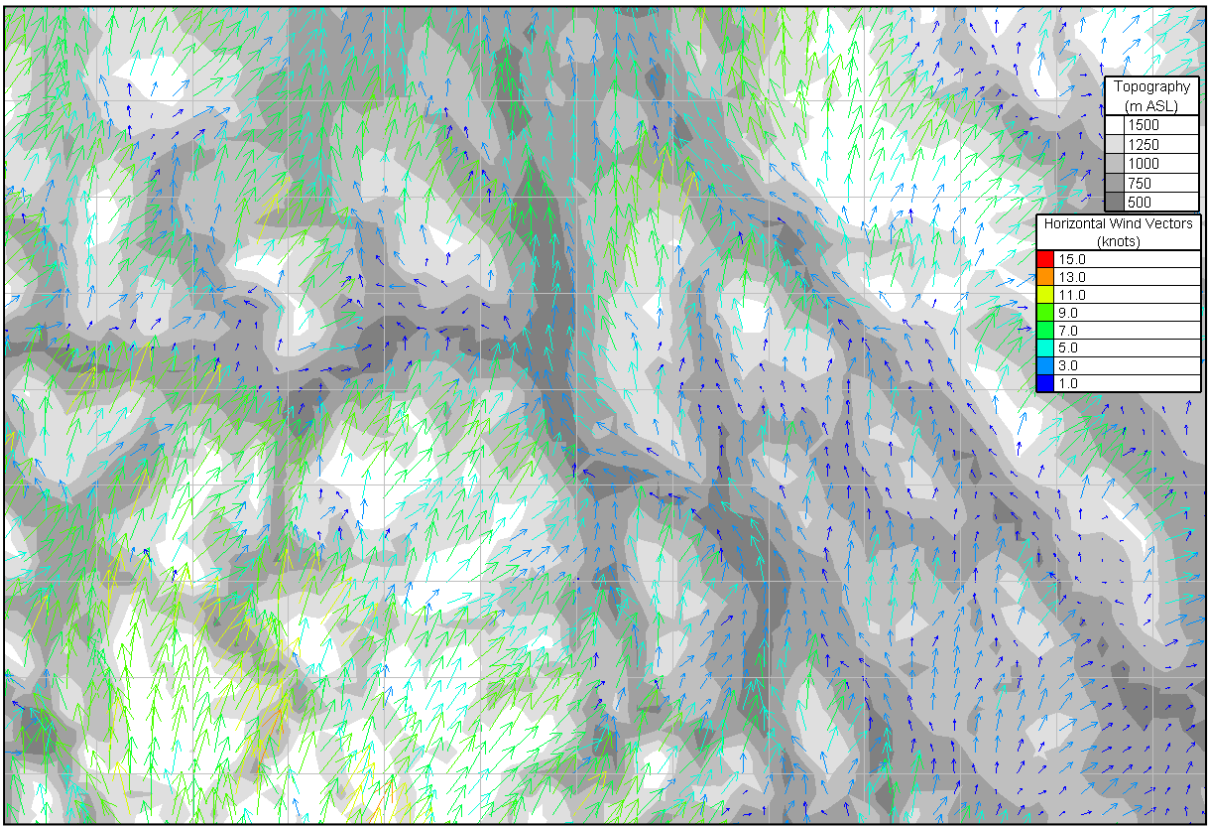

Figure 5.12 The simulated wind flow of the climate states from WEST database and used in Pinard *et al.* (2009)

CHAPTER 6

FINAL SIMULATION

6.1 Results

In the final simulation, all the modifications and modules have been implemented: the new classification scheme with Froude number, the correction factor that modifies the climate state frequencies, the initial reference topography raised at 600, and the kdrop module set to one that allows the initialization to ignore the Reanalysis data below the topography and instead uses the data level above it. The MC2 results of the 736 climate states were obtained, and similarly to all simulations in this study, they were post processed in WESTATS to give the directions shown in Figure 6.1 and the wind magnitude in Figure 6.2. The overall directions of the wind in the Whitehorse Valley, Takhini Valley, and at higher altitudes are northward, eastward, and north-eastward respectively. As for the magnitude, we see wind speeds of 1-3 m/s in the valleys, and 3-5 m/s in the mountains. In addition, the wind frequency roses of the final simulation were obtained at the position of the 16 wind stations in annex XV. Most of these wind direction roses are in general agreement with the observed wind directions found in Figure 5.2, except for wind stations HaeckelHill(#3), FoxLake(#6), Watson(#8), MtSima(#13) and Jubilee(#15).

The Whitehorse Upper-air Radiosondes in Figure 5.2 were also compared with extracted direction frequency roses at the same heights (714, 1200, 1400, 1700, 1900 and 2500 m ASL) for the location of Whitehorse. The simulations were able to capture the clockwise veering of the wind with height. However; the northward wind at the first level changed direction much faster and settles in a more eastward direction as early as 1200 m, where as the Upper-air Radiosondes tends to gradually veer to the north-eastern in the span of 2500m. As for the wind speeds, although increasing with height, the simulated wind speeds are lower than ones recorded by Upper-air Radiosondes. We believe these low wind speeds are effect of the correction factors reducing the wind speeds not only throughout the region but also in altitude.

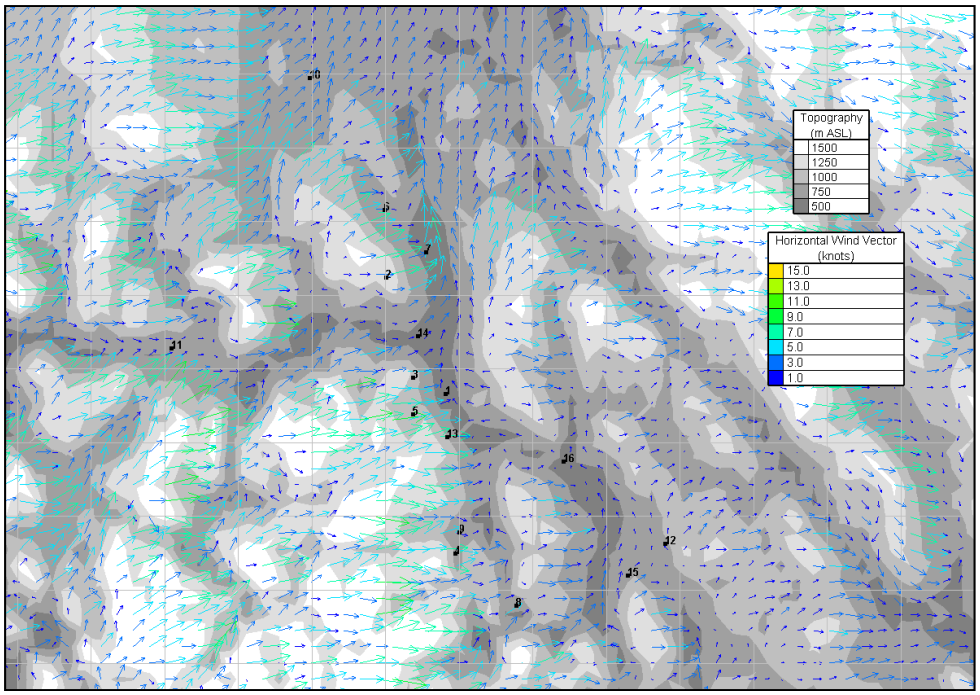

Figure 6.1 The simulated wind flow for the climate states of the final simulation involving all the modifications

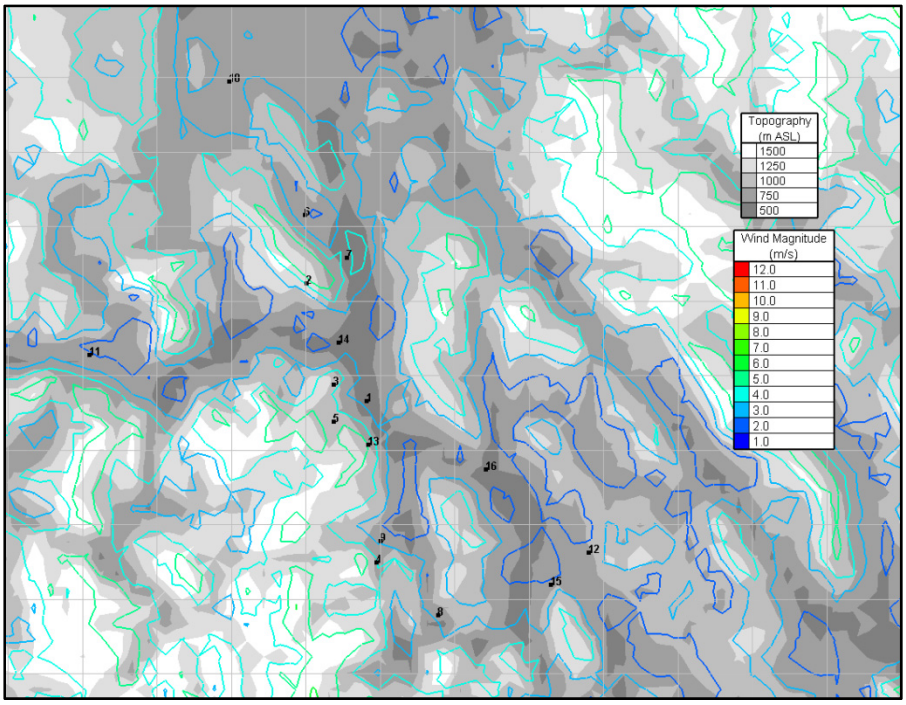

Figure 6.2 Wind speed for final simulations

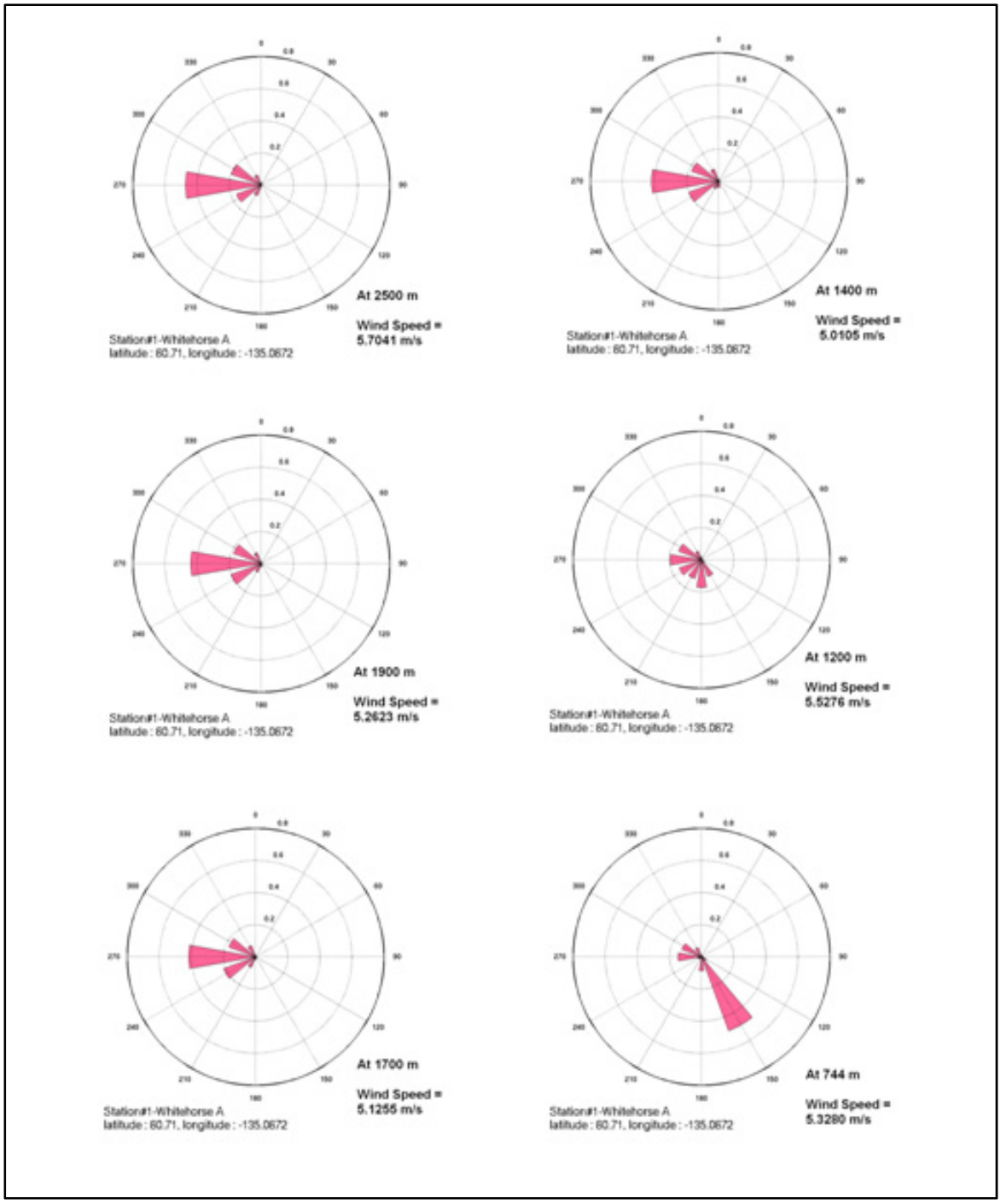

Figure 6.3 Simulated direction frequency rose of Whitehorse at height levels

6.2 Comparison

The results are first compared with the simulation that involved all the modifications, except the kdrop module. This will allow us to see the changes to the results that the kdrop module brings, with respect to the results from the preceding simulated case. Table 6.1 shows the wind speed differences for each wind stations. The wind is increased and decreased at different points due to the difference in the initialization using values at higher levels and the mean wind speed difference is -0.05 m/s and standard deviation is 0.14 m/s; however, no clear improvement could be highlighted.

Table 6.1 Wind speed difference between the final simulation and Variant 2 with init_topo

Station Name	Station #	Reference	Simulations	Difference (m/s)
		Variant 2 topo	Final	
Whitehorse A	1	3,284	3,238	-0,05
Flat Mtn	2	5,542	5,494	-0,05
Haeckel Hill	3	5,001	4,729	-0,27
Annie	4	4,159	4,088	-0,07
Fish	5	4,507	4,501	-0,01
Fox Lake	6	2,585	2,638	0,05
Laberge	7	3,725	3,840	0,11
Watson	8	3,775	3,875	0,10
Wheaten	9	2,518	2,377	-0,14
Braeburn	10	2,789	2,900	0,11
Champagne	11	3,867	4,073	0,21
Jakes	12	2,305	2,123	-0,18
Mt Sima	13	5,286	5,167	-0,12
Nursery	14	3,498	3,307	-0,19
Jubilee Mtn	15	2,675	2,509	-0,17
Marsh Lake	16	2,475	2,344	-0,13
Mean Difference (m/s)				-0,05
Standard Deviation (m/s)				0,14

Next, the wind speed results of the 16 wind stations for this simulation were compared with the observations, as shown in Table 6.2, and a scatter point graph comparing both data is shown in Figure 6.4. The mean wind speed difference and standard deviation are -0.5 m/s and 1.1 m/s, respectively. In Figure 6.4, the simulated points are closer to the 1:1 diagonal line, but we still observe the wind stations FlatMtn(#2), HaeckelHill(#3) and JubileeMtn(#15) with underestimated wind speeds, similar to the case in Figure 5.5.

Table 6.2 Wind speed difference between the final simulations and the observations

Station Name	Station #	Reference	Simulations	Difference (m/s))
		Observation	Final	
Whitehorse A	1	4,6	3,238	-1,4
Flat Mtn	2	8,4	5,494	-2,9
Haeckel Hill	3	6,9	4,729	-2,2
Annie	4	3,0	4,088	1,1
Fish	5	4,1	4,501	0,4
Fox Lake	6	2,7	2,638	-0,1
Laberge	7	4,5	3,840	-0,7
Watson	8	4,1	3,875	-0,2
Wheaten	9	2,2	2,377	0,2
Braeburn	10	3,1	2,900	-0,2
Champagne	11	2,9	4,073	1,2
Jakes	12	2,5	2,123	-0,4
Mt Sima	13	5,1	5,167	0,1
Nursery	14	3,5	3,307	-0,2
Jubilee Mtn	15	4,5	2,509	-2,0
Marsh Lake	16	3,0	2,344	-0,7
Mean Difference (m/s)				-0,5
Standard Deviation (m/s)				1,1

For the sake of perspective, a comparison between the results of the modeled wind in the final simulation with all the modification implemented, and the results obtained with the original classification and original version of MC2 was performed. It is clear that there was

an improvement of the simulated winds with WEST. Indeed, the wind speed difference with the observations went from 0.8 m/s to -0.5 m/s (Table-A XIV-1). The biggest improvement to the simulated wind speeds was due to the classification involving the Froude number with the correction factors, where the mean wind speed difference was reduced to a value of -0.1 m/s. The Froude number criterion allowed the classification scheme to capture stable climate states (as seen in the Whitehorse climatology), and the correction factors augmented the frequency of these climate states, giving them more importance in the overall results after post processing through WESTATS. This in turn, would reduce the wind speeds and make them approach the observation values. On a side note, it is worth mentioning that the classification variant 3 (in annex VI) was able to obtain a mean wind speed difference of 0.0 m/s and a standard deviation of 0.1 m/s, which seems to indicate that good predictions are possible even without the shear classifying criterion; and this variant takes significantly less computing time.

Furthermore, with the implementation of the initial reference plane at 600 m ASL, a further reduction, averaging 0.3 m/s for all 16 wind stations, has been observed for simulated wind speeds. This reduction is small compared to the effect of the correction factors, but it was consistent throughout all 16 wind stations and is caused by raising the initial reference topography, which reduced the flow drainage by the contours of the domain. Lastly, the modification by the kdrop module provided the least improvement to the simulated wind speeds. The changes by adding the module were not significant, and no distinct pattern on the wind speeds could be discerned, as some simulated wind speed increased, and others decreased. Had the climate states used to initialize been different, such as the dubious 0m ASL states used in Pinard *et al.* (2009) with erroneous geostrophic wind directions, larger improvements might have been possible.

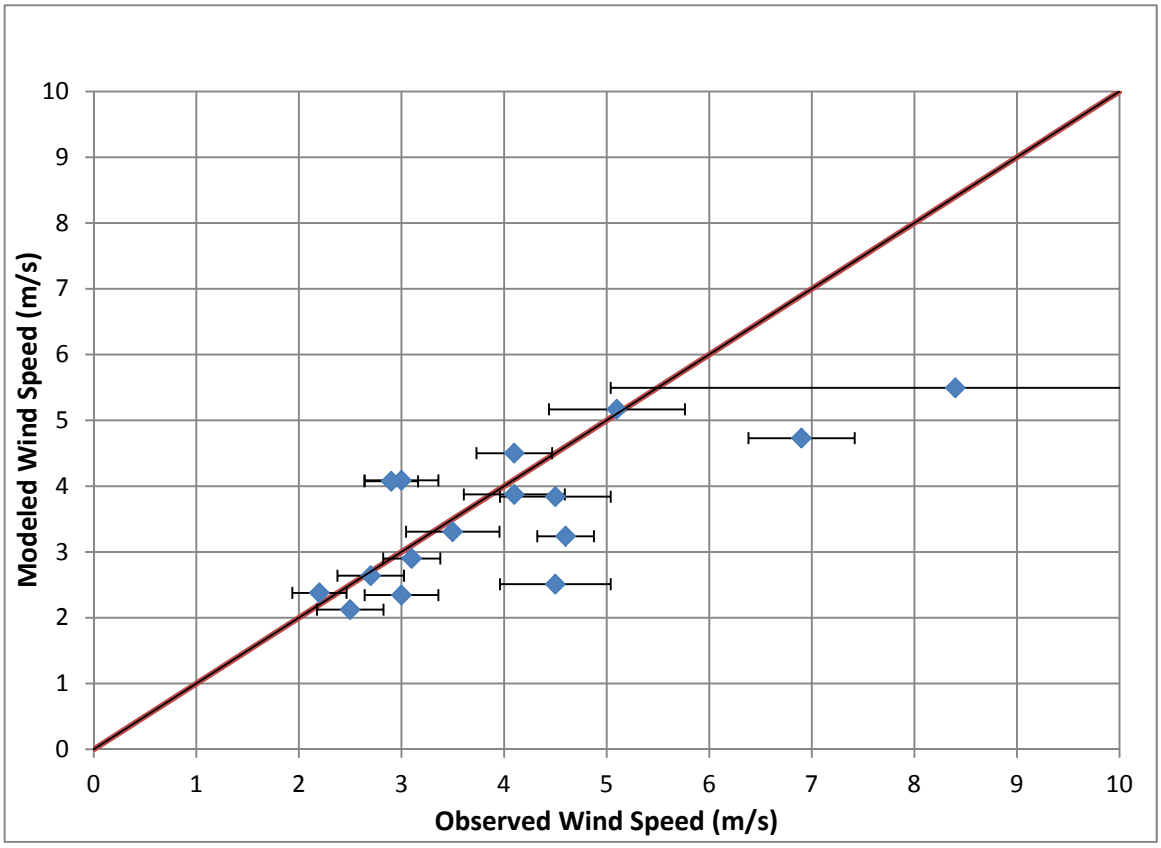

Figure 6.4 Comparison of wind speed in m/s between the observations and the final simulations

CONCLUSION

To conclude, it was shown that the new classification including Froude numbers was able to capture the distinct stability of the climate states, and with the essential aid of correction factors, the simulated wind speeds of the region of Whitehorse were reduced and closer to the observations. In addition, the implementation of raising the initial reference topography also reduced the overall modeled wind speed of the domain, but only by a marginal amount compared to the new classification. Another improvement allowed by this study was the correction of the direction of the simulated wind. Depending on the case and the profile available to initialize, the new module kdrop is able to use the higher profile values to initialize and correct the wind directions. Out of all the classification variants and modifications implemented, the classification variant 2 was closest to the observations, with a mean wind speed difference of -0.1 m/s.

It is important to mention that these modifications and improvements have only been tested on the region of Whitehorse, using a specific NCEP/NCAR Reanalysis point as input for the classification scheme. If other regions are tested, one must remember that the correction factors were only generated for the Western Canada and should not be applied globally anywhere. This type of correction is deemed applicable in cold mountain regions. If considered useful to apply this technique, Radiosonde data from the region surrounding the targeted wind mapping area should be used to derive new generalized correction factors to obtain accurate climate state frequencies. One might also have to perform a study on the climatology of the region in question in order to see the relevance of using the kdrop module.

Other outlooks related to this study may be considered, such as:

An improvement on the method of the correction factors being applied to the frequencies of the climate states. Instead of modifying the frequencies of the climate states across the board that simply match the Froude bin of the correction factors, an additional step should be added such that the original frequency of a climate state family is maintained, but the climate state

Froude subdivision frequencies would change. Meaning the correction factors would only change the frequencies of the Froude bins within the same climate states, but whenever these frequencies are added again, the sum of the same frequency remains as originally.

A study on the sensitivity of the wind flow with respect to the value of the initial reference topography may bring a more thorough understanding of the effects of this modification.

Program and automate the process of getting the temperature values directly from the NCEP/NCAR Reanalysis database and link them to the model setting files for the purpose of calculating the horizontal temperature gradient for thermal wind.

Verification of the frequencies of the Froude number bins of Yukon using another large scale data set, such as NARR (North American Regional Reanalysis), and compare them with respect to NCEP

Port the MC2 4.9.6 version used in the WEST software to the MC2 4.9.8 version and to the MC2 4.9.9 version, so as to test again the merit of the new classification with Froude number and the init_topo and kdrop modules. Pinard *et al.* (2009) had mentioned the benefits of better numerics for rugged terrain to improve the wind resource mapping.

ANNEX I

CLASSIFICATION ALGORITHM

This section enumerates and details the steps of the classification algorithm used in this study. The classification algorithm can basically be divided into 7 main steps.

1) Definition of parameters, variables, and settings.

2) Loop over entries of the climate data base by time:

    a) Read *gz, tt, hr* of each grid point;
    b) Use *gz, tt* and *hu* (converted from hr) to calculate the geostrophic wind vg;
    c) Use *vg* and *tt (th)* and calculate the Brunt-Väisälä frequency and Froude number;
    d) Classify into shear bins and Froude bins (if activated);
    e) Classify *vg* in wind direction sector and wind speed class of the sector.

3) Post processing:

    a) Modifying the frequency of each Froude bins with correction factors;
    b) Ignore shear distinction for the first wind speed class and no shear distinction for classes with frequency < 0.02;
    c) Calculate the mean profiles for each class;
    d) Calculate the frequency for each class at each grid point.

4) Write the results into one big standard file.

5) Prepare the output directories.

6) Use the standard file to write one text file for each grid point with all occurring classes into the output directory.

7) Calculate the weight of each class for each grid point and sort the classes output in table.ef files

The following describes the seven steps enumerated above, and explains thoroughly the procedure and the important keys and variables used.

1) The basic parameters must be defined. This includes the directories for in- and output, the time period, the seasons, the heights, the method of interpolation ("hydrostatic" or "linear"), the number of wind sectors, the wind speed classes, the class division of the wind speed. All these parameters must be chosen in classification.ksh

   In addition, the new classification incorporates a parameter (“nofrd”) that can be toggled on or off, depending if the classification by Froude number is desired. If “nofrd” is set to .true., Froude number is not used as a classification criterion and Froude number bins are not incorporated into the classification. If “nofrd” is set to .false., Froude number is used as a classification criterion and Froude number bins will be incorporated into the classification.

   The variable “xmesh” defines the limit of Froude number bins. There are 32 set of numbers increasing in size, where the first number defines the lower limit of the bin and is inclusive and the following number sets the higher limit of the bin and is non-inclusive. ex: [0, 0.0516); [0.0516, 0.1032)

   The variable “fcorr” goes in tandem with “xmesh” and defines the correction factor at which each frequency of the Froude number bins will be multiplied to. There is the same amount of numbers as the variable “xmesh”, and each number in the sequence of “fcorr” corresponds to its respective Froude number bins defined in “xmesh”.

Furthermore, when “nofrd” is set to .false., the new classification offers the possibility to classify without shear. The key “noshear” controls that function of the classification program. When the key “noshear” is set to .false., the classification program will classify the data in terms of direction sectors, speed classes, Froude numbers bins and shear bins. However, when the key “noshear” is set to .true., the classification program will classify the data in terms of direction sectors, speed classes and Froude number bins. Therefore, ignoring the shear bins. This key allows the number of possible climate states to be reduced by half, and facilitate the computational load.

&gz2vg_cfg
season = '${s}', version = 1
ip1s = 1000, 850, 700, 500
height = 0., 1500., 3000., 5500.
method = 'hydrostatic'
shearvec = .false.
byear =1958, bmonth = 01, bday = 01, bhour = 00, sampling = 6
eyear = 2000, emonth = 01, eday = 01, ehour = 00
region = ''
indir = '${INDIR}'
outdir = '${DATADIR}'
ofile = 'classes_${s}.fst'
swtt = .true., swph = .true.
nofc = .false., noms = .false.
nsect = 16
nclass = 14
classes = 0.2, 2., 4., 6., 8., 10., 12., 14., 16., 18., 22., 26., 30., 34.
generalclas = .true.
flat_s = -5., flat_n = 10.
nofrd = .true.
noshear = .false.
xmesh = 0.0000, 0.0516, 0.1032, 0.1548, 0.2065, 0.2581, 0.3097, 0.3613, 0.4129, 0.4645, 0.5161, 0.5677, 0.6194, 0.6710, 0.7226, 0.7742, 0.8258, 0.8774, 0.9290, 0.9806, 1.0323, 1.0839, 1.1355, 1.1871, 1.2387, 1.2903, 1.3419, 1.3935, 1.4452, 1.4968, 1.5484, 1.6000
fcorr = 24.967, 8.877, 3.818, 2.030, 1.306, 0.931, 0.775, 0.704, 0.638, 0.595, 0.587, 0.516, 0.517, 0.513, 0.526, 0.521, 0.654, 0.671, 0.594, 0.753, 0.730, 0.716, 0.774, 0.841, 0.945, 1.083, 1.042, 0.966, 1.339, 1.570, 1.264, 0.800

The parameters for the grid of the climate data base must be set in */grids/classification_settings.nml*. Therefore the number of grid points, the grid

resolution, the grid projection, and for rotated grids the coordinates of the center and the equator and the reference point must be specified.

&grille
Grd_ni = 60 , Grd_nj = 26, Grd_dx= 2.5,
Grd_iref= 1, Grd_jref= 1, Grd_latr= 30. , Grd_lonr= 140.
Grd_proj_S= 'L', Grd_phir= 0.0 , Grd_dgrw= 0.0
Grd_xlat1= 0., Grd_xlon1= 240.,Grd_xlat2= 0., Grd_xlon2= 330.,
/

2) In order to use the classification program, the input climate data files must be stored in monthly std-files names *yearmonth*. Otherwise, the *"read data"* passage of the code in *gz2vg.ftn* must be changed.

A loop over each time steps begins for the input climate data files. In the case of seasonal statistics, dates out of the season are skipped.

a) Fields with the dimension of the grid are allocated to store the results. At each time step, the geopotential height, *gz*; the temperature, *t*; and the relative humidity, *hr*; are read from the input files of the climate database files.

b) After the importation of the data, the pressure *pp* is interpolated to the four heights by the chosen interpolation method (linear or hydrostatic) specified in step 1). The relative humidity is also converted to specific humidity, *hu*; and linear interpolation is performed on the specific humidity and temperature.

The parameters *pp, hu* and *tt* are then used to calculate the geostrophic wind at the four heights in the code *subroutines.ftn*

c) In *subroutines.ftn*, the potential temperature *th* is calculated from *tt* and the two lower height levels of *th* and their corresponding heights are used to calculate the Brunt-Väisälä frequency. Using the Brunt-Väisälä frequency and the geostrophic wind *vg*, the Froude number is calculated for each time steps.

d) Sort each time step into its corresponding shear bins. The shear is calculated as the sign of the difference between the near surface geostrophic wind at 0 and at 1500m. If the difference is a negative number, the time step is stored in the first shear bin. If the difference is a positive number, the time step is stored in the second bin.

   The new classification allows the possibility to classify the data by Froude number. If the key "nofrd" is set to false, the classification program creates 64 Froude number bins. The first 32 bins are for negative shear and the bins go from low Froude numbers to high Froude numbers. The last 32 bins are for positive shear and the bins go from the same low Froude numbers to the high Froude numbers as seen in the first 32 bins. The Froude numbers bins are defined in step 1 by the variable "xmesh".

e) The wind direction sectors are defined to the chosen number in step 1) by the key "nsect". And for each sector, the number of wind speed classes is defined by the key "nclass" and the limits of the classes are set by the key "classes".

   The direction of the geostrophic wind at 0m is used to select the wind direction sector and the wind speed class in that sector.

f) Once the time step has been classified by geostrophic wind direction, speed, shear and Froude number (if applicable), the frequency for that precise classification category (specific direction sector, speed class, shear and Froude bin) is incremented by one. Furthermore, the shear and the values of wind speed in x-direction (u), wind speed in y-direction and temperature (t) for the four heights are added to the existing values in that climate state.

At the end of the loop, there are dimensional field grids that contain: the number of occurrence for each climate state; the total number of the shear; and the added values for *u, v* and *t* at the four heights for each classification category.

3)

a) In the case where “nofrd” is false, the frequencies of the classification categories in step 2 are multiplied by a correction factors defined by the key “fcorr” in step 1. More precisely, each classification category is multiplied by a correction factor that corresponds to their Froude number and shear bins.

   Next, the 64 Froude number bins (32 for positive shear and 32 for negative shear) are collapsed and combined into 8 new Froude number bins (4 Froude number bins for positive shear and 4 Froude number bins for negative shear). The new Froude number bins will have new bin limits defined by the end limits of every former 8 Froude number bins.

   Ex.: The 8 Froude number bins:
   [0.0000, 0.0516); [0.0516, 0.1032); [0.1032, 0.1548); [0.1548, 0.2065); [0.2065, 0.2581); [0.2581, 0.3097); [0.3097, 0.3613); [0.3613, 0.4029) becomes a single new Froude number bin: [0.0000, 0.4029).

   In the case where “nofrd” is true, this entire step is skipped.

b) At this point the shear distinction is removed for the first wind class in each sector (weak wind) and for classes with a frequency less than 0.02 by merging the classes.

c) Each climate state has their mean values calculated by dividing the values for shear, *u, v* and *t* for the four heights by the frequency.

d) Afterwards, the percentage frequency is calculated by multiplying the frequency with 100 and dividing by the total number of records or time steps respectively in each climate state.

4) The grid dimensional fields are written into a standard file in the output directory called *classses_season.fst*. This file contains the grid-positions, the frequency, the mean geostrophic wind direction and speed at 0m and the mean values for *u, v* and *t* for the four heights for each class.

5) The output directories are prepared by creating folders for the latitude numbers of grid points, which will contain the table files with the longitude numbers of grid points after finishing the classification.

6) The content of the standard file is subdivided into the records for each grid point. One text file per grid point is generated which contains all occurring classes and its frequency, mean geostrophic wind direction *dd* and speed *ff* at 0m, the mean shear, the mean values for *u, v, t* for the 4 heights and the weight as *ff* * frequency and the coordinates and indices for the grid point additionally.

7) For sorting the classes the text file for each grid point is read and the eweight is calculated by multiplying the cubic of the mean geostrophic wind speed at 0m with the frequency. The classes are then sorted in descending order of the eweight and at last printed into the table.ef file.

ANNEX II

PROCEDURE TO CHANGE CLASSIFICATION VARIANT

1) Go to classification.ksh, and change keys to
   nofrd = .false.
   noshear = .true.

In *classification.ksh*, change the values of "xmesh" and "fcorr" to control the correction factors. "xmesh" defines the limits of the bins. There should be 32 set of numbers increasing in size. First number is inclusive, the second is non-inclusive.

Ex.: [0, 0.0516); [0.0516, 0.1032)

"fcorr" defines the factor at which the frequency will be multiplied by. Each set of number corresponds to the bins defined by xmesh. There should be 32 set of numbers and "xmesh" and "fcorr" should have the same amount of values. The variable in *gz2vg2.ftn* named "nshear" controls the amount of values "xmesh" and "fcorr" will have. "nshear" is the value desired multiplied by two.

2) Go to Fortran code *gz2vg.ftn* and change the variable values of nshear and mshear. If only shear is being used with no Froude bins, change the variable values to:

   nshear = 2
   mshear = 4

If shear and Froude bins are used, change the variables:

   nshear = 64
   mshear = 8

If shear is not used, but Froude bins are used, change variables to:

nshear = 64
mshear = 8

3) Go to Fortran code *gz2vg.ftn* and change the lines "data cshear / [...] /" to the following case:

If one shear is being used with no Froude bins, replace the line with
data cshear /'M', 'P'/

If shear and Froude bins are used, replace the line with
data cshear /'A', 'B', 'C', 'D', 'M', 'N', 'O', 'P'/

If shear is not used, but Froude bins are used, replace the line with
data cshear /'A', 'B', 'C', 'D'/

4) Go to Fortran code prep_table.ftn and change the lines
parameter (nsect=16, nshear=4, nclass=14, nvar=3, kmx=4, sshear=2, mshear=2)

If only shear is used, with no Froude bins, replace the line with
parameter (nsect=16, nshear=2, nclass=14, nvar=3, kmx=4, sshear=2, mshear=2)

If shear and Froude bins are used, replace line with
parameter (nsect=16, nshear=8, nclass=14, nvar=3, kmx=4, sshear=2, mshear=2)

If shear is not used, but Froude bins are used, replace the line with
parameter (nsect=16, nshear=4, nclass=14, nvar=3, kmx=4, sshear=2, mshear=2)

5) Go to Fortran code *prep_table.ftn* and change the lines
data cshear / 'A', 'B','C','D'/ AND data fshear / -1., -1., -1., -1./

If only shear is used, with no Froude bins, replace the line with:
data cshear / 'M', 'P'/
data fshear / -1., 1./

If shear and Froude bins are used, replace lines with:
data cshear /'A', 'B', 'C', 'D', 'M', 'N', 'O', 'P'/
data fshear / -1., -1., -1., -1., 1., 1., 1., 1./

If shear is not used, but Froude bins are used, replace the line with:
data cshear / 'A', 'B','C','D'/
data fshear / -1., -1., -1., -1./

ANNEX III

CALCULATED CORRECTION FACTORS

Table-A III-1 Correction factors of 5 cities and their arithmetic average (Merged)

	Correction Factors					
xmesh	**Whitehorse**	**Prince George**	**Port Hardy**	**Norman Wells**	**Fort Nelson**	**Merged**
0	21,151	5,507	7,278	11,894	9,932	11,1524
0,0516	7,177	2,821	2,871	5,605	5,17	4,7288
0,1032	3,406	1,573	1,509	2,66	2,638	2,3572
0,1548	1,685	1,042	0,985	1,435	1,536	1,3366
0,2065	1,031	0,833	0,816	0,987	1,038	0,941
0,2581	0,743	0,683	0,718	0,695	0,711	0,71
0,3097	0,679	0,642	0,692	0,537	0,565	0,623
0,3613	0,636	0,597	0,694	0,439	0,476	0,5684
0,4129	0,622	0,593	0,696	0,396	0,429	0,5472
0,4645	0,648	0,64	0,726	0,405	0,426	0,569
0,5161	0,605	0,758	0,826	0,42	0,375	0,5968
0,5677	0,565	0,846	1,045	0,441	0,383	0,656
0,6194	0,545	1,07	1,175	0,471	0,449	0,742
0,671	0,589	1,201	1,187	0,511	0,498	0,7972
0,7226	0,693	1,252	1,362	0,489	0,525	0,8642
0,7742	0,719	1,548	1,508	0,59	0,629	0,9988
0,8258	0,747	1,797	1,736	0,744	0,764	1,1576
0,8774	0,819	1,911	1,791	0,697	0,775	1,1986
0,929	0,916	2,265	2,007	0,829	0,854	1,3742

	Correction Factors					
xmesh	**Whitehorse**	**Prince George**	**Port Hardy**	**Norman Wells**	**Fort Nelson**	**Merged**
0,9806	1,034	2,696	2,216	0,87	1,145	1,5922
1,0323	1,17	2,861	2,026	1,011	1,08	1,6296
1,0839	1,246	2,862	1,901	0,893	1,216	1,6236
1,1355	1,161	3,322	1,759	1,231	1,818	1,8582
1,1871	1,216	4,442	1,853	1,957	2,044	2,3024
1,2387	1,608	7,368	2,434	1,704	2,199	3,0626
1,2903	1,734	5,843	2,775	1,716	3,261	3,0658
1,3419	1,723	6,497	2,687	2,235	3,056	3,2396
1,3935	1,718	9,407	2,666	4,212	4,778	4,5562
1,4452	1,755	12,974	2,03	2,995	6,195	5,1898
1,4968	2,557	15,927	6,601	2,501	3,555	6,2282
1,5484	2,623	14,082	3,393	4,863	4,763	5,9448
1,6	0,986	7,938	1,528	1,792	1,673	2,7834

ANNEX IV

FROUDE FREQUENCY CURVE

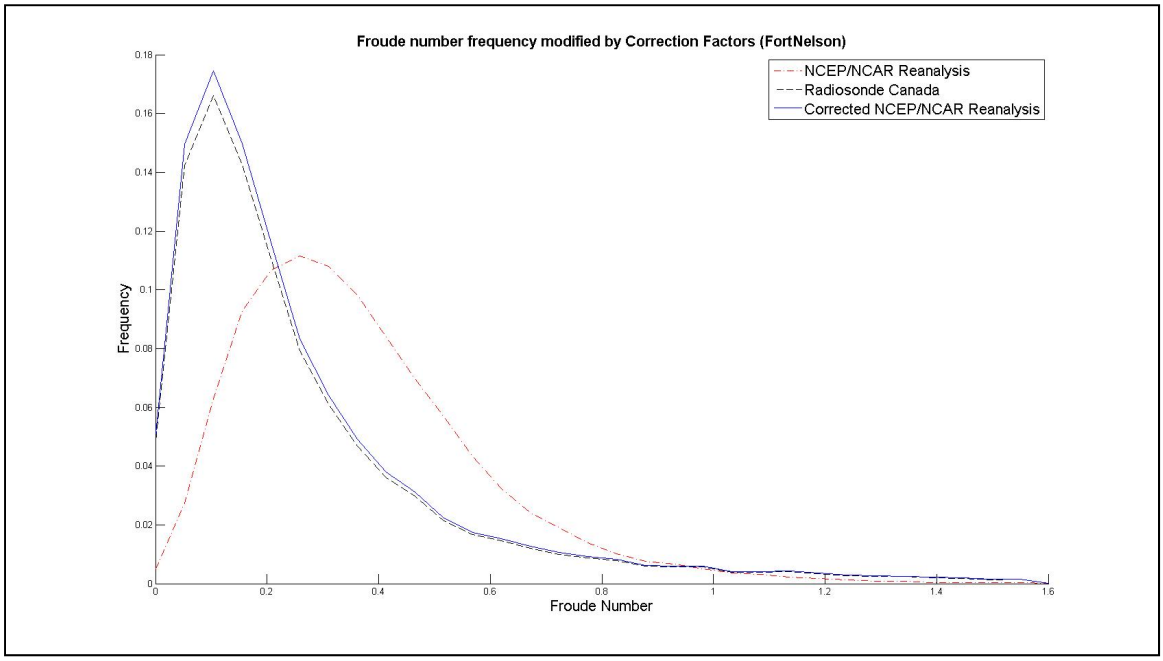

Figure-A IV-1 Froude number frequency curve of Fort Nelson modified by correction factors

The frequency curves of the Froude number bins of Fort Nelson. The dash-dotted line is the frequency curve of the NCEP/NCAR Reanalysis data points closest to Fort Nelson. The dashed line is the frequency curve of the Radiosonde in Whitehorse. The continuous line is the frequency curve of the Reanalysis modified by the correction factors to resemble the Radiosondes. There is a slight off-set between the Radiosonde curve (dashed line) and the modified curve (continuous line) in order to distinguish both curves.

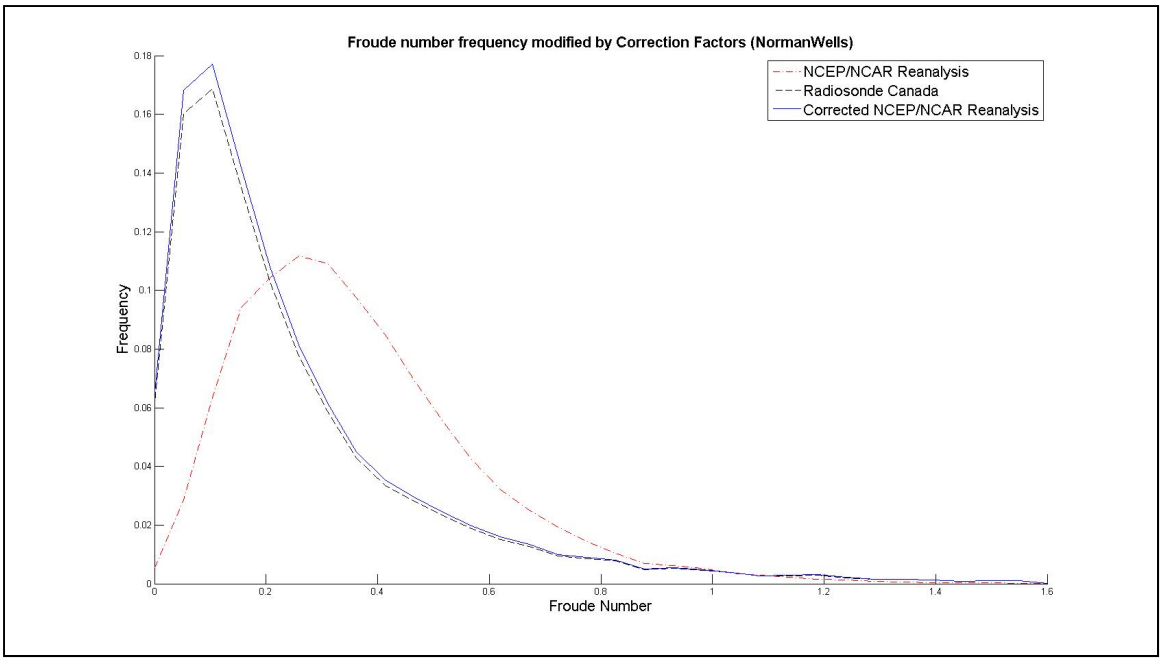

Figure-A IV-2 Froude number frequency curve of Norman Wells modified by correction factors

The frequency curves of the Froude number bins of Norman Wells. The dash-dotted line is the frequency curve of the NCEP/NCAR Reanalysis data points closest to Norman Wells. The dashed line is the frequency curve of the Radiosonde in Whitehorse. The continuous line is the frequency curve of the Reanalysis modified by the correction factors to resemble the Radiosondes. There is a slight off-set between the Radiosonde curve (dashed line) and the modified curve (continuous line) in order to distinguish both curves.

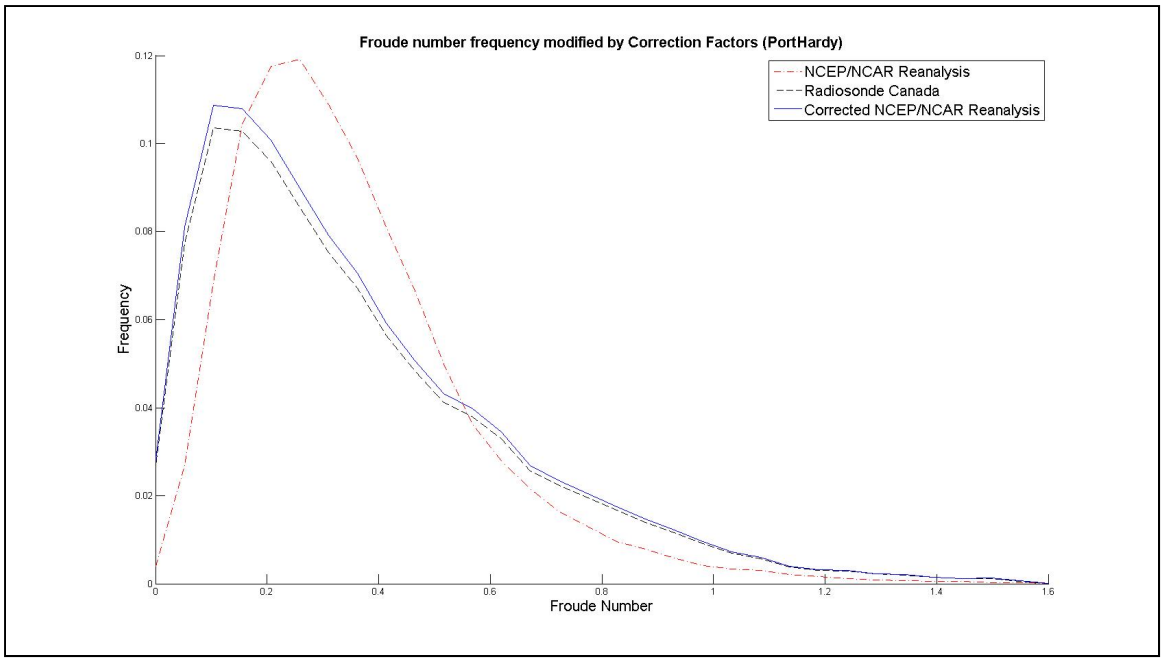

Figure-A IV-3 Froude number frequency curve of Port Hardy modified by correction factors

The frequency curves of the Froude number bins of Port Hardy. The dash-dotted line is the frequency curve of the NCEP/NCAR Reanalysis data points closest to Port Hardy. The dashed line is the frequency curve of the Radiosonde in Whitehorse. The continuous line is the frequency curve of the Reanalysis modified by the correction factors to resemble the Radiosondes. There is a slight off-set between the Radiosonde curve (dashed line) and the modified curve (continuous line) in order to distinguish both curves.

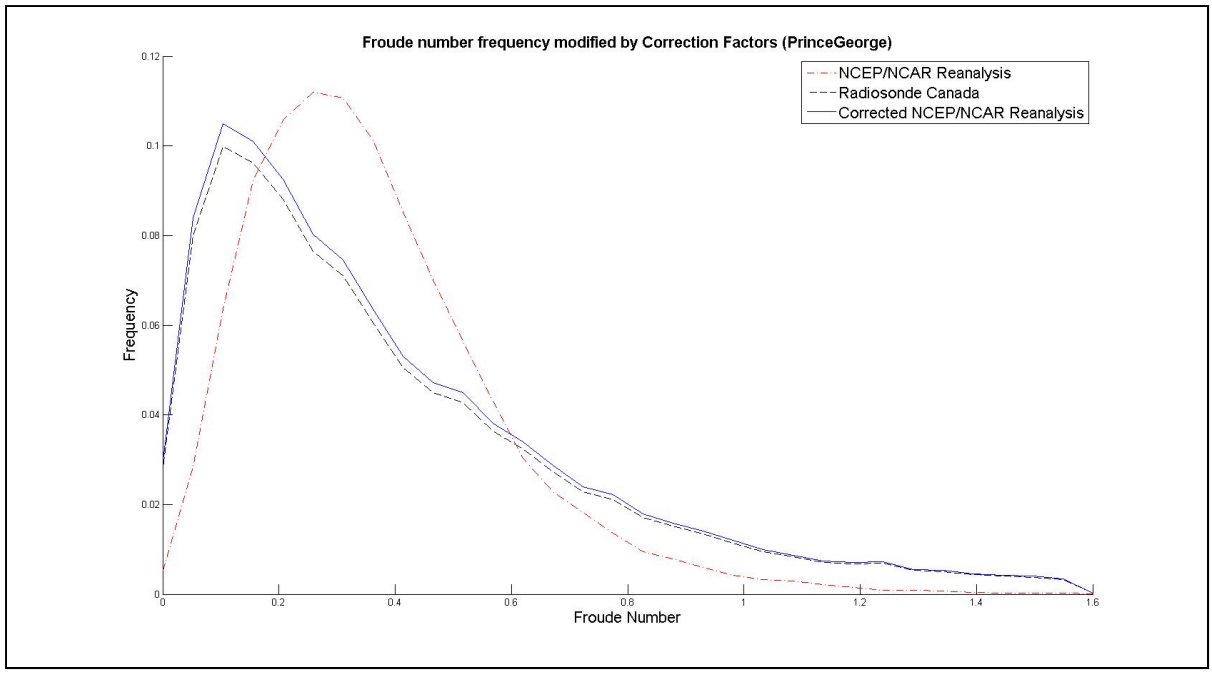

Figure-A IV-4 Froude number frequency curve of Prince George modified by correction factors

The frequency curves of the Froude number bins of Prince George. The dash-dotted line is the frequency curve of the NCEP/NCAR Reanalysis data points closest to Prince George. The dashed line is the frequency curve of the Radiosonde in Prince George. The continuous line is the frequency curve of the Reanalysis modified by the correction factors to resemble the Radiosondes. There is a slight off-set between the Radiosonde curve (dashed line) and the modified curve (continuous line) in order to distinguish both curves.

ANNEX V

FROUDE FREQUENCY CURVE WITH MERGED FACTORS

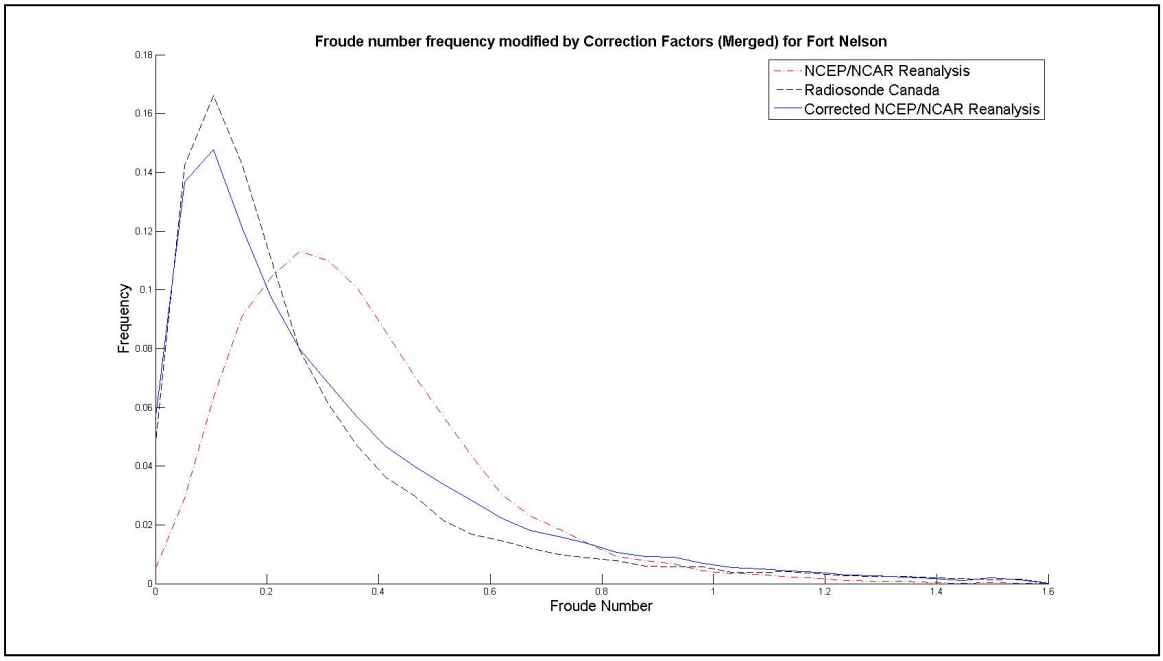

Figure-A V-1 Froude number frequency curve of Fort Nelson modified by merged correction factors

The figure shows the frequency curves of the different Froude number bins for Fort Nelson with the merged correction factors derived of 5 cities (Whitehorse, Norman Wells, Port Hardy, Prince George and Fort Nelson). The dash-dotted line indicates the frequency curve of the NCEP/NCAR Reanalysis data points closest to Fort Nelson. The dashed line indicates the frequency curve of the Radiosonde in Fort Nelson. The continuous line is the frequency curve of the Reanalysis modified by the merged correction factors to resemble the Radiosondes.

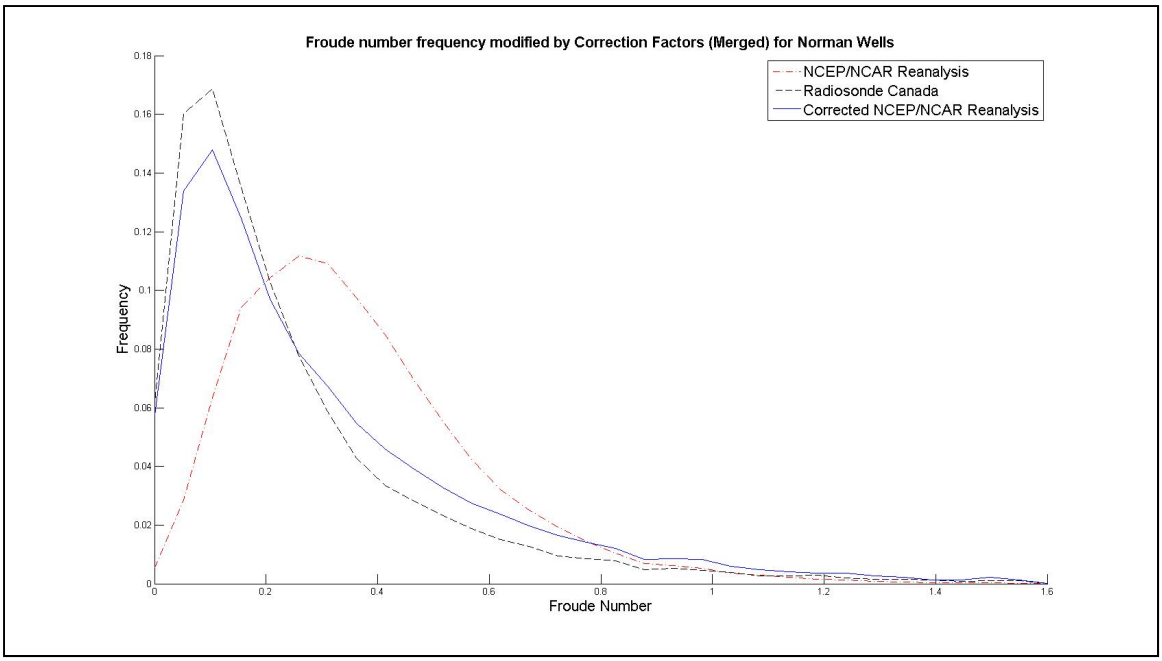

Figure-A V-2 Froude number frequency curve of Norman Wells modified by merged correction factors

This shows the frequency curves of the different Froude number bins for NormanWells with the merged correction factors derived of 5 cities (Whitehorse, NormanWells, Port Hardy, Prince George and Fort Nelson). The dash-dotted line indicates the frequency curve of the NCEP/NCAR Reanalysis data points closest to NormanWells. The dashed line indicates the frequency curve of the Radiosonde in NormanWells. The continuous line is the frequency curve of the Reanalysis modified by the merged correction factors to resemble the Radiosondes.

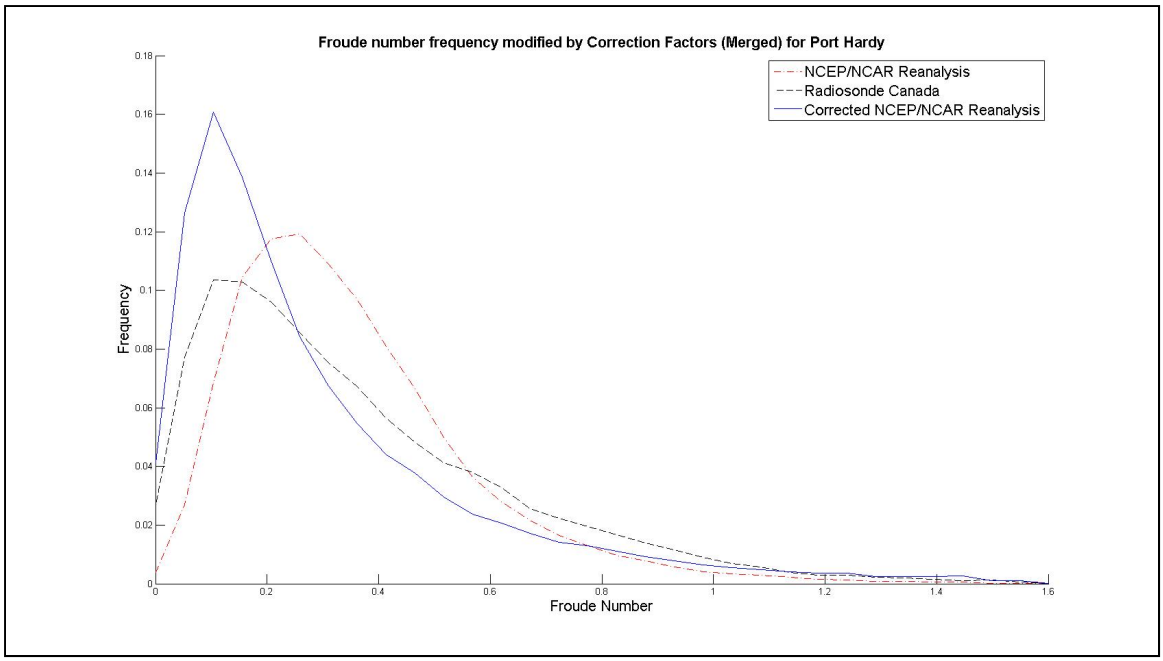

Figure-A V-3 Froude number frequency curve of Port Hardy modified by merged correction factors

This shows the frequency curves of the different Froude number bins for Port Hardy with the merged correction factors derived of 5 cities (Whitehorse, Norman Wells, Port Hardy, Prince George and Fort Nelson). The dash-dotted line indicates the frequency curve of the NCEP/NCAR Reanalysis data points closest to Port Hardy. The dashed line indicates the frequency curve of the Radiosonde in Port Hardy. The continuous line is the frequency curve of the Reanalysis modified by the merged correction factors to resemble the Radiosondes.

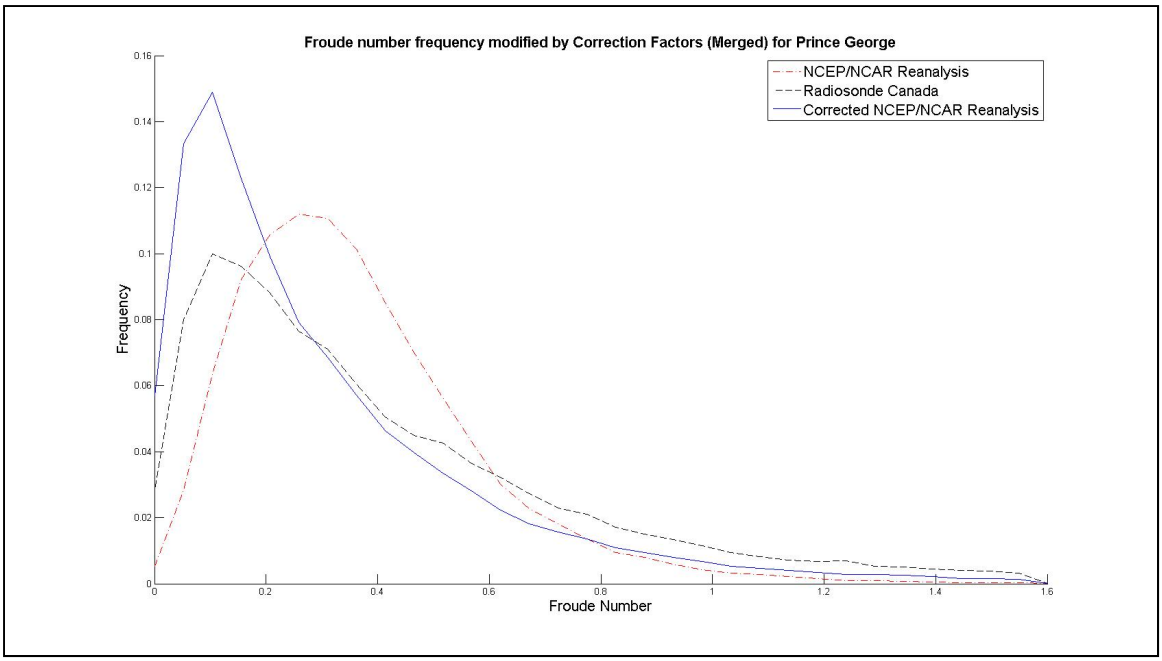

Figure-A V-4 Froude number frequency of Prince George modified by merged correction factor

This shows the frequency curves of the different Froude number bins for Prince George with the merged correction factors derived of 5 cities (Whitehorse, Norman Wells, Port Hardy, Prince George and Fort Nelson). The dash-dotted line indicates the frequency curve of the NCEP/NCAR Reanalysis data points closest to Prince George. The dashed line indicates the frequency curve of the Radiosonde in Prince George. The continuous line is the frequency curve of the Reanalysis modified by the merged correction factors to resemble the Radiosondes.

ANNEX VI

RESULTS AND ANALYSIS OF CLASSIFICATION VARIANT 3

The result of the simulated wind for the Classification Variant 3 (the classification with Froude criterion, but without Shear bins) is shown in Figure-A I. The color and size of the arrows give the direction and horizontal vector of the wind flow over the region of the Whitehorse in knots. The topography is defined by the filled contour lines in m ASL and the numbers indicate the position of the different observation wind stations used in this study. The wind in the Whitehorse Valley and Takhini Valley flow northward and eastward respectively; the horizontal wind vector speeds in the valleys are slower, varying between 1-5 knots. The wind higher up in the mountain flow in the northeast-eastward direction and the wind speeds at that altitude are faster, varying from 5-9 knots.

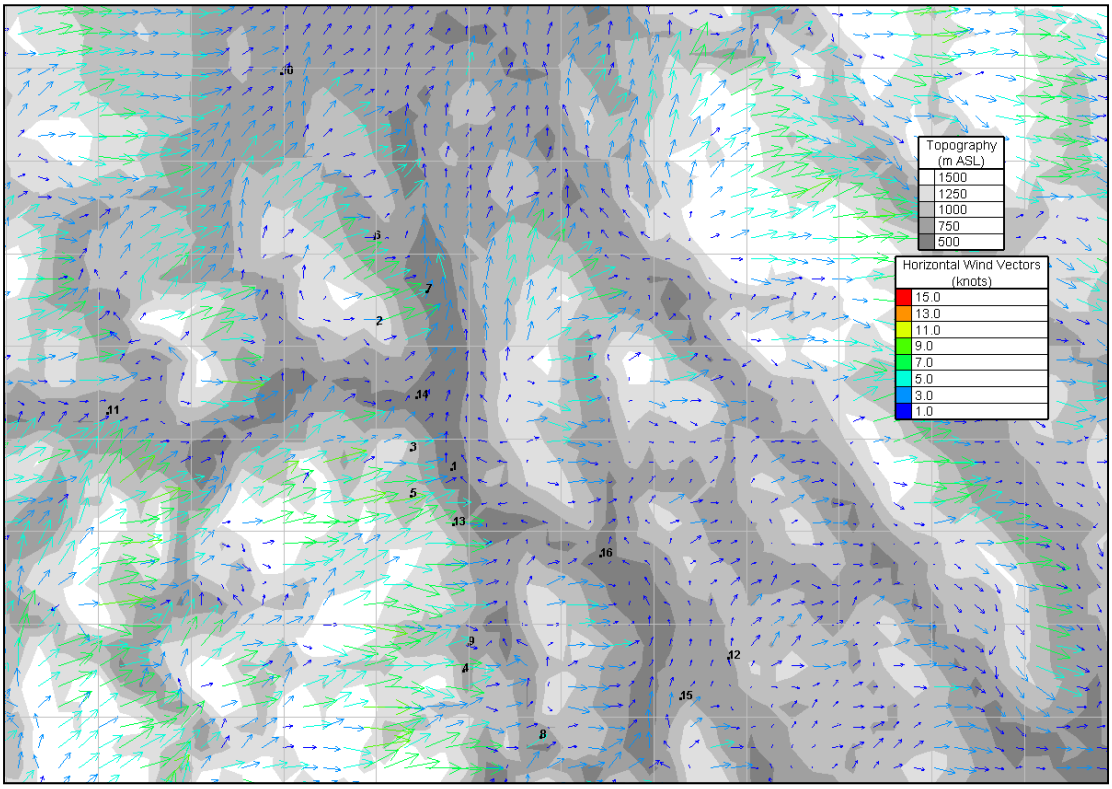

Figure-A I The simulated wind flow for the climate states of
the classification variant 3

When the wind speeds of these results are compared to the observation values, we obtain Figure-A II. The thick diagonal like shows the 1 to 1 ratio line in an ideal case. The dashed line shows the trend line of the 16 data points. Each observed wind speed values have their own long term mean wind speed standard deviation.

The modeled results hover around the diagonal, indicating some similarity with the observations. Unfortunately, there are still certain wind values that are overestimated and underestimated. However, when calculating the mean wind speed difference and its standard deviation between Variant 3 and the observations in Table-A XIII-1, we obtain a difference of 0.0 m/s and 0.1 m/s respectively. Furthermore, when comparing the wind speeds of Variant 3 with Variant 2, as presented in Table-A VI-1, we only see a mean difference of 0.114 m/s. The small differences between the two cases suggest that the exclusion of shear bins does not divert the results from values with respect to the case with the shear bins.

These results indicate that with the introduction of the Froude and correction factors, but without the use of shear bins, there is still an improvement in the wind speeds, and according to the mean difference with observations, yields the best results out of all the experiments. The Froude number aids greatly with the objective of reducing wind speed and approaching the observation values, and the shear seems to be of little help and contribution. This means, if needed, the shear bin can be ignored, in order to lighten the number of climate states and the computational requirements.

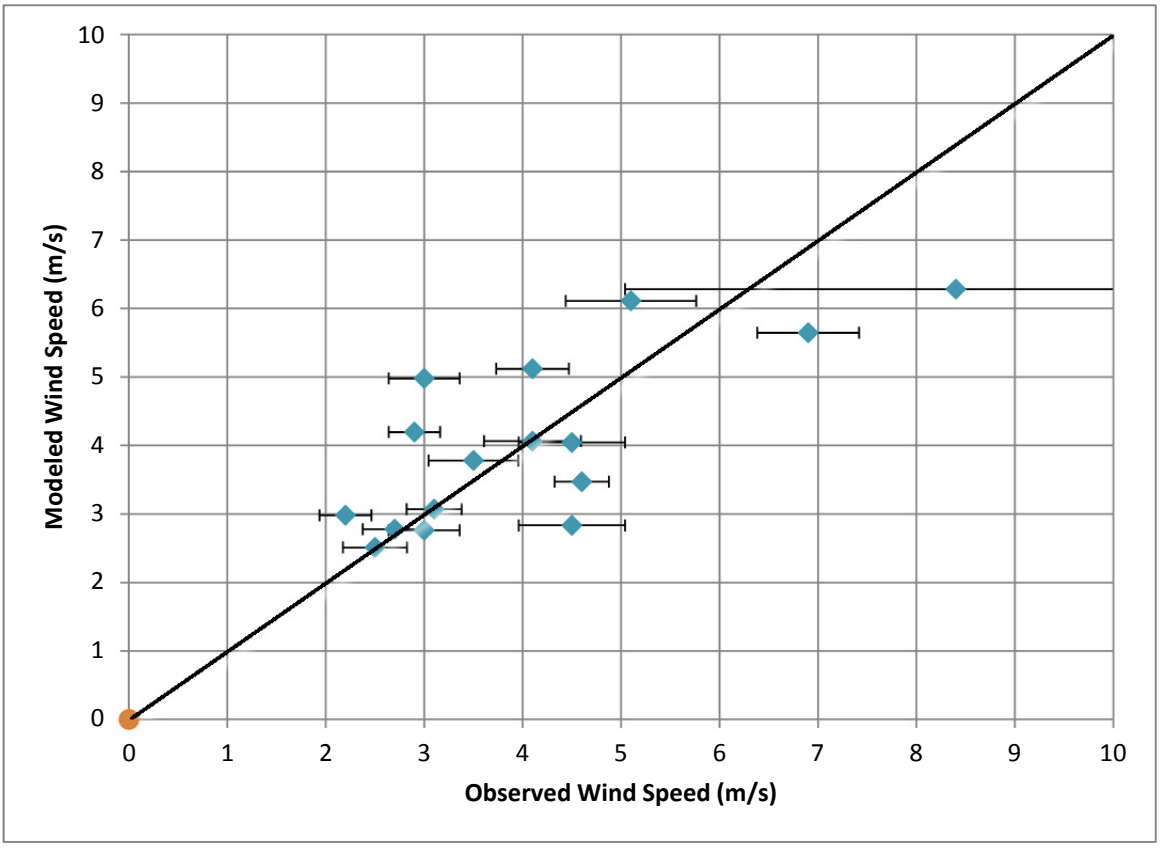

Figure-A II The comparison of wind speeds in m/s between the observations and the classification variant 3

Table-A VI-1: Difference between variant 3 and variant 2

Station Name	Station #	Reference	Simulations	Difference (m/s))
		Variant 2	Variant 3	
Whitehorse A	1	3,498	3,470	-0,028
Flat Mtn	2	6,113	6,282	0,169
Haeckel Hill	3	5,425	5,646	0,221
Annie	4	4,475	4,978	0,503
Fish	5	4,797	5,119	0,322
Fox Lake	6	2,803	2,776	-0,026
Laberge	7	4,048	4,044	-0,003
Watson	8	3,950	4,062	0,112
Wheaten	9	2,884	2,980	0,096
Braeburn	10	3,014	3,071	0,057
Champagne	11	3,915	4,195	0,279
Jakes	12	2,492	2,510	0,017
Mt Sima	13	5,920	6,111	0,192
Nursery	14	3,849	3,781	-0,069
Jubilee Mtn	15	2,825	2,834	0,009
Marsh Lake	16	2,789	2,761	-0,028
Mean Difference (m/s)				0,114
Standard Deviation				0,158

ANNEX VII

WIND SPEEDS CONTOUR LINES FOR ORIGINAL CLASSIFICATION

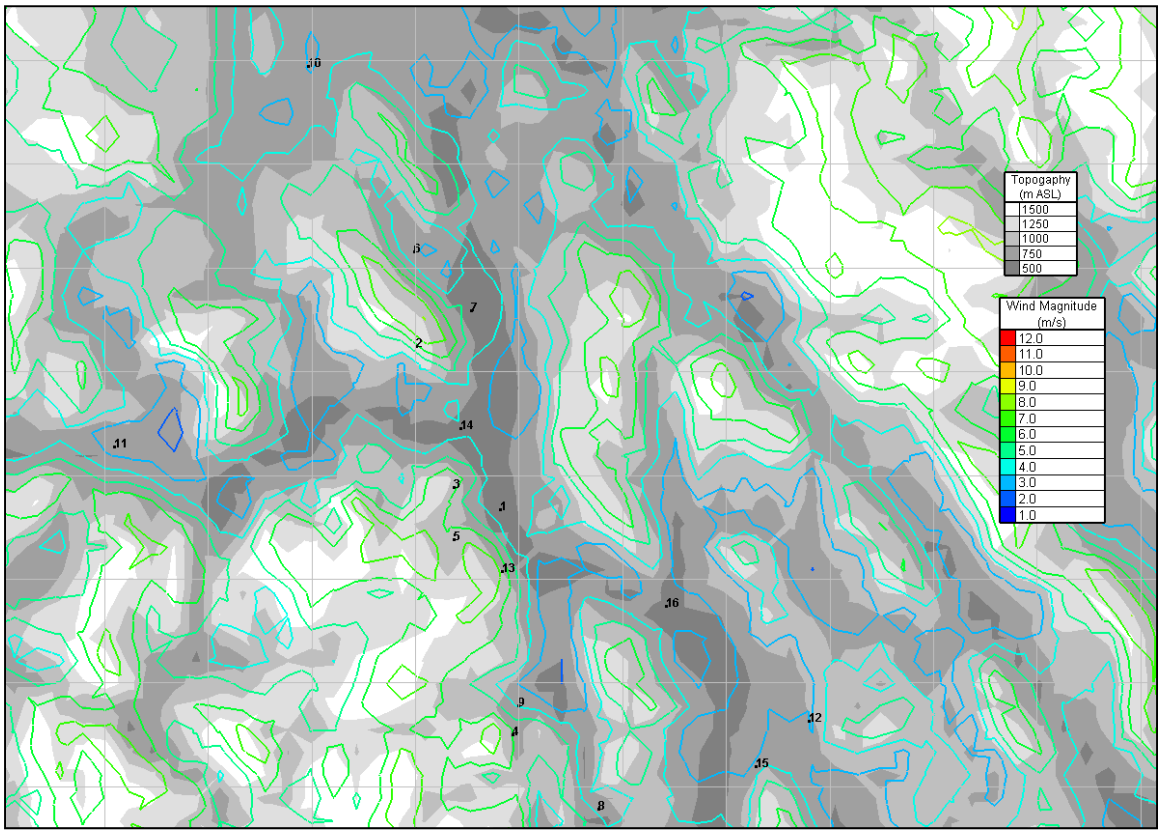

Figure-A III The magnitude of the wind for original classification

The wind speed from the climate states of the original classification. The colour of the contour lines gives the magnitude of the wind in m/s, for the region of Whitehorse. The topography is defined by the filled contour lines in m ASL and the numbers indicates the position of the different observation wind stations used in this study.

ANNEX VIII

WIND SPEED CONTOUR LINES FOR CLASSIFICATION VARIANT 1

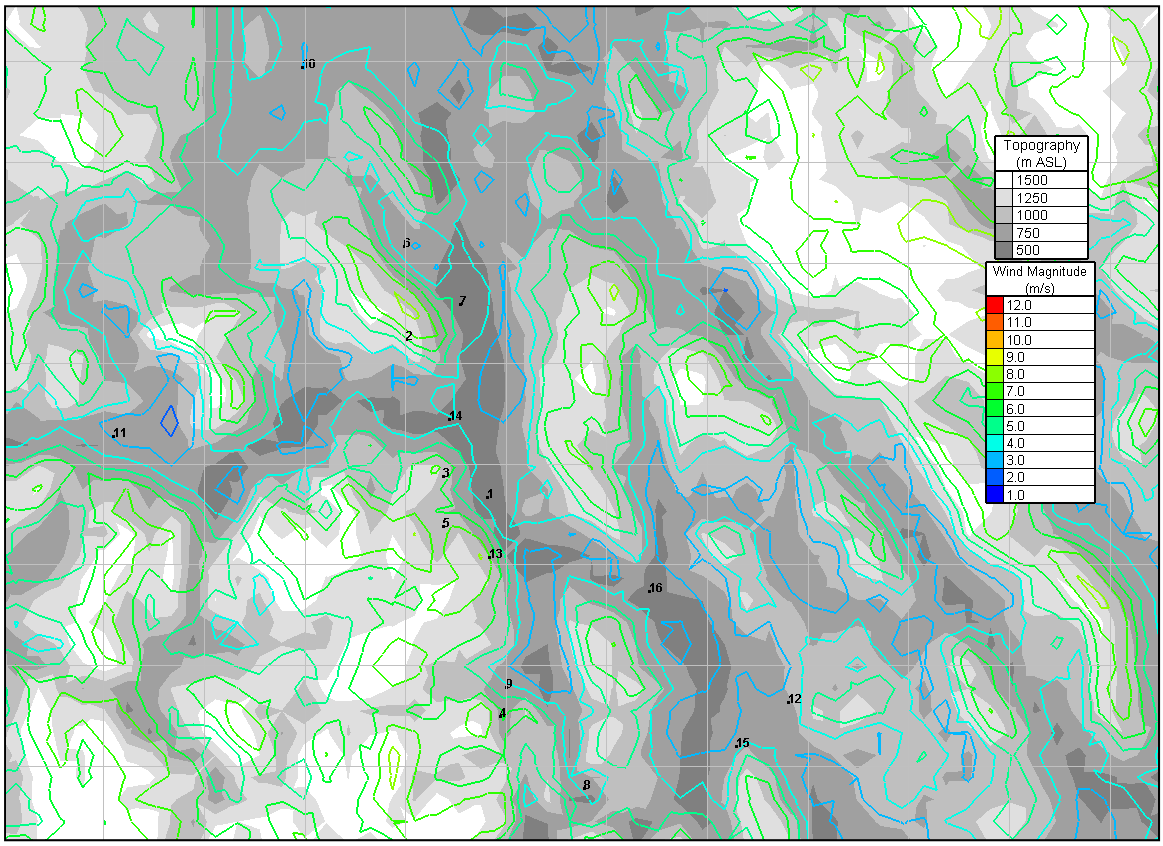

Figure-A IV The magnitude of the wind for classification variant 1

The wind speed from the climate states of the classification variant 1. The colour of the contour lines gives the magnitude of the wind in m/s, for the region of Whitehorse. The topography is defined by the filled contour lines in m ASL and the numbers indicates the position of the different observation wind stations used in this study.

ANNEX IX

WIND SPEED CONTOUR LINES FOR CLASSIFICATION VARIANT 2

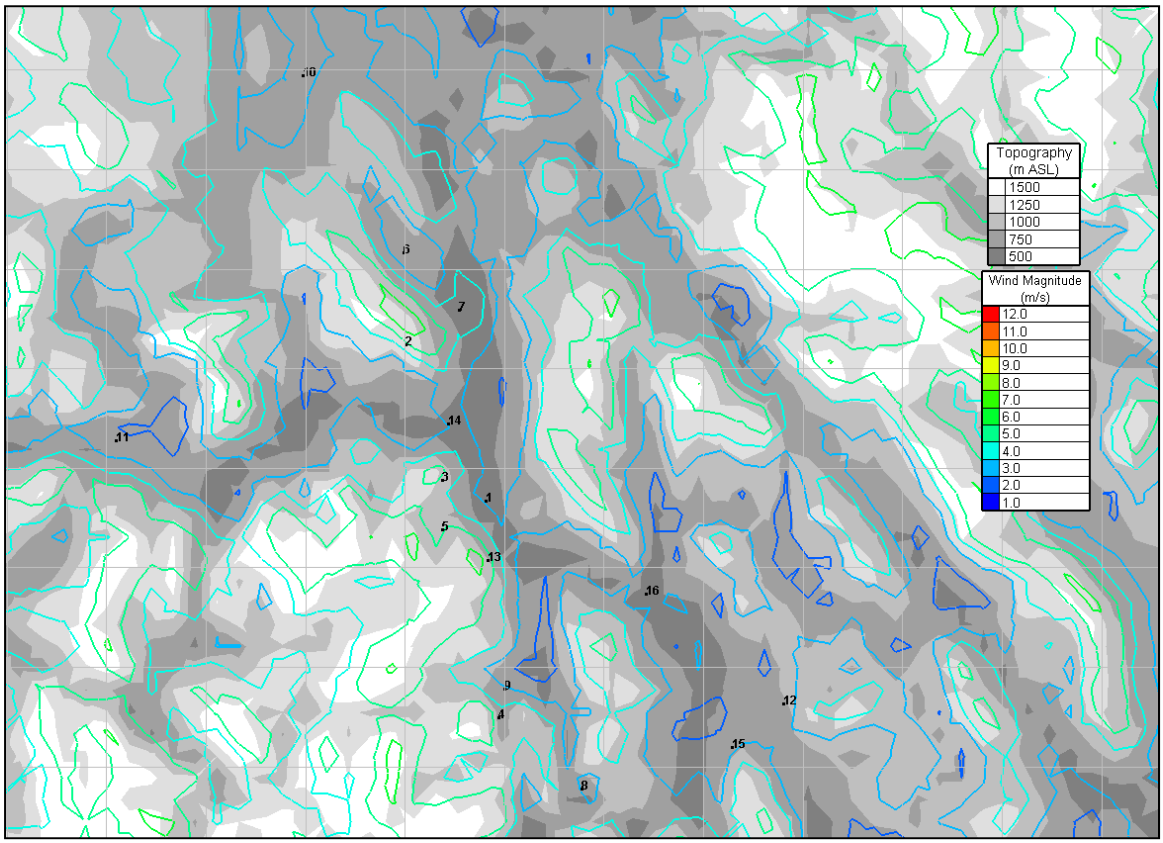

Figure-A V The magnitude of the wind for classification variant 2

The wind speed from the climate states of the classification variant 2. The colour of the contour lines gives the magnitude of the wind in m/s, for the region of Whitehorse. The topography is defined by the filled contour lines in m ASL and the numbers indicates the position of the different observation wind stations used in this study.

ANNEX X

WIND SPEED CONTOUR LINES FOR INITIAL REFERENCE TOPOGRAPHY

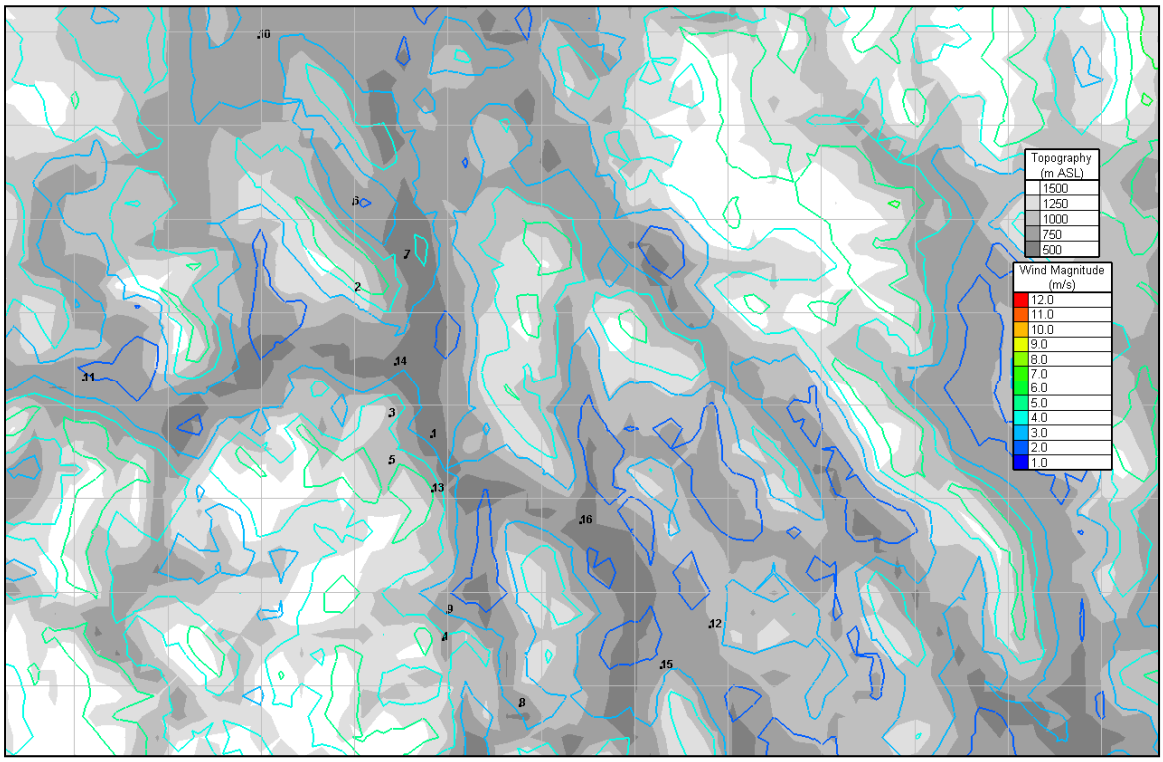

Figure-A VI The magnitude of the wind for classification variant 2 with initial reference topography

The simulated wind speed for the classification variant 2 with the initial reference topography (init_topo) at 600m ASL. The colours of the contour lines give the magnitude of the wind in m/s, for the region of Whitehorse. The topography is defined by the filled contour lines in m ASL and the numbers indicates the position of the different observation wind stations used in this study.

ANNEX XI

DESCRIPTION OF KEY KNCEP_DROP

In order to use the modification that ignores the u,v profile during initialization and bring down the value in the level above using the thermal wind, an additional key was added to the mc2_settings.nml file. This key name is “kncep_drop”, and controls which data level will be ignored and which data level will be used to extrapolate (using wind thermal equations) and replace that ignored level. It can be set to a value from 0 to 3, where 0 indicates that no levels will be ignored; 1 will ignore the data level 0m ASL and data from level 1500m ASL will be used; 2 will ignore the 2 bottom data levels (0 and 1500m ASL) and level 3000m ASL will be used; 3 will ignore the 3 bottom data levels (0, 1500 and 3000m ASL) and level 5500m ASL will be used. Note, that “ncep_kdrop” cannot be set to 4, as the model still requires 1 level to be used as a reference and to be extrapolated to the other levels below.

ANNEX XII

DETAILED DESCRIPTION OF WIND STATIONS

Table-A XII-1 Full description of wind stations

Station Name	Station #	Latitude (°)	Longitude (°)	Period	Period Length	Uncertainty on average (%)	Elevation (m)	Valley/ Mtn	grid coordinates		Surface Rough-ness	Wind Speed (m/s)	Variation (±m/s)
									I	J			
Whitehorse A	1	60,710	-135,067	2001-2005	5 years	6	706	V	50	49	0,02	4,6	0,276
Flat Mtn	2	60,994	-135,370	June-August 1992	3 months	40	1930	M	46	58	n/a	8,4	3,36
Haeckel Hill	3	60,749	-135,231	1998-2001	4 years	8	1430	M	48	51	0,01	6,9	0,5175
Annie	4	60,319	-135,020	2000-2001	2 years	12	876	V	51	39	n/a	3	0,36
Fish	5	60,659	-135,230	2001-2003	3 years	9	1175	M	48	48	n/a	4,1	0,369
Fox Lake	6	61,160	-135,380	2001-2002	2 years	12	793	V	47	61	3,85	2,7	0,324
Laberge	7	61,057	-135,170	2001-2002	2 years	12	645	V	49	58	0,01	4,5	0,54
Watson	8	60,190	-134,720	2001-2002	2 years	12	702	V	54	36	3,55	4,1	0,492
Wheaten	9	60,370	-135,000	2002-2003	2 years	12	783	V	52	41	n/a	2,2	0,264
Braeburn	10	61,481	-135,770	June03-Sept06	3 years	9	725	V	41	69	n/a	3,1	0,279
Champagne	11	60,811	-136,448	May03-Sept06	3 years	9	732	V	33	51	n/a	2,9	0,261
Jakes	12	60,339	-133,980	March05-Sept06	1.5 years	13	814	V	64	40	n/a	2,5	0,325
Mt Sima	13	60,604	-135,060	Dec04-Sept06	1.75 years	13	939	M	50	46	n/a	5,1	0,663
Nursery	14	60,851	-135,210	June05-Sept06	1.25 years	13	674	V	49	53	n/a	3,5	0,455
Jubilee Mtn	15	60,262	-134,170	1993-1994	2 years	12	1280	M	62	38	0,05	4,5	0,54
Marsh Lake	16	60,542	-134,480	2001-2002	2 years	12	656	V	57	45	0,01	3	0,36

ANNEX XIII

SIMULATED WIND SPEED OF SIMULATIONS

Table-A XIII-1 Wind speed of wind stations for observation and simulations

Station Name	Station #	Observation (m/s)	Surface Roughness of grid (m)	Simulations (m/s)						
				Original	Variant 1	Variant 2	Variant 2 + init_topo	Variant 2 + kdrop1	Final Simulation	Variant 3
Whitehorse A	1	4,6	0,010	4,33	4,53	3,50	3,28	3,41	3,24	3,47
Flat Mtn	2	8,4	0,016	7,52	7,74	6,11	5,54	6,03	5,49	6,28
Haeckel Hill	3	6,9	0,010	6,91	7,21	5,43	5,00	5,10	4,73	5,65
Annie	4	3	0,038	5,81	6,10	4,48	4,16	4,49	4,09	4,98
Fish	5	4,1	0,019	6,30	6,53	4,80	4,51	4,86	4,50	5,12
Fox Lake	6	2,7	0,695	3,81	3,91	2,80	2,59	2,83	2,64	2,78
Laberge	7	4,5	0,010	4,39	4,47	4,05	3,73	4,16	3,84	4,04
Watson	8	4,1	0,021	5,04	5,19	3,95	3,77	4,10	3,87	4,06
Wheaten	9	2,2	0,231	3,67	3,92	2,88	2,52	2,65	2,38	2,98
Braeburn	10	3,1	0,485	3,53	3,69	3,01	2,79	3,16	2,90	3,07
Champagne	11	2,9	0,832	4,70	4,87	3,92	3,87	4,12	4,07	4,19
Jakes	12	2,5	1,311	2,98	3,12	2,49	2,30	2,17	2,12	2,51
Mt Sima	13	5,1	0,010	7,26	7,65	5,92	5,29	5,84	5,17	6,11
Nursery	14	3,5	0,804	4,57	4,74	3,85	3,50	3,47	3,31	3,78
Jubilee Mtn	15	4,5	0,770	3,43	3,66	2,83	2,67	2,55	2,51	2,83
Marsh Lake	16	3	0,070	3,20	3,42	2,79	2,47	2,55	2,34	2,76
Correlation of Coefficient				**0,750**	**0,743**	**0,782**	**0,773**	**0,739**	**0,742**	**0,739**

ANNEX XIV

DIFFERENCE BETWEEN OBSERVATIONS AND SIMULATIONS

Table-A XIV-1 Difference between observations and simulations

Station Name	Station #	Original	Variant 1	Variant 2	Variant 2 + init_topo	Variant 2 + kdrop1	Final Simulation	Variant 3
Whitehorse A	1	-0,3	-0,1	-1,1	-1,3	-1,2	-1,4	-1,1
Flat Mtn	2	-0,9	-0,7	-2,3	-2,9	-2,4	-2,9	-2,1
Haeckel Hill	3	0,0	0,3	-1,5	-1,9	-1,8	-2,2	-1,3
Annie	4	2,8	3,1	1,5	1,2	1,5	1,1	2,0
Fish	5	2,2	2,4	0,7	0,4	0,8	0,4	1,0
Fox Lake	6	1,1	1,2	0,1	-0,1	0,1	-0,1	0,1
Laberge	7	-0,1	0,0	-0,5	-0,8	-0,3	-0,7	-0,5
Watson	8	0,9	1,1	-0,1	-0,3	0,0	-0,2	0,0
Wheaten	9	1,5	1,7	0,7	0,3	0,4	0,2	0,8
Braeburn	10	0,4	0,6	-0,1	-0,3	0,1	-0,2	0,0
Champagne	11	1,8	2,0	1,0	1,0	1,2	1,2	1,3
Jakes	12	0,5	0,6	0,0	-0,2	-0,3	-0,4	0,0
Mt Sima	13	2,2	2,5	0,8	0,2	0,7	0,1	1,0
Nursery	14	1,1	1,2	0,3	0,0	0,0	-0,2	0,3
Jubilee Mtn	15	-1,1	-0,8	-1,7	-1,8	-2,0	-2,0	-1,7
Marsh Lake	16	0,2	0,4	-0,2	-0,5	-0,5	-0,7	-0,2
Mean Difference (m/s)		**0,8**	**1,0**	**-0,1**	**-0,4**	**-0,2**	**-0,5**	**0,0**
Standard Deviation (m/s)		1,1	1,1	1,0	1,1	1,1	1,1	1,1

ANNEX XV

WIND FREQUENCY ROSE OF FINAL SIMULATIONS AT 16 WIND STATION

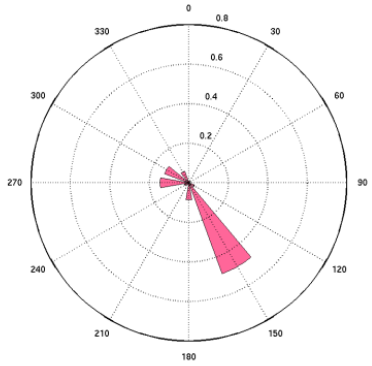

Station#1-Whitehorse A
latitude : 60.71, longitude : -135.0672

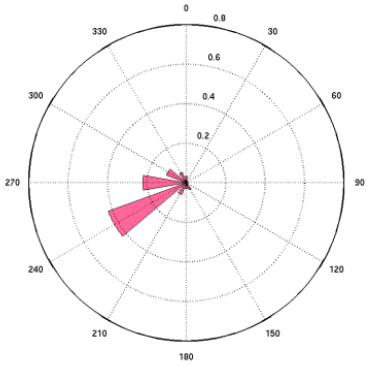

Station#2-Flat Mtn
latitude : 60.994, longitude : -135.37

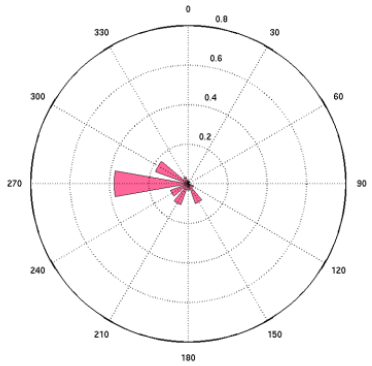

Station#3-Haeckel Hill
latitude : 60.749, longitude : -135.231

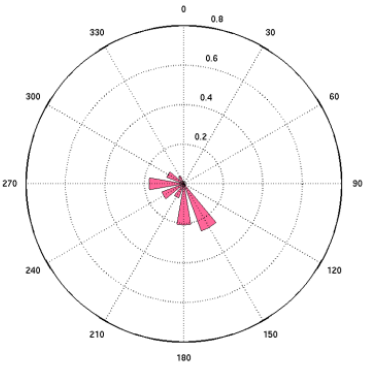

Station#4-Annie
latitude : 60.319, longitude : -135.02

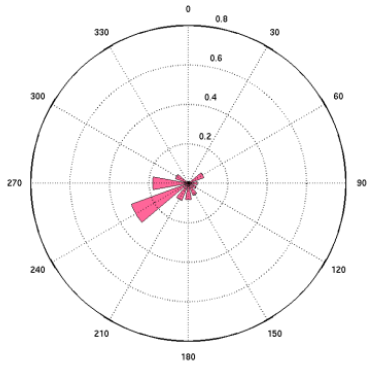

Station#5-Fish
latitude : 60.659, longitude : -135.23

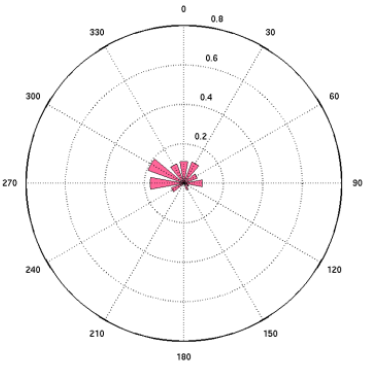

Station#6-Fox Lake
latitude : 61.16, longitude : -135.38

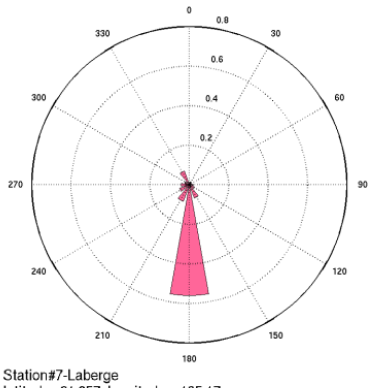

Station#7-Laberge
latitude : 61.057, longitude : -135.17

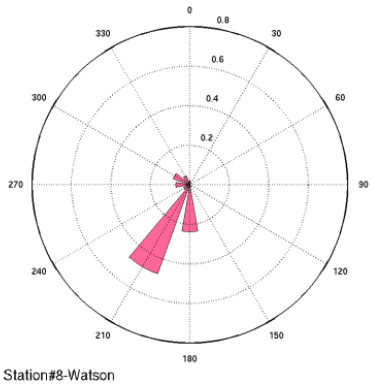

Station#8-Watson
latitude : 60.19, longitude : -134.72

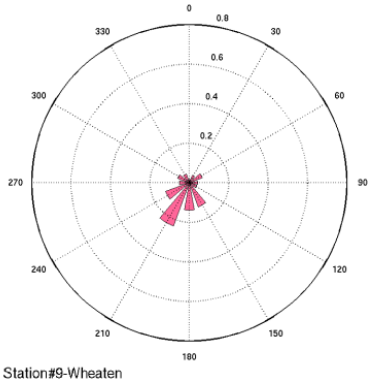

Station#9-Wheaten
latitude : 60.37, longitude : -135

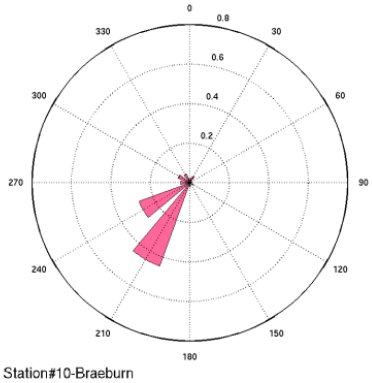

Station#10-Braeburn
latitude : 61.481, longitude : -135.77

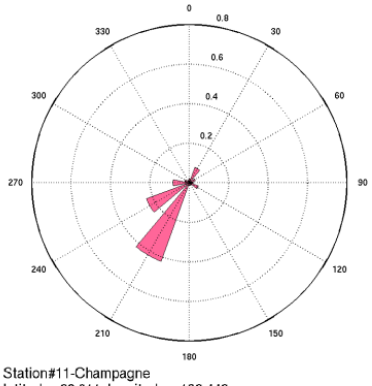

Station#11-Champagne
latitude : 60.811, longitude : -136.446

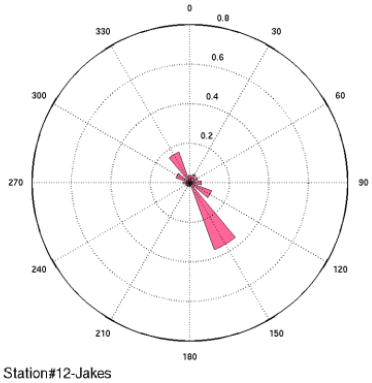

Station#12-Jakes
latitude : 60.339, longitude : -133.98

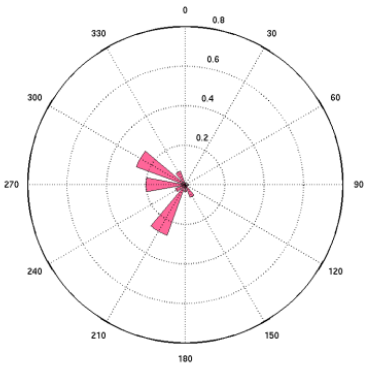

Station#13-Mt Sima
latitude : 60.604, longitude : -135.06

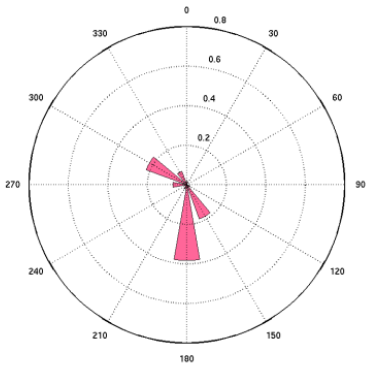

Station#14-Nursery
latitude : 60.851, longitude : -135.21

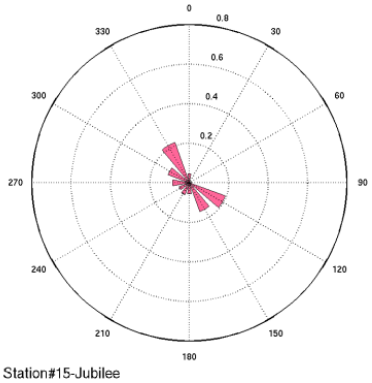

Station#15-Jubilee
latitude : 60.262, longitude : -134.17

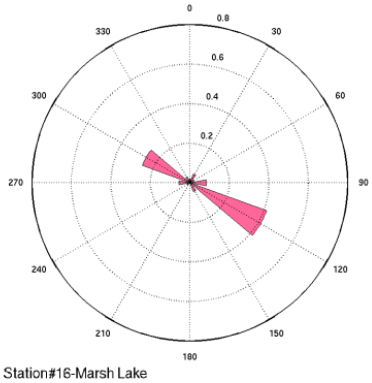

Station#16-Marsh Lake
latitude : 60.542, longitude : -134.48

LIST OF BIBLIOGRAPHICAL REFERENCES

Adrian, G. and F. Fiedler (1991). "Simulation of unstationary wind and temperature fields over complex terrain and comparison with observations." Beitrage zur Physik der Atmosphere **64**: 27-48 p.

Benoit, R. and W. Yu (2004). "Cartographie et analyse du gisement éolien du Québec par le système WEST".Online. <http://www.anemoscope.ca/References/EOLE_Quebec_2004.pdf>.Visited on March 1st 2013.

Bergstrom, H. and N. Juuso (2006). "A study of valley winds using the MIUU mesoscale model." Wind Energy **9**: 109-129 p.

CanadianHydraulicsCentre (2006). "Anemoscope Wind Energy Simulation and Mapping Reference guide." Online. <ftp://kenueftp.chc.nrc.ca/AnemoScope/AnemoScope_ReferenceGuide.pdf>. Consulted on November 24th 2012.

Frank, H. and L. Landberg (1997). "Modelling the wind climate of Ireland." Boundary-Layer Meteorology **85**(3): 359-377 p.

Frank, H. P., O. Rathmann, N. G. Mortensen and L. Landberg (2001). "The numerical wind atlas of the KAMM/WAsP method." Riso-R-1252 (EN) **60**.

Frey-Buness, F., D. Heimann and R. Sausen (1995). "A statistical-dynamical downscaling procedure for global climate simulations." Theoretical and Applied Climatology **50**(3): 117-131 p.

Gal-Chen, T. and R. C. J. Somerville (1975). "On the use of a coordinate transformation for the solution of the Navier-Stokes equations." Journal of Computational Physics **17**(2): 209-228 p.

Girard, C., R. Benoit and M. Desgagne (2005). "Finescale topography and the MC2 dynamics kernel." Monthly weather review **133**(6): 1463-1477 p.

Grell, G. A., J. Dudhia and D. R. Stauffer (1994). "A description of the fifth-generation Penn State/NCAR mesoscale model (MM5)."

Holton, J. R. and D. Staley (1973). "An introduction to dynamic meteorology." American Journal of Physics **41**: 752 p.

Jackson, P. and J. Hunt (1975). "Turbulent wind flow over a low hill." Quarterly Journal of the Royal Meteorological Society **101**(430): 929-955 p.

Kalnay, E., M. Kanamitsu, R. Kistler, W. Collins, D. Deaven, L. Gandin, M. Iredell, S. Saha, G. White and J. Woollen (1996). "The NCEP/NCAR 40-year reanalysis project." Bulletin of the American meteorological Society **77**(3): 437-471 p.

Laprise, R., D. Caya, G. Bergeron and M. Giguere (1997). "The formulation of the Andre Robert MC2 (mesoscale compressible community) model." Atmosphere-Ocean **35**(sup1): 195-220 p.

Mortensen, N. G., U. S. Said and J. Badger (2006). Wind Atlas of Egypt, RISO National Laboratory, New and Renewable Energy Authority, Egyptian Meteorological Authority.

Pinard, J. D. J. P., R. Benoit and W. Yu (2005). "A WEST wind climate simulation of the mountainous Yukon." Atmosphere-Ocean **43**(3): 259-281 p.

Pinard, J. P. (2007). "Wind climate of the Whitehorse area." Arctic: 227-237 p.

Pinard, J. P., R. Benoit and J. D. Wilson (2009). "Mesoscale wind climate modelling in steep mountains." Atmosphere-Ocean **47**(1): 63-78 p.

Robert, A., T. L. Yee and H. Ritchie (1985). "A semi-Lagrangian and semi-implicit numerical integration scheme for multilevel atmospheric models." Monthly weather review **113**(3): 388-394 p.

Recherche en Prévision Numérique (2003). "Canadian Wind Energy Atlas". Online. < http://www.windatlas.ca/en/index.php>. Visited on March 1st 2013

Scire, J. S., F. R. Robe, M. E. Fernau and R. J. Yamartino (2000). "A users guide for the CALMET Meteorological Model." Earth Tech, USA.

Tanguay, M., A. Robert and R. Laprise (1990). "A Semi-implicit Send-Lagrangian Fully Compressible Regional Forecast Model." Monthly weather review **118**(10): 1970-1980 p.

Thomas, S., C. Girard, R. Benoit, M. Desgagne and P. Pellerin (1998). "A new adiabatic kernel for the MC2 model." Atmosphere-Ocean **36**(3): 241-270 p.

Vosper, S. (2004). "Inversion effects on mountain lee waves." Quarterly Journal of the Royal Meteorological Society **130**(600): 1723-1748 p.

Walmsley, J., P. Taylor and T. Keith (1986). "A simple model of neutrally stratified boundary-layer flow over complex terrain with surface roughness modulations (MS3DJH/3R)." Boundary-Layer Meteorology **36**(1): 157-186 .p

Yim, S. H. L., J. C. H. Fung, A. K. H. Lau and S. Kot (2007). "Developing a high-resolution wind map for a complex terrain with a coupled MM5/CALMET system." Journal of geophysical research **112**(D5): D05106.

Yu, W., R. Benoit, C. Girard, A. Glazer, D. Lemarquis, J. R. Salmon and J. P. Pinard (2006). "Wind Energy Simulation Toolkit (WEST): A wind mapping system for use by the WindEnergy Industry." Wind Engineering **30**(1): 15-33 p.